Studies on dynamic nuclear polarization using photo-excited triplet electron spins

Kazuyuki Takeda

March, 2003

Acknowledgments

Before starting studies on dynamic nuclear polarization by photo-excited triplet electron spins, the main subject of this work, I had been a graduate student in master's program at Molecular Chemical Physics laboratory in Department of Chemistry, Kyoto University, and had been developing a solid-state NMR technique to measure interatomic distances, which was intended to be utilized to extract structual information of molecules. Just around the same time, a research group at Department of Physics in Kyoto University, which is placed just a few hundred meters north to ours, were about to complete their project on the development of a polarized target for scattering experiments of particle beams.

Their experimental result was fascinating; ^{1}H spin polarization was enhanced by 80,000 times, which meant that ^{1}H NMR sensitivity was improved by 80,000 times! They said that they had finished their work on it and would not use instruments such as laser and microwave power amplifier any more, and that we may use them for a while if we wanted. Being very stimulated, we immediately seized on their kind offer. Therefore, I had begun this work as a research task for my doctoral course because I happened to be given a fortunate opportunity to do this and I felt it fascinating.

In the course of my research, I had frequently encountered machine troubles, and I had a plenty of time to repair them. Sometimes the troubles were so serious that I thought I could not go on the subject any longer. Very fortunately, however, I managed to continue progress in my research under the direction of professor Takehiko Terao, an expert on NMR, our boss, and

my immediate supervisor. Throughout my student days, he have supervised me, encouraged me, and sometimes fired me up to continue my tasks. Discussions with him have been very stimulating and enjoyable, and were very helpful for me to delve into the essence of things.

In our department, undergraduate students are supposed to be put in one of a dozen laboratories when they get into their forth year. I, however, had informally had joined the Terao group when I was still in my third year, thanks to our associate professor Kiyonori Takegoshi, who has taken care of me in many respects. He happened to be having a training class on electrical circuits when I chose it as an elective subject for the third-year student, and influenced me to develop a sample-spinning-speed controller which he had designed and was to be used for solid-state NMR experiments. At the class he challenged me to a game, saying that if I could successfully develop it within I was in my third year, then he would offer me a drink, but if I carried it over to my forth year, there would be no reward as it would no longer be an extra job, but would become my research subject. I managed to make it just in time, and so I had had a free feast as promised. During this game, I had enjoyed learning the principles of operation of electric circuits.

I owe a lot to the members of Department of Chemistry. I have had many helps and suggestions from professor Okitsugu Kajimoto. My skill in metalwork has been trained by attentive advice from Fujitsugu Amita. Atushi Kubo and Fumio Imashiro had frequently gave me suggestions. Clerical works by Chiyoe Sakata and Hiromi Kumamoto have been very helpful. I have had a lot of help with my own work from colleague students, Takayuki Imaizumi, Jun Mizokami, Ryoji Koumura, and Tomohiko Abe. I am also grateful to other colleague students, Yoshitaka Ishii, Toshikazu Miyoshi, Kaoru Nomura, Mitsuru Ito, Yusuke Nishiyama, Koichi Hirao, Shinji Nakamura, Shinji Ichikawa, Takashi Mizuno, Toshiki Ito, Tomomi Yano, and Ryutaro Ohashi, for giving me helps, stimulations, and enjoyable laboratory lifetime.

The support from the members of Department of Physics were very helpful. Professor Tsutomu Yabuzaki, associate professor Yoshiro Takahashi, and professor Akira Masaike allowed us to use many expensive devices such a flashlamp dye laser, a TWT microwave am-

plifier, an electromagnet, microwave components, a digital oscilloscope, DC power supplies, and so on. Masataka Iinuma, who had been working on the production of a ^{1}H-polarized beam target, kindly helped me to start my subject, despite his busyness in moving to Hiroshima University. I also have had a lot of advice from him when I have come to a deadlock. Masahiro Oda, who had been trying to polarize deuterium (^{2}H) spins instead of ^{1}H spins, showed me a series of operations that they had been doing to polarize nuclear spins by means of dynamic nuclear polarization using photo-excited triplet electron spins.

From April in 1998 to March in 2000, I received financial support from Fellowships of the Japan Society for the Promotion of Science. I could use the research fund in purchasing electronic parts and computer softwares. The salary I received was very, very helpful; it made me possible to get married. I am very grateful to my wife Fusae Takeda for continuously encouraging me in doing my work since days long before our wedding, and to my father Shigemi Takeda and my mother Mineko Takeda for supporting me all the time.

I was surprised when I heard that my work on polarizing nuclear spins has been attracting interests of quantum information scientists. Professor Masahiro Kitagawa at Osaka University had invited me to join their research project on nuclear spin network quantum computing, and the CREST[1] program of the Japan Science and Technology Corporation has been providing financial support for me to work at Kitagawa's group, where I have been receiving clerical support by Madoka Konishi. I have just begun study on quantum computation, and have a lot to learn.

I would like to express my heartfelt thanks to them all.

— K. Takeda

March 2003

[1] Core Research for Evolutional Science and Technology

Contents

1 Introduction **1**

1.1 Nuclear spin polarization 1

1.2 NMR sensitivity enhancement by Dynamic Nuclear Polarization (DNP) 5

1.3 The purpose and the structure of this thesis 8

2 Basic Principles **11**

2.1 Electronic energy levels of pentacene. 11

2.2 Properties of the electron spin in the photo-excited triplet state 13

2.3 Hyperfine coupling of a triplet electron spin with ^{1}H spins 18

2.4 Cross polarization between the electron spins in the rotating frame and the ^{1}H spins in the laboratory frame 21

2.4.1 The concept of spin precession in the rotating frame of reference 21

2.4.2 Integrated cross polarization using adiabatic sweep 25

3 Experimental strategies and setup **31**

3.1 Strategies for maximizing the ^{1}H polarization 31

3.2 Experimental 34

3.2.1 Sample 34

3.2.2 Experimental setup 34

4 Results **47**

4.1 Optimization of the experimental parameters 47

4.2 Enhancement of ^{1}H polarization by ICP in pentacene-doped naphthalene 50

4.3 Polarization of dilute spins 53

4.3.1 Polarization of residual protons in a deuterated sample 53

4.3.2 Polarization transfer from triplet electron spins to ^{13}C spins via ^{1}H spins 59

5 Toward better understanding of DNP by photo-excited triplet electron spins **65**

5.1 A model for the buildup process 66

5.2 Intramolecular polarization transfer from a triplet electron spin to nuclear spins 71

5.2.1 Extraction of the flip-flop term that causes the polarization transfer . . . 71

5.2.2 Simulation of the polarization transfer by ICP 81

5.3 Evaluation of ^{1}H spin diffusion constants in naphthalene 87

5.4 Simulations of buildup curves 91

5.4.1 Simulations of the buildup behaviors 91

5.4.2 Buildup behavior in the rapid spin diffusion limit 93

6 Dynamic nuclear polarization by photo-excited triplet states in polycrystalline samples 97

6.1 Introduction 97

6.2 Calculation of ESR powder spectra 98

6.3 Result and discussion 102

7 Study of light penetration into single crystal and polycrystalline material doped with molecules photoexcitable to the triplet state via intersystem crossing 107

7.1 Theory 111

7.2 Experimental 116

7.3 Results and discussion 118

7.3.1 Single crystal samples of *p*-terphenyl doped with pentacene 118

7.3.2 Polycrystalline samples of *p*-terphenyl and naphthalene doped with pentacene 124

7.4 Summary of this chapter 128

8 Conclusion 131

9 Appendix **135**

9.1 Program list for the simulation of the intramolecular polarization transfer by ICP 135

9.2 Program list for the simulation of the ^{1}H polarization buildup 151

Chapter 1

Introduction

1.1 Nuclear spin polarization

■□■ Nuclear magnetic resonance ■□■

The subject matter of this work, dynamic nuclear polarization by photo-excited triplet electron spins, has a close connection to scientific researches using nuclear magnetic resonance (NMR) spectroscopy. NMR spectroscopy in bulk matter was firstly developed independently by F. Bloch and E.M. Purcell in 1946[1, 2, 3, 4]. Since then the macroscopic magnetic properties of assemblies of nuclear spins have extensively been studied. Amazingly, NMR spectroscopy had turned out to be a very, very powerful tool not only for nuclear physics, but also for condensed matter physics, organic chemistry, structual chemistry, biochemistry, material science, pharmacology, medical science, and quantum information science. Even at present, more than 50 years after its invention, researches on NMR are still making progresses, in which nuclear spins are utilized as probes for investigating chemical structures, molecular conformations, molecular dynamics, and so on.

NMR, as a branch of spectroscopy, has a unique feature that it deals with electromagnetic fields of frequencies ranging from a few kHz to a thousand MHz (radiofrequency (RF) region), being much lower than any other spectroscopic methods do. The low frequency affords NMR the following two advantageous features. First, in RF region, electromagnetic fields can be treated classically due to the tiny photon energy[5]; very weak power suffices to produce an astronomically large number of photons, so that the uncertainty Δn in the number of photons can be suppressed to be negligibly small while the uncertainty $\Delta\phi$ in the phase of the electromagnetic field being minimized, without violating the uncertainty principle $\Delta n \Delta\phi < h$. One therefore does not have to use a complicated quantum mechanical description of radiation. Second, nuclear spin interactions, such as chemical shielding and dipole-dipole interactions, are weak, ranging from a few Hz to tens of kHz. The weakness of these interactions allows one to artificially modify nuclear spin Hamiltonians simply by rotating a sample or by irradiating RF fields. A large number of techniques have been developed, and are being developed, to manipulate spin Hamiltonians to serve special needs such as the removal of an internal interaction for the spectral simplification and resolution enhancement or the selective recovery of an anisotropic interaction under magic-angle spinning to obtain structual information.

■□■ Nuclear spin polarization ■□■

On the other hand, NMR spectroscopy suffers from low sensitivity, which means that a large amount of nuclear spins are necessary for its resonance signal to be detected with an appreciable signal-to-noise ratio. Now let us look at what makes NMR so insensitive. Suppose that N nuclear spins $I = \frac{1}{2}$, say, proton (^{1}H) spins, are placed in a static magnetic field B_0. Each ^{1}H spin will be in one of the eigenstates $|+\frac{1}{2}\rangle$ and $|-\frac{1}{2}\rangle$. The NMR signal intensity is proportional to the total macroscopic magnetization M, which is given by

$$M = N_-\mu - N_+\mu, \tag{1.1}$$

$$\mu = \frac{1}{2}\gamma_{\mathrm{H}}\hbar, \tag{1.2}$$

where γ_{H} is the gyromagnetic ratio of ^{1}H, and N_- and N_+ are the populations on the eigenstates

$|-\frac{1}{2}\rangle$ and $|+\frac{1}{2}\rangle$, respectively (thus, the total number N of ^{1}H spins are given by $N = N_- + N_+$). We rewrite Eq.(1.1) as

$$\begin{aligned} M &= \mu N \frac{N_- - N_+}{N_- + N_+} = N\mu P, \\ P &\equiv \frac{N_- - N_+}{N_- + N_+}. \end{aligned} \tag{1.3}$$

Accordingly, the total magnetization M, and therefore the NMR signal intensity, is proportional to both the number N of the spins in the system and the quantity P called the *spin polarization*, which is a measure of how much the population distribution is one-sided. By its definition, P ranges from -1 (the case in which all the spins are in the $|+\frac{1}{2}\rangle$ state) to 1 (all the spins in the $|-\frac{1}{2}\rangle$ state).

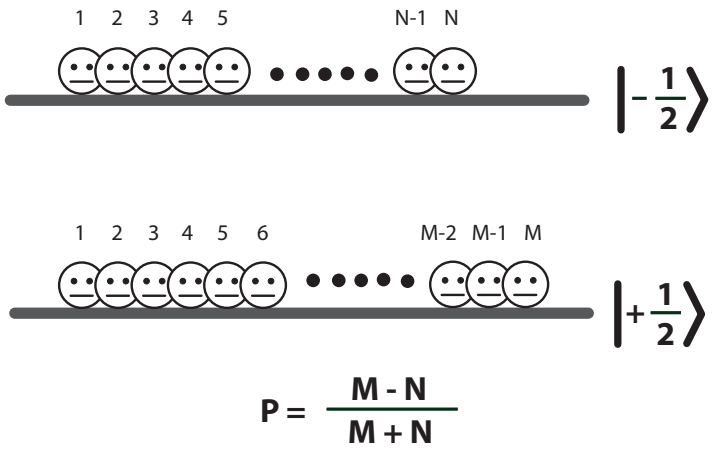

Figure 1.1: Definition of spin polarization.

When the spin system is in thermal equilibrium with the lattice, N_- and N_+ can be calculated from Boltzmann's law:

$$N_\mp \propto \exp\left[\pm\frac{\gamma_{\rm H}\hbar B_0}{2kT}\right]. \tag{1.4}$$

where k is the Boltzmann constant and T is a temperature. Then, the thermal equilibrium

polarization $P_{\rm th}$ is obtained from Eq. (1.3-1.4) as

$$\begin{aligned} P_{\rm th} &= \frac{\exp(\gamma_{\rm H}\hbar B_0/2kT) - \exp(-\gamma_{\rm H}\hbar B_0/2kT)}{\exp(\gamma_{\rm H}\hbar B_0/2kT) + \exp(-\gamma_{\rm H}\hbar B_0/2kT)} \\ &= \tanh\left[\frac{\gamma_{\rm H}\hbar B_0}{2kT}\right]. \end{aligned} \tag{1.5}$$

For ^{1}H spins ($\gamma_{\rm H} \sim 2\pi \cdot 4.26 \times 10^7$ rad·s^{-1}·T^{-1}), $P_{\rm th}$ is given by

$$P_{\rm th} \sim \tanh(1.0225 \times 10^{-3} B_0/T), \tag{1.6}$$

where the magnetic field B_0 and the temperature T should be given in Tesla and Kelvin, respectively. In Fig. 1.2, the ^{1}H thermal polarizations are plotted as a function of the magnetic field for $T = 77$ and 300 K. In magnetic fields conventionally used nowadays ($1 \sim 20$ T), and

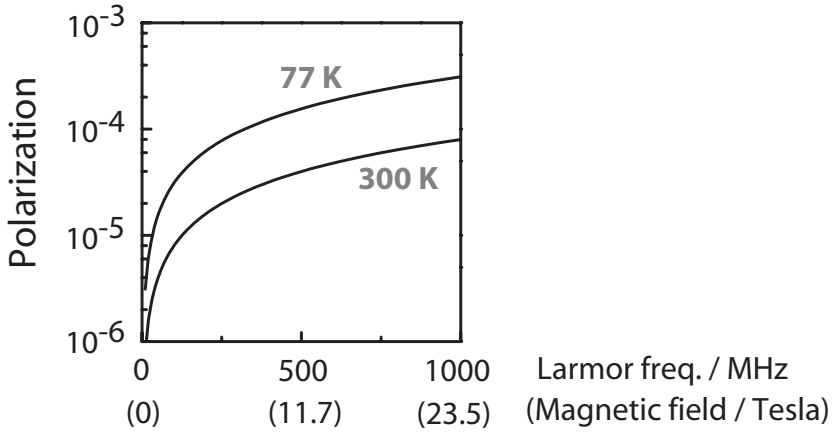

Figure 1.2: ^{1}H spin polarization in thermal equilibrium as a function of magnetic field strength.

at temperatures ranging from liquid helium to room temperatures, $P_{\rm th}$ is always much less than 1, so that one can approximate Eq. (1.6) by

$$P \sim 1.0225 \times 10^{-3} B_0/T. \tag{1.7}$$

Thus, under the conventional conditions, nuclear spin polarization is on the order of $10^{-6} \sim 10^{-5}$, which means that signals coming from 99.999% of the total spins cancel each other (Fig. 1.3). This is one of the major reasons why a large number ($10^{19} \sim 10^{20}$) of nuclear spins must be present in order to detect the NMR signal with an appreciable signal-to-noise ratio.

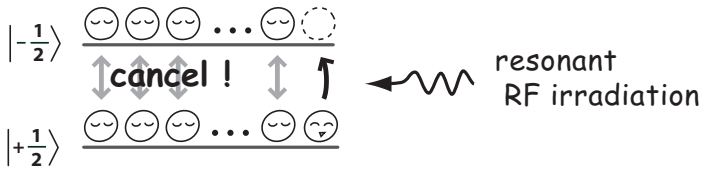

Figure 1.3: Low sensitivity in NMR arises from a tiny population difference on the Zeeman sublevels.

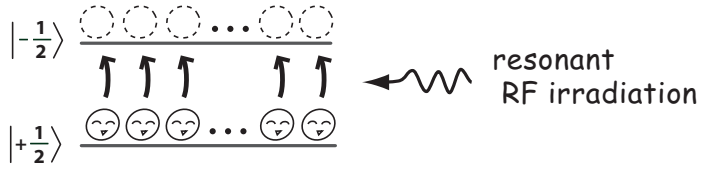

Figure 1.4: If nuclear spin polarization could significantly be enhanced, the NMR sensitivity would dramatically be improved...

1.2 NMR sensitivity enhancement by Dynamic Nuclear Polarization (DNP)

■□■ DNP by permanent paramagnetic electrons ■□■

In a paper published in 1953, A.W. Overhauser pointed out that nuclear spin polarization in metals should be enhanced if the electron spin resonance of the conduction electron is saturated by applying microwave irradiation[6]. This effect, called the Overhauser effect, was experimentally confirmed by T.R. Carver and C.P. Slichter[7, 8]. This was the first example of *dynamic nuclear polarization* (DNP)[5], known as a phenomenon or technique in which nuclear spin polarization is increased by polarization transfer from electron spins. DNP by the Overhauser effect was then shown to be expected in nonmetallic paramagnetic substances as well[9], and its theoretical basis was well established by I. Solomon[10]. The Overhauser effect can take place between a pair of spins, regardless of whether they are electron or nuclear spins, if the fluctuation of the local field produced by one spin causes the relaxation of the other spin, or vice versa. Thus, it can occur between spins whose relative position varies with time, for instance,

those in liquids, metals[7, 8], or conducting polymers[11]. On the other hand, the Overhauser effect cannot be expected to occur in rigid solid material, because the spins are fixed in space. However, it turned out that polarization transfer between electron and nuclear spins is possible even in rigid solids, by other mechanisms such as the solid effect[12, 13, 14], thermal mixing effect[15], and cross polarization[16, 17].

The limit to the attainable nuclear polarization by DNP is set by the polarization of electron spin being used. In thermal equilibrium, a permanent paramagnetic electron has spin polarization given by a formula similar to Eq. (1.5) but γ_H is replaced by electron's gyromagnetic ratio γ_e, which is about 660 times as large as that of ^{1}H . It follows that the enhancement factor of ^{1}H polarization cannot exceed $\gamma_e/\gamma_{\mathrm{H}} \sim 660$ as long as permanent paramagnetic electrons are used.

■□■ DNP by photo-excited triplet electrons ■□■

An electron spin in the photo-excited triplet state is another candidate for the source of electron polarization in DNP experiments. Fig. 1.5 shows simplified electronic energy levels of a molecule photo-excitable to the triplet state. Light-irradiation excites the electronic state of the molecule from the ground state S_0 to the excited singlet state S_1. The electronic state of a part of the excited molecules is transferred to the lowest triplet state T_1, where the spin-orbit coupling very selectively populates the triplet sublevels independent of temperature and magnetic field. Thus a high, non-equilibrium electron spin polarization is created simply by applying a laser pulse. If the electron spin-lattice relaxation of the photo-excited triplet state of pentacene is not so fast compared to the decay rate of the triplet state, the high electron spin polarization is retained during its lifetime. Therefore, we can perform DNP to transfer the large polarization to the ^{1}H spins even at high temperature. Moreover, the ^{1}H polarization can be accumulated by repeating this triplet DNP process, because the ^{1}H spins remain polarized after the decay of the triplet state. In NMR spectroscopy, the use of the photoexcited triplet electron spins instead of paramagnetic impurities has another advantage that the enhanced NMR signal

is not disturbed by the electron paramagnetism, since the triplet state decays to the diamagnetic ground state in a finite lifetime.

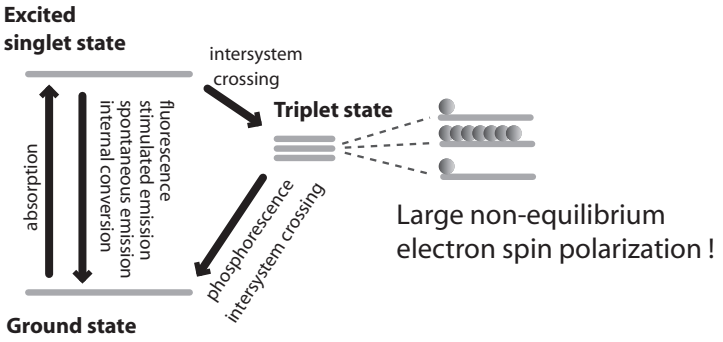

Figure 1.5: Energy levels of a molecule photoexcitable to the triplet state via intersystem crossing.

The first example of the polarization transfer from photo-excited triplet electron spins to nuclear spins was demonstrated in a single crystal sample of anthracene, in which UV irradiation in very low magnetic field (¡25 mT) enhanced ^{1}H polarization in anthracene[18]. Since then a number of studies were made on this kind of dynamic ^{1}H polarization in very low fields[19, 20, 21, 22, 23, 24], and it was found that the polarization transfer is induced in magnetic fields close to that at which level-anticrossing occur between the triplet sublevels[25, 26, 27]. (Also, in some exceptional cases, it was found that relaxation caused by the mobility of triplet excitons induces the dynamic ^{1}H polarization by the Overhauser effect[28, 29].)

The idea that photo-excited triplet electron spins can be utilized for DNP experiments, just as permanent paramagnetic electrons can, was first put forward by M. Deimling et al. in 1980[30]. At first, however, the enhancement factor of ^{1}H polarization was quite small (Fig. 1.6). The breakthrough was brought about by A. Henstra et al., who invented a very efficient DNP technique based on cross polarization and realized a 5,000-fold enhancement of ^{1}H polarization, which was the first successful demonstration of the enhancement of ^{1}H polarization beyond the limit of 660 when permanent paramagnetic electrons are used[31]. The essence of their technique is the simultaneous application of microwave irradiation and external field sweep, with which each electron spin packet in the ESR line, broadened by the hyperfine coupling with the

surrounding nuclear spins, is locked along the effective field in the rotating frame. With an appropriate choice of the intensity of the locking field, the Hartmann-Hahn condition is fulfilled between the electron spin in the rotating frame and the ^{1}H spins in the laboratory frame. This technique, originally called the Integrated Solid Effect (ISE)[31] and later the Integrated Cross Polarization (ICP)[32], has successfully been applied to polarize ^{1}H spins in a single crystal sample of pentacene-doped naphthalene by M. Iinuma et al., who realized ^{1}H polarization of 0.32 at 77 K in 0.3 T[33], being 8×10^4 times as large as the thermal ^{1}H polarization!

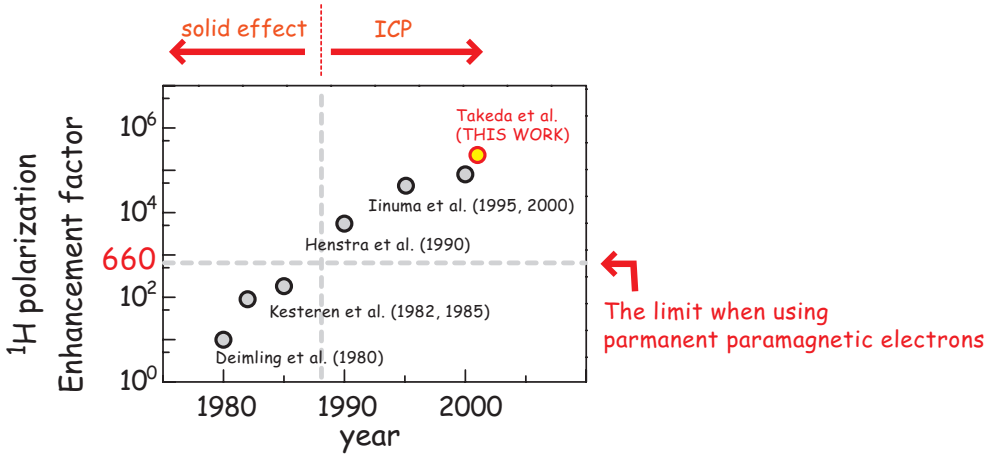

Figure 1.6: History of the DNP experiments using triplet electron spins[30, 34, 35, 31, 36, 33, 37, 38]. Each point represents the enhancement factor with respect to the corresponding thermal equilibrium ^{1}H polarization under study.

1.3 The purpose and the structure of this thesis

The triplet DNP technique has successfully been performed to obtain fantastically large ^{1}H polarization compared to the thermal equilibrium polarization. Nevertheless, there are some interesting questions still being left unanswered:

Q1: Can we further improve the buildup efficiency, and if we can, how much can we? In the experiments by Iinuma, ^{1}H polarization was exponentially built up to 0.32 with a time

constant of about 6 hours. Is it possible to obtain even larger nuclear spin polarization, and to realize such high polarization in even shorter experimental time?

Q2: Why is ^{1}H polarization built up in the way it is? What kind of elementary processes lie behind the buildup behavior, and how do they affect it?

Q3: Is it possible to apply the triplet DNP technique to various systems of interest? For instance, can we polarize nuclear spins other than protons, and can we polarize nuclear spins in non-crystal materials, such as powder or glass? And further, is it possible to enhance NMR signals in chemically or biologically interesting systems such as proteins?

The principal purpose of this work is to tackle these stimulating questions. In Chapter 2, I describe basic concepts and ideas that are necessary to understand the principle of DNP by photo-excited triplet electron spins, explaining the properties of photo-excited triplet electrons, the concept of spin precession in the rotating frame, and the principle of cross polarization. Then, in Chapter 3, the strategy is presented for maximizing the efficiency of the polarization transfer from the triplet electron spin to ^{1}H spins[37], and the sample, the experimental setup, and the experimental procedure are briefly introduced. The experimental results are shown in Chapter 4[37, 38], and are discussed in Chapter 5, where I propose a theoretical model to explain the results of the buildup experiments. In Chapter 6, the application of the buildup experiment to polycrystalline samples is demonstrated[32]. Chapter 7 deals with the problem of light penetration, where a theory is proposed to calculate the depth of light penetration in material photo-excitable to the triplet state for both single crystal and polycrystalline samples[39]. The theory is examined by measuring the signal amplitudes of zero-field ESR of photo-excited triplet electron spins for various sample thicknesses. And finally, in Chapter 8, I shall reply to the questions Q1-Q3 mentioned above, and make some comments on the possible future progress of this work.

Chapter 2

Basic Principles

In this chapter, I review concepts and theories that are necessary to understand the principles of polarization of nuclear spins by DNP using electron spins in the photoexcited triplet state. For concreteness, let us focus on a pentacene molecule ($C_{22}H_{14}$). It is convenient to assign numbers on 22 carbon atoms and 14 hydrogen atoms. The numbering shown in Fig. 2.1 follows the definition by D.J. Sloop et al.[40], who have published a number of reports on photoexcited triplet pentacene.

2.1 Electronic energy levels of pentacene.

Fig. 2.2 shows simplified electronic energy levels of pentacene. The electronic state of pentacene is excited from the ground state S_0 to the excited singlet state S_1 by irradiating light whose wavelength is shorter than 600 nm[41]. A part of the excited molecules is known to transfer first to the third triplet state T_3 by intersystem crossing (ISC), and then undergoes a rapid internal conversion (IC) to the lowest triplet state T_1[42, 43]. The probability for transferring to the triplet state, which is called the ISC quantum yield, depends on the host molecule.

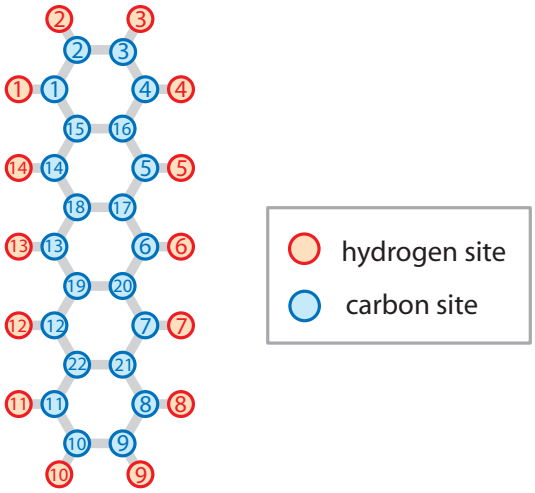

Figure 2.1: A pentacene molecule ($C_{22}H_{14}$).

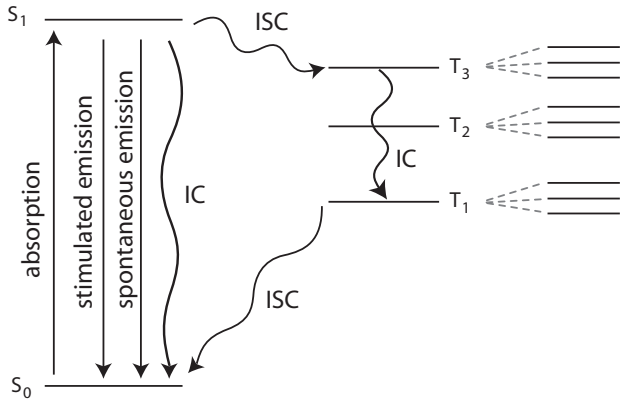

Figure 2.2: Electronic energy levels of pentacene. The straight and the wavy arrows indicate the radiative and the radiationless transitions, respectively.

For example, for a pentacene guest molecule doped in naphthalene, the ISC quantum yield was measured at 2 K to be ca. 0.03[44], while another study performed at 1.9 K reported it to be 0.003[45]. On the other hand, when pentacene is doped in *p*-terphenyl host, the ISC quantum yield varies from 0.004 to 0.64, depending on four different substitution sites in the host crystal lattice[44, 46, 47, 48]. There had been two models to account for this large difference in the ISC quantum yields for pentacene doped in *p*-terphenyl. The first model assumes that the triplet energy levels for two of four substitution sites lie below the singlet energy level, while that for the other two sites lie above the single energy level[49]. Thus, the former sites are much more likely to undergo ISC than the latter. In the second model, pentacene molecules embedded in the four possible substitution sites are twisted in different ways, and the extent of deviation from planary shape affects the perturbation that causes ISC[50]. The problem of which is the correct picture was worked out by the study by Köhler et al. on optically-detected electron spin resonance, which supported the first idea of the accidental allocation of the energy levels[48].

In all cases, the ISC quantum yield is less than 1, so one may worry that only a part of pentacene molecules in a sample can transfer to the T_1 state, which is prerequisite for triplet DNP experiments. However, as I will show in Chapter 7 (p. 107∼), one can really pump all the pentacene molecules up to the T_1 state with a laser whose pulse width and beam intensity are appropriately chosen, by taking advantage of the fact that the lifetime of the S_1 is much shorter than that of T_1.

2.2 Properties of the electron spin in the photo-excited triplet state

■□■ Zero-field splitting (ZFS) ■□■

Now consider a pentacene molecule in the T_1 state, which is composed of three Zeeman

substates. Even in the absence of an external magnetic field, the degeneracy of energy levels is removed due to an interaction called the zero-field splitting (ZFS) interaction arising from the dipole-dipole interaction between the two electron spins in the triplet state[51, 52]. The

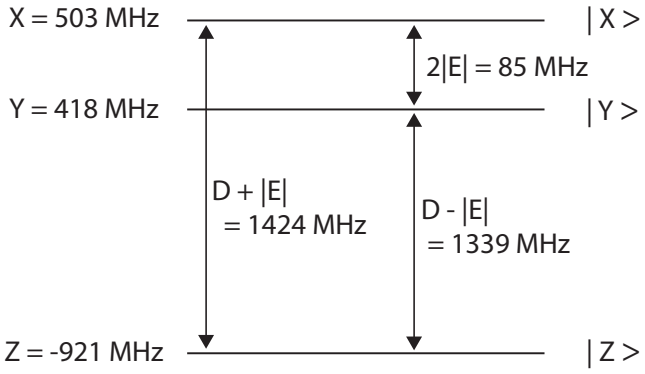

Figure 2.3: Three energy sublevels for the triplet state of pentacene in zero external field.

Hamiltonian $\mathscr{H}_{\rm ZFS}$ representing the ZFS interaction is written using a spin operator $\mathbf{S}(S=1)$ as

$$\begin{aligned}\mathscr{H}_{\rm ZFS} &= D\left[S_Z^2-\frac{1}{3}S(S+1)\right]+E(S_X^2-S_Y^2)\\ &= D\left(S_Z^2-\frac{2}{3}\right)+E(S_X^2-S_Y^2),\end{aligned} \tag{2.1}$$

where D and E are so-called ZFS parameters. In zero field, the ZFS Hamiltonian $\mathscr{H}_{\rm ZFS}$ is diagonalized in a basis set $\{|X\rangle,|Y\rangle,|Z\rangle\}$ defined by

$$|X\rangle = \frac{1}{\sqrt{2}}(|-1\rangle-|1\rangle)$$

$$|Y\rangle = \frac{i}{\sqrt{2}}(|-1\rangle+|1\rangle) \tag{2.2}$$

$$|Z\rangle = |0\rangle, \tag{2.3}$$

where $\{|1\rangle,|0\rangle,|-1\rangle\}$ denote the eigenstates of S_Z. The energy eigenvalues $\{X,Y,Z\}$ are related to the ZFS parameters D and E through

$$D = \frac{1}{2}(X+Y)-Z \tag{2.4}$$

$$E = -\frac{1}{2}(X-Y). \tag{2.5}$$

From ESR studies, the eigenvalues have been determined to be (X,Y,Z) =($2\pi\cdot$503 MHz·rad, $2\pi\cdot$418 MHz·rad, $-2\pi\cdot$921 MHz·rad)[53]. It follows from Eqs. (2.4-2.5) that (D,E) =($2\pi\cdot$1381.5 MHz·rad, $-2\pi\cdot$42.5 MHz·rad).

In the course of the transition to the T_1 state by ISC, the spin-orbit coupling very selectively populates the triplet sublevels. For pentacene, the populations on the triplet substates $|X\rangle, |Y\rangle, |Z\rangle$ are 0.76, 0.16, 0.08, respectively[40, 54]. As a consequence, the electron spin polarization of the photoexcited triplet pentacene becomes much larger than the thermal equilibrium polarization.

■□■ Energy levels in the presence of an external field ■□■

When an external magnetic field is applied to the spin, the energy splittings between the triplet sublevels are lifted up by Zeeman interaction $\mathscr{H}_Z$, which is represented as

$$\mathscr{H}_Z = g\beta B_0 S_Z = \omega_S S_Z. \tag{2.6}$$

Here β ($\sim 2\pi\cdot$14 GHz·rad/T) is the Bohr magneton, and g (~ 2)[53] is a g-factor. Now we have to consider both contributions from the Hamiltonians $\mathscr{H}_Z$ and $\mathscr{H}_{ZFS}$. The eigenvalues ω_{+1}, ω_0, and ω_{-1} will then depend on the orientation of the magnetic field with respect to the ZFS tensor, each of whose principal axis aligns along one of the symmetry axes (X,Y, and Z axes) of the pentacene molecule as shown in Fig. 2.4. Also shown in Fig. 2.4 is the external field tilted by Θ and Φ with respect to the ZFS principal axes. In the special cases that the magnetic field aligns along one of these principal axes, one can obtain the energy eigenvalues analytically[55]:

1. $\Theta = 90^\circ, \Phi = 0$ ($B_0 \parallel X$)

   This corresponds to the case in which the field aligns along the long molecular axis (X-

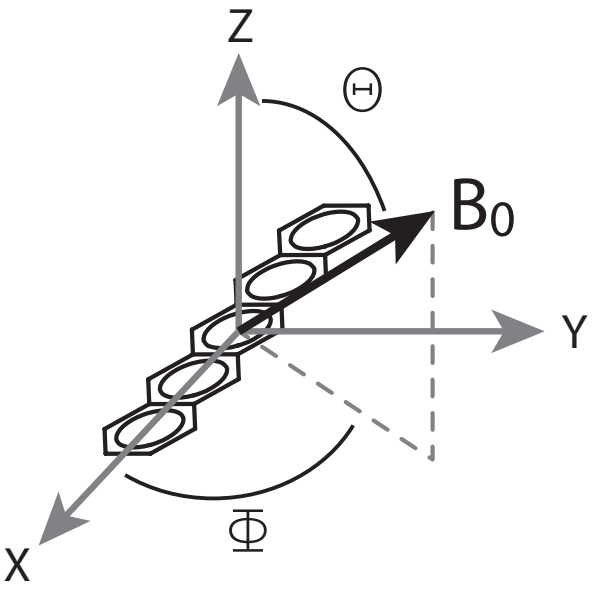

Figure 2.4: Principal axes of the zero-field splitting (ZFS) tensor of the photoexcited triplet state of pentacene.

axis) of pentacene.

$$\begin{aligned} \omega_{+1} &= \frac{Y+Z}{2} + \sqrt{\frac{1}{4}(Y-Z)^2 + \omega_S^2}, \\ \omega_0 &= X, \qquad (2.7) \\ \omega_{-1} &= \frac{Y+Z}{2} - \sqrt{\frac{1}{4}(Y-Z)^2 + \omega_S^2}. \end{aligned}$$

(2.8)

2. $\Theta = 90^\circ, \Phi = 90^\circ$ ($B_0 \parallel Y$)

$$\begin{aligned} \omega_{+1} &= \frac{X+Z}{2} + \sqrt{\frac{1}{4}(X-Z)^2 + \omega_S^2}, \\ \omega_0 &= Y, \qquad (2.9) \\ \omega_{-1} &= \frac{X+Z}{2} - \sqrt{\frac{1}{4}(X-Z)^2 + \omega_S^2}. \end{aligned}$$

(2.10)

3. $\Theta = 0$ ($B_0 \parallel Z$)

$$\begin{aligned} \omega_{+1} &= \frac{X+Y}{2} + \sqrt{\frac{1}{4}(X-Y)^2 + \omega_S^2}, \\ \omega_0 &= Z, \\ \omega_{-1} &= \frac{X+Y}{2} - \sqrt{\frac{1}{4}(X-Y)^2 + \omega_S^2}. \end{aligned} \tag{2.11}$$

The energy levels for these three special cases are plotted as a function of external field in Fig. 2.5

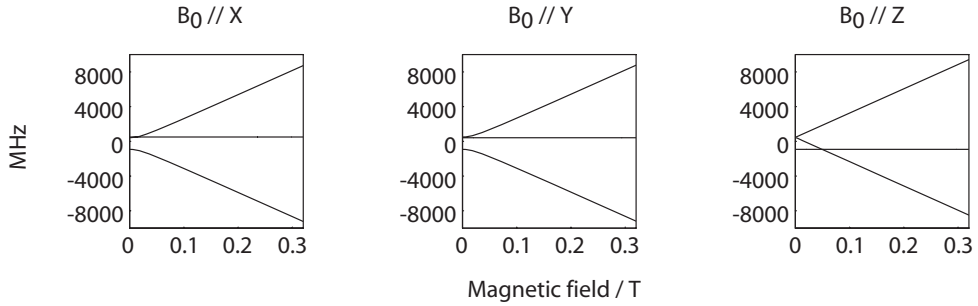

Figure 2.5: The triplet energy levels of pentacene, when one of the ZFS principal axes is parallel to the external field.

■□■ High-field approximation ■□■

In general, the energy eigenvalues cannot be obtained analytically, and have to be obtained numerically by diagonalizing the Hamiltonian matrix, which will be shown in Chapter 6 (page 99). However, in high magnetic fields where the magnitude of the Zeeman interaction is much larger than that of the ZFS interaction, those terms that do not commute with $\mathscr{H}_Z$ do not contribute to the energy levels in first order and can be dropped. In the high-field approximation, the expressions for $\omega_{+1,0,-1}$ are given by

$$\begin{aligned} \omega_{+1} &= \omega_S + \frac{1}{3}\omega_{ZFS}(\Theta,\Phi), \\ \omega_0 &= -\frac{2}{3}\omega_{ZFS}(\Theta,\Phi), \\ \omega_{-1} &= -\omega_S + \frac{1}{3}\omega_{ZFS}(\Theta,\Phi), \end{aligned} \tag{2.12}$$

where

$$\omega_{\mathrm{ZFS}} = \frac{1}{2}D(1-3\cos^2\Theta) + \frac{3}{2}E\sin^2\Theta\cos 2\Phi. \tag{2.13}$$

2.3 Hyperfine coupling of a triplet electron spin with ^{1}H spins

A coupling of an electron spin with a nuclear spin is called a hyperfine coupling, because it makes the electron resonance line to split slightly. For the nuclear spin, however, the effect of this interaction is not small at all; the "hyperfine" interaction can be so large that it can outweigh the effect of other nuclear spin interactions such as chemical shielding, J coupling, dipole-dipole coupling, and so on. There are two kinds of hyperfine couplings, namely, an isotropic hyperfine coupling and an anisotropic hyperfine coupling. The former interaction, sometimes called the contact interaction, arises from a finite (non-zero) probability density of an electron wave function at the position of a nucleus, whereas the latter is a dipole-dipole interaction between the electron and nuclear spins.

■□■ Spin densities ■□■

Since one cannot specify a single, definite position of an electron spin in a molecule, it may seem formidable to represent the Hamiltonian for the isotropic as well as the anisotropic hyperfine couplings. Fortunately, H.M. McConnell succeeded in describing the hyperfine couplings by introducing the concept of spin density[56, 57, 58]. McConnell's theory states that a single electron spin appears to break up into segments, each of which being distributed over the molecule and having its own "spin density". For aromatic hydrocarbons, including pentacene, each fractional spin is thought to be located at either carbon atomic site with a spin density given by the π electron density at the carbon atom. Thus, the spin densities can be obtained from MO calculations[59, 60]. Fig. 2.6 shows the spin densities for the triplet state of pentacene calculated by T.-S.T. Lin et al.[61].

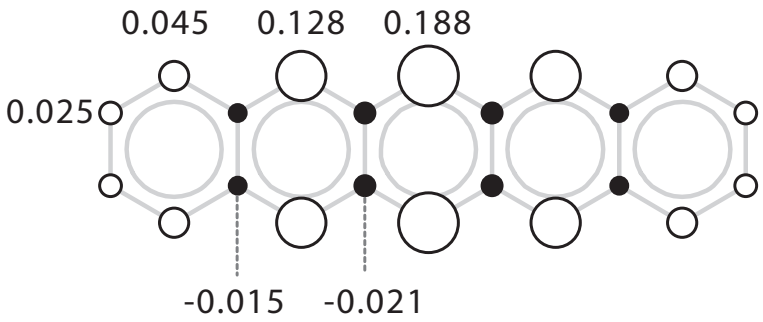

Figure 2.6: Spin densities of the pentacene triplet calculated by T.-S.T. Lin et al. (page 194 in Ref. [61]). The area of each circle is described to be proportional to the spin density. The open and filled circles represent positive and negative spin densities, respectively.

■□■ Isotropic hyperfine coupling ■□■

McConnell's theory also states that, for aromatic hydrocarbons, an isotropic hyperfine coupling acts between a fractional electron spin and a ^{1}H spin, only if they are adjacent to each other. For instance, the electron spin segment at the kth carbon site on a pentacene molecule has the isotropic hyperfine coupling only with the kth ^{1}H spin. The isotropic hyperfine coupling between an electron spin S and a ^{1}H spin I has the Hamiltonian of the form

$$\mathscr{H}_{\mathrm{HF}}^{\mathrm{iso}} = \sum_k Q_k I_Z^k S_Z^k \tag{2.14}$$

$$Q_k = \rho_k \gamma_S B_{\mathrm{C}}. \tag{2.15}$$

Here, ρ_k is the spin density at the kth carbon site, and the value for B_{C} has been empirically obtained to be ca. -2.3 mT[57, 58].

■□■ Anisotropic hyperfine coupling ■□■

On the other hand, the anisotropic hyperfine interactions, or the dipolar interactions, act on every pair of spins. Also, the coupling of a fractional electron spin with the surrounding

nuclei is proportional to its spin density, and is represented as

$$\mathscr{H}_{\mathrm{HF}}^{\mathrm{aniso}} = \sum_{j,k} d_{jk} \left[\mathbf{I}^j \cdot \mathbf{S}^k - 3 \frac{(\mathbf{I}^j \cdot \mathbf{r}_{jk})(\mathbf{S}^k \cdot \mathbf{r}_{jk})}{r_{jk}^2} \right], \tag{2.16}$$

$$d_{jk} = \left(\frac{\mu_0}{4\pi} \right) \frac{\gamma_I \gamma_S \hbar}{r_{jk}^3}, \tag{2.17}$$

where $\mathbf{r}_{jk}$ is a vector connecting the jth hydrogen and the kth carbon atomic sites. The above formulas for the hyperfine couplings will be used later (page 71∼) to evaluate the efficiency of polarization transfer from the triplet electrons to protons.

■□■ Inhomogeneous broadening ■□■

The effect of an isotropic hyperfine interaction between a pair of electron and nuclear spins is to lift the energy levels of both spins. As a consequence, the resonance frequencies shift from those they would take had the interaction not been present. The frequency shift of one spin can be both positive and negative, depending on the state of the other spin. Thus, when one measures the resonance signal coming from a large numbers of molecules contained in the sample, its apparent spectrum would be a pair of peaks, whose splitting is twice the shift. The anisotropic hyperfine interaction, in part, has the same effect as the isotropic hyperfine interaction, giving spectrum a peak splitting that depends on both the distance between the spins and the orientation of the vector connecting them. Then, the effect of the sum of the isotropic and the anisotropic hyperfine couplings would be to produce four resonance lines; each doublet due to the isotropic hyperfine coupling splits again into doublet due to the anisotropic hyperfine coupling. In actual situations, each of these spin pairs is not isolated from the other many spins nearby, which bring additional hyperfine interactions, making each multiplet resonance lines to split further. Consequently, the apparent spectrum becomes a single, broadened resonance line made up of many, many peaks having different resonance frequencies (Fig. 2.7). This is an example of what is called the “inhomogeneously broadened” resonance line, which is composed of a large number of peaks, or *spin packets*, as they are called.

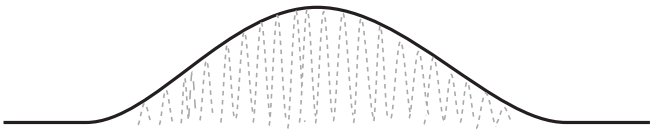

Figure 2.7: An example of a inhomogeneously broadened resonance line (solid line), consisting of a large number of "spin packets" (broken lines).

2.4 Cross polarization between the electron spins in the rotating frame and the ^{1}H spins in the laboratory frame

In order to understand the principle of the polarization transfer by the ICP technique, it is necessary first to explain cross polarization, and in turn, in order to understand cross polarization, you have to be familiar with the concept of spin precession in the rotating frame of reference.

2.4.1 The concept of spin precession in the rotating frame of reference

■□■ Spin precession in the laboratory frame ■□■

A spin placed in a static magnetic field $\mathbf{B_0} = (0, 0, B_0)$ precesses around $\mathbf{B_0}$ with an angular frequency $\omega_0 = \gamma B_0$ called the Larmor frequency, where γ is the gyromagnetic ratio of the spin (Fig. 2.8(a)). If an additional small field $\mathbf{B_1} = (B_1 \cos \omega t, B_1 \sin \omega t, 0)$ is applied perpendicular to $\mathbf{B_0}$ and rotating around $\mathbf{B_0}$ (Fig. 2.8(b)), then a transition occurs to the spin system, provided that the frequency ω of the rotating field is close to the precession frequency ω_0. This is what we observe in the laboratory frame of reference.

■□■ Spin precession in the rotating frame ■□■

Now let us look at how the motions of the spin look in a reference frame rotating around $\mathbf{B_0}$ with the angular frequency ω of the transverse field $\mathbf{B_1}$. Obviously, $\mathbf{B_1}$ looks stationary in

this reference frame. On the other hand, the field felt by the spin along $\mathbf{B_0}$ is apparently reduced when viewed in the rotating frame. Suppose for a moment that the frequency ω of the transverse field exactly coincides with the Larmor frequency ω_0. Then, the field along $\mathbf{B_0}$ completely vanishes (Fig. 2.8(c)), and the only field that remains to be felt by the spin is the transverse field $\mathbf{B_1}$ apparently being static. Thus, in the rotating frame, the spin will precess around an

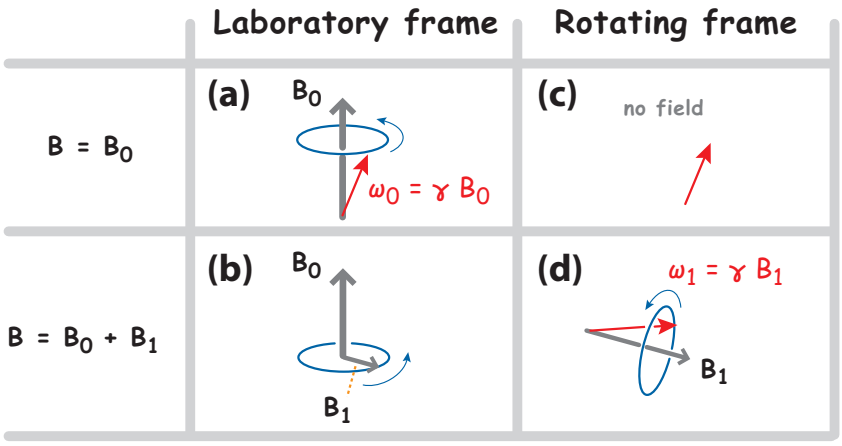

Figure 2.8: Magnetic fields felt by a spin in the laboratory and the rotaing frames of reference. A static magnetic field $\mathbf{B_0}$ applied in the laboratory frame, shown in (a), disappears in a reference frame rotaing around $\mathbf{B_0}$ with an angular frequency $\omega_0 = \gamma B_0$, so the apparent motion of the spin should be stationary in the rotating frame ((c)). (b) When an additional field $\mathbf{B_1} = (B_1 \cos \omega t, B_1 \sin \omega t, 0)$ is applied perpendicular to $\mathbf{B_0}$ and rotating around $\mathbf{B_0}$, it causes a transition in the spin system. (d) The effect of application of $\mathbf{B_1}$, when viewed in the rotating frame, is to rotate the spin around $\mathbf{B_1}$ which looks to be stationary.

axis perpendicular to the Z-axis at an angular frequency $\omega_1 = \gamma B_1$, which is proportional to the amplitude of the applied transverse field (Fig. 2.8(d)).

On the other hand, if the frequency ω of the transverse field is not the same as the frequency ω_0 of the spin precession, but differs slightly by $\Delta\omega = \omega_0 - \omega$, then a small field $\Delta\mathbf{B} = \Delta\omega/\gamma$ survives along the Z-axis in the rotating frame. Now the spin precesses around the vector sum $\Delta\mathbf{B} + \mathbf{B_1}$ called the effective field, which is tilted by an angle $\alpha = \tan^{-1}(B_1/\Delta B)$ with respect to the Z-axis, with an effective precession frequency ω_{eff} given by

$$\omega_{\text{eff}} = \sqrt{\Delta\omega^2 + \omega_1^2}. \tag{2.18}$$

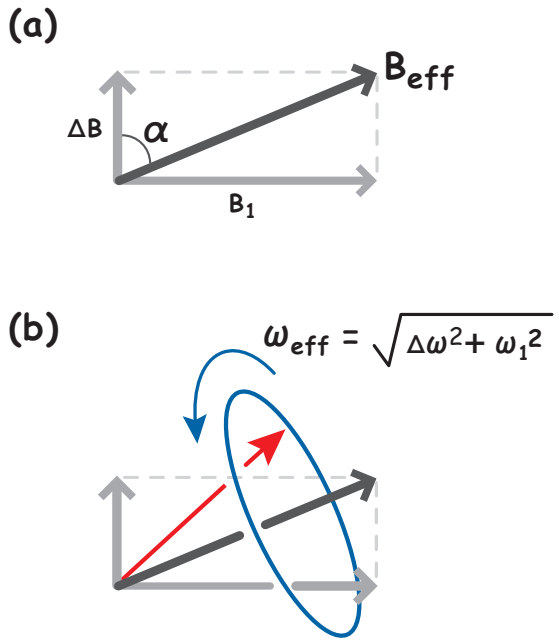

Figure 2.9: In the presence of a resonance offset ΔB, the effective precession of a spin in the rotating frame is around an axis tilted by $\alpha = \tan^{-1}(B_1/\Delta B)$ with respect to $\mathbf{B_0}$, and its precession frequency ω_{eff} is given by $\gamma\sqrt{\Delta B^2 + B_1^2}$.

■□■ Hartmann-Hahn matching and cross polarization ■□■

One noticeable feature of the spin precession in the rotating frame is that its effective precession frequency ω_{eff} is *artificially adjustable*, by choosing either ΔB or B_1, and a remarkable effect can take place when the effective precession of a spin synchronizes with the precession of another spin of different species. What happens to a pair of unlike spins, if one gradually varies one of their precession frequencies, is a bit like oscillations observed in a coupled pendulum when one changes the length of one of the strings, just as described in Fig. 2.10. When the lengths of strings differs so much that the characteristic frequency of one pendulum considerably deviates from that of the other pendulum, their oscillations will not affect each other (Fig. 2.10(a)). On the other hand, if one adjust the length of the strings so that their charac-

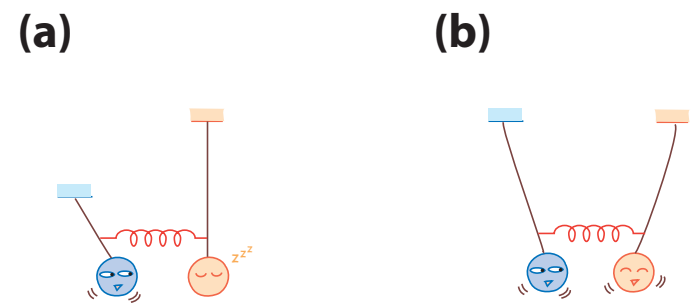

Figure 2.10: One can see an analogy between a coupled pair of spins and a coupled pendulum, if one corresponds the spin states $|\frac{1}{2}\rangle$ and $|-\frac{1}{2}\rangle$ to the pendulum's states of maximum and the minimum oscillation amplitudes.

teristic frequencies coincides, the pendulums will resonate with each other, exchanging kinetic energy again and again through the spring that connects the pendulums (Fig. 2.10(b)). Similarly, if the precession frequency of, say, an electron spin is adjusted in the rotating frame to that of a ^{1}H spin in the rotating frame, they can exchange their spins states with each other. In this case, what corresponds to the spring in the case of the coupled pendulum is the "flip-flop" term of the dipolar interaction, which include a term of the form $(I_+S_- + I_-S_+)$.

The ingenious idea of matching the precession frequencies in the rotating frame was first put forward by S.R. Hartmann and E.L. Hahn[62], and their idea was so innovative that Slichter says in his famous textbook on NMR, in a phrase with a literary flavor, that[63]

> *... if by magic one could apply one magnetic field at the I spins, a second magnetic field at the S spins. How can one do this to spins which are neighbors on the atomic scale? The magical solution was found by the Wizard of Resonance, Erwin Hahn and demonstrated by the Wizard and his Sorcerer's Apprentice Sven Hartmann.*

The condition for the synchronization of the precession frequencies is called the Hartmann-Hahn condition. The fact that different spin species can exchange their spin states implys that one can exchange the population distribution of one species with that of the other species. That is, one can transfer spin polarization from one spin to another spin, provided that the spin sys-

tem are made to fulfill the Hartmann-Hahn condition. The polarization transfer of this type is called cross polarization[64], and is widely utilized in modern solid state NMR experiments to enhance the sensitivity of dilute nuclei such as ^{13}C and ^{15}N, where polarization is transferred from abundant and relatively polarized ^{1}H spins[65, 64, 63]. We can expect a similar effect between an electron spin and a ^{1}H spin; when one adjusts the effective precession frequency of an electron spin in the rotating frame to the precession frequency of protons, a significant enhancement of ^{1}H polarization is expected by cross polarization. Specifically, the triplet electron spin having very large polarization is promising for dramatic improvement of NMR sensitivity.

2.4.2 Integrated cross polarization using adiabatic sweep

If an X-band ($\sim$9 GHz) microwave source is used for the electron spin resonance, the static magnetic field has to be set around 0.3 T, in which ^{1}H spins resonate at $\sim$13 MHz. Then, in order to satisfy the Hartmann-Hahn condition between the electron spin in the rotating frame and the ^{1}H spin in the laboratory frame, the required intensity ω_1 of the microwave irradiation is on the order of 10 MHz. Since this is considerably smaller than the resonance linewidth broadened by hyperfine couplings (several tens of MHz), the effective field felt by one spin packet becomes very different from that felt by other spin packets (Fig. 2.11). Thus, it is impossible to satisfy the Hartmann-Hahn condition for all spin packets simultaneously. However, all of these spin packets can be made to successively participate cross polarization by an elegant technique proposed by A. Henstra et al.[31].

■□■ Successive Hartmann-Hahn matching by adiabatic sweep ■□■

In their method, the external field is swept over the electron resonance during which microwave is continuously applied. The field may be swept from lower to upper values (upfield sweep) or vice versa (downfield sweep). Suppose, for instance, the case of the upfield sweep. The effective field is initially far below the resonance condition for every spin packet (Fig. 2.12(a)), so that the effective field is only slightly tilted from the $-Z$ direction (Fig. 2.12(d)). As the field increases gradually, the effective field gets up, and when the field

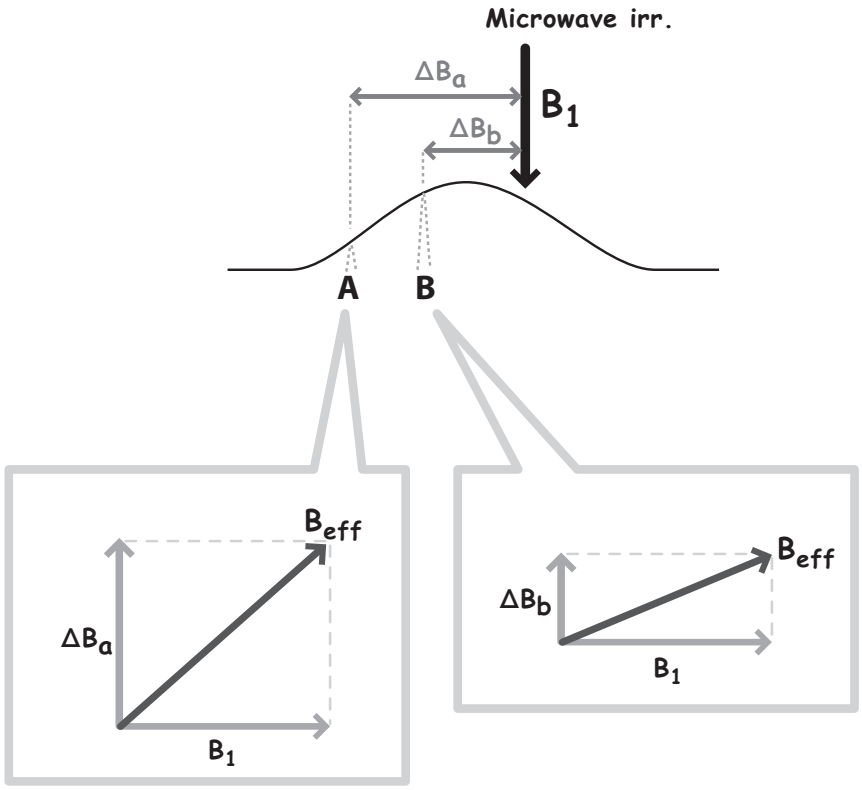

Figure 2.11: When the resonance line is inhomogeneously broadened (what is meant by the word "inhomogeneous" has been explained in page 21), the effective field felt by one spin packet (spin packet **A**, for instance) differs from that felt by another spin packet (spin packet **B**). Hence, the Hartmann-Hahn condition cannot be fulfilled simultaneously for all spin packets.

becomes on-resonance (Fig. 2.12(b)), its vertical component vanishes (Fig. 2.12(d)). Eventually the sweeping field becomes far above the resonance (Fig. 2.12(c)) and the effective field points in a direction close to the $+Z$ axis (Fig. 2.12(f)).

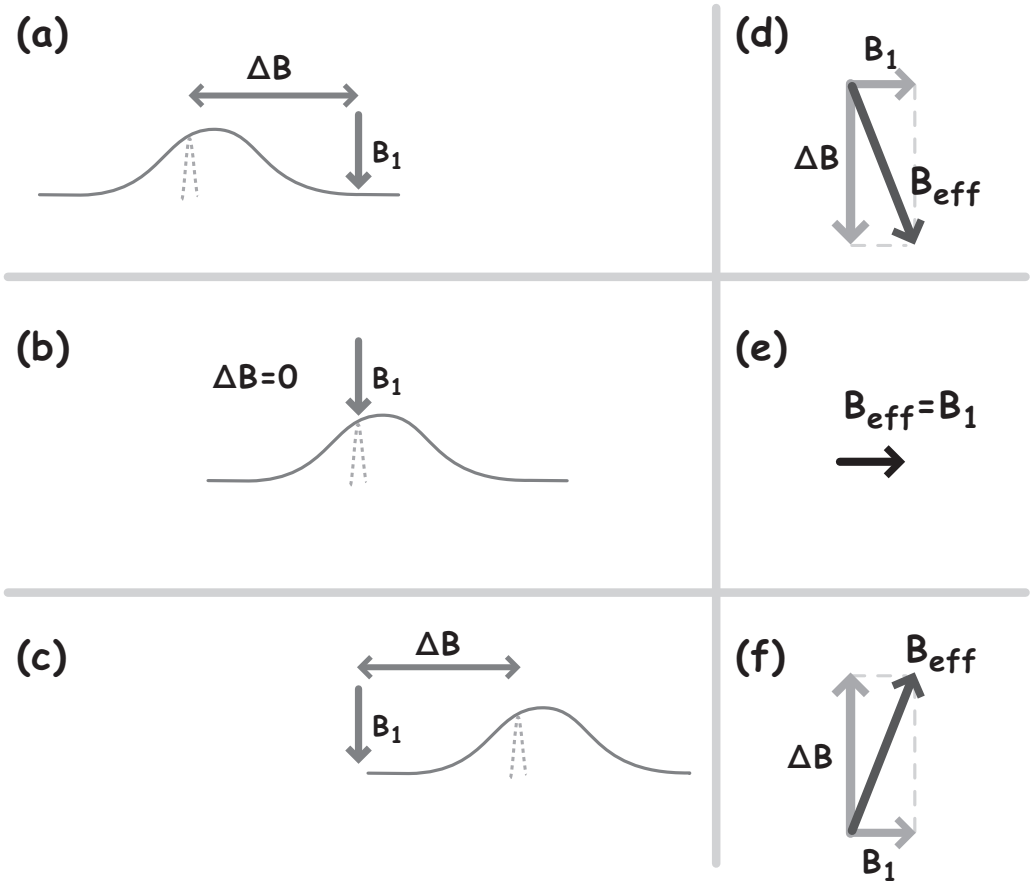

Figure 2.12: When the field is swept from lower to upper values (upfield sweep), the effective field is initially far below the resonance condition for every spin packet ((a)), so that the effective field is only slightly tilted from the $-Z$ direction ((d)). As the field increases gradually, the effective field gets up, and when the field becomes on-resonance ((b)), its vertical component vanishes ((d)). Eventually the sweeping field becomes far above the resonance ((c)) and the effective field points in a direction close to the $+Z$ axis ((f)).

In the course of the sweep, the effective field felt by each spin packet follows a path depicted in a solid line in Fig. 2.13, and the effective precession frequency changes with time as shown in Fig. 2.14. Therefore, every spin packet is ensured to experience the Hartmann-Hahn matching twice during the sweep, provided that ω_1 is chosen below the ^{1}H Larmor frequency.

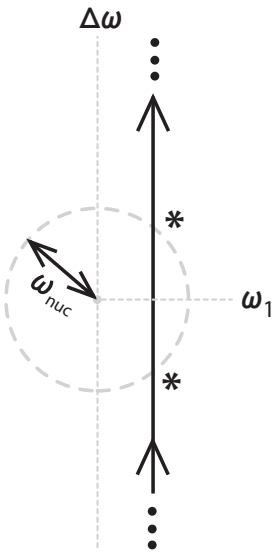

Figure 2.13: A trajectory (a solid line) of the effective field felt by each spin packet, when the external field is swept far-below the resonance to far-above resonance. The Hartmann-Hahn condition is fulfilled when the trajectory of the effective field crosses the circle of a radius equal to the ^{1}H Larmor precession frequency, as marked by asterisks

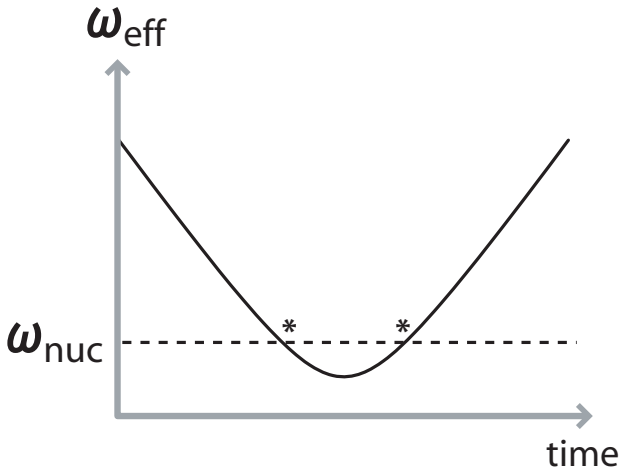

Figure 2.14: Time dependence of the effective field strength when the field sweep is performed. The Hartmann-Hahn condition is satisfied when the effective field strength matches the ^{1}H Larmor precession frequency, as marked by asterisks

This field sweeping technique realizes a very efficient polarization transfer based on cross polarization, because all of the electron-spin packets can successively satisfy the Hartmann-Hahn condition, and participate the polarization transfer. We shall call this technique the integrated cross polarization (ICP).

■□■ adiabatic condition ■□■

It is important to perform the field sweep sufficiently slowly, so that each spin packet is "locked" along the effective field in the rotating frame. That is, the rate of change in the external field has to be sufficiently slow compared to the effective precession frequency so as to satisfy the so-called adiabatic condition given by

$$\gamma \frac{dB_0}{dt} \ll \frac{\omega_e^2}{\sin\alpha(t)}, \tag{2.19}$$

where $\alpha(t)$ is the angle of the effective field with respect to the static field[5].

■□■ An experimental sequence for ICP ■□■

The ICP technique can be carried out by using both permanent paramagnetic impurities and photo-excited triplet electrons. In the latter case, one should notice that the photo-excited triplet electrons decay to the diamagnetic ground state in a finite lifetime. Thus, the sweep must be performed quickly enough. At the same time, the sweep must be slow enough not to violate the adiabatic condition (Eq. 2.19). When one tries to perform ICP using photo-excited triplet electron spins, the experimental sequence will be something like a schematic diagram as shown in Fig. 2.15. Beforehand pulsing a laser beam for the photo-excitation, a field offset is made by half the sweep width, and immediately after the laser pulse the sweep is performed together with microwave irradiation. When the sweep is over, the microwave irradiation is switched off and the field is restored to the original value. The field sweep width has to exceed the ESR linewidth, and the field sweep has to complete within the lifetime of the triplet state, For the photo-excited triplet electron spins in pentacene, I found the appropriate field sweep width and sweep time to be ca. 7 mT and ca. 15 μs, respectively, as will be shown in Chapter 4

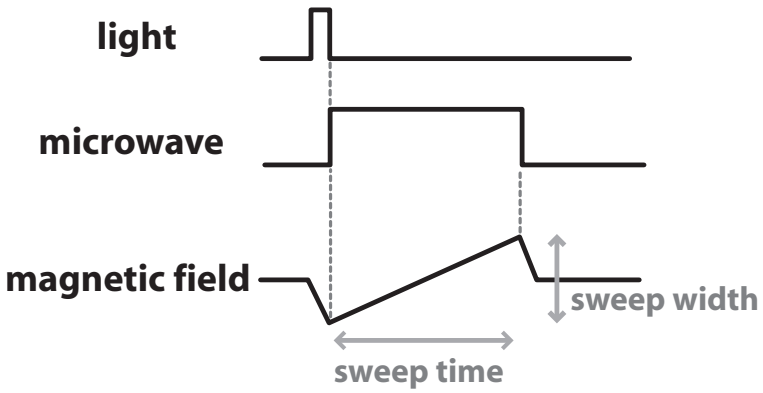

Figure 2.15: An ICP sequence using photo-excited triplet electron spins. Just before pulsing a laser beam, a field offset is made by half the sweep width, and immediately after the laser pulse the sweep is performed together with microwave irradiation. When the sweep is over, the microwave irradiation is switched off and the field is restored to the original value.

■□■ Summary of this chapter ■□■

In this chapter I have explained the principle of the polarization transfer from photo-excited triplet electron spins to nuclear spins. Polarization transfer by cross polarization is much more efficient than that by the solid effect, because the former is induced by an allowed flip-flop transition, whereas the latter is caused by a forbidden transition. I have explained that the adiabatic field sweep over the triplet-electron resonance lines enables all the spin packets to participate the polarization transfer successively. I would like to stress that the technique which we call the integrated cross polarization (ICP) was invented by Henstra et al.[31], who named the technique the integrated solid effect (ISE). However, since the polarization transfer is *not* caused by the solid effect but by cross polarization, it is better, I believe, to call the technique the integrated cross polarization.

The explanation of the principle of ICP presented here is only qualitative. A more detailed, quantitative discussion will be made in Chapter 5, where I attempt to explain the experimental results shown in Chapter 4.

Chapter 3

Experimental strategies and setup

3.1 Strategies for maximizing the ^{1}H polarization

■□■ Sample ■□■

Molecules having the following conditions among a number of molecules photo-excitable to the triplet state should be chosen for polarization sources in DNP experiments. The electron polarization in the triplet state should be as large as possible, by which the attainable ^{1}H polarization is limited. The concentration of the triplet guest molecules in the host molecules are desirable to be as high as possible, because the ^{1}H Zeeman reservoir can efficiently be cooled down under the high concentration, and the quantum yield of the triplet state is desired to be large to shorten the polarization buildup time. In order to realize a high dynamic ^{1}H polarization, nuclear spin-lattice relaxation rate should be very low, since it acts to restore the nuclear spin system towards thermal equilibrium. The lifetime of the triplet state must be long enough to transfer the electron polarization to the nuclear spins. However, it should not be unnecessarily long, because the paramagnetism of the triplet state accelerates the nuclear spin-lattice relaxation.

Pentacene-doped naphthalene seems to be one of the best systems for the triplet DNP experiments, because pentacene exhibits a large electron polarization of ca. 0.7 in the triplet state[40], and the triplet lifetime ($20 \sim 80\ \mu$s[66]) is long enough to carry out the ICP sequence. Moreover, the electron spin-lattice relaxation is not so fast compared to the triplet lifetime, so that the large electron polarization is retained until it is transferred to the surrounding protons by ICP. Since the ^{1}H spin-lattice relaxation time of naphthalene is extremely long at temperatures around 77 K[67, 33], the buildup experiment should be carried out at this temperature region.

We tried to dope pentacene molecules into naphthalene as much as possible unless clustered. If they are doped too much, recognizable clusters of pentacene molecules appeared in the naphthalene crystal, and we found that they seriously shorten the ^{1}H spin-lattice relaxation time. We could dope pentacene with a concentration of 0.018 mol% without clustering. It is best to orient the long molecular axis of the pentacene molecule along the external field, because the polarization of the triplet electron spin becomes the largest (0.7)[40]. We tried to align the crystal so that the normal line to the cleavage plane (*ab*-plane) makes an angle of 23° with respect to the external field around the crystal *b*-axis. In this crystal orientation, both long molecular axes of pentacene molecules at either of the two substitution sites align along the external field[53].

■□■ Laser ■□■

Recently we have proposed a theory to calculate the penetration depth of light, the triplet excitation depth to which the guest molecules can undergo ISC to the triplet state, and the fraction of the guest molecules in the triplet state, and we have verified the theory by ESR measurements[39]. Based on the theory, the triplet excitation depth and the triplet fraction can be simulated for given guest concentration, ISC rate, natural lifetime, laser beam intensity, and laser pulse width. Therefore, if the ISC rate and the natural lifetime are known, we can know the laser beam intensity and pulse width required to maximize both of the triplet excitation depth and the triplet fraction for various guest concentrations. Some hints are given in the following: The ISC rate is desired to be high, because a popularly available laser with a short pulse width

($1 \sim 10$ ns) can be used. If the ISC rate is low, the guest molecules should be photoexcited many times during a laser pulse to increase the triplet fraction; thus, the pulse width is desirable to be much longer than the lifetime of the excited singlet state as far as it is shorter than the lifetime of the triplet state. The laser beam is desirable to be very intense to increase the triplet excitation depth. However, it should not be so intense that the effect of the stimulated emission is no longer negligible, because it decreases the ISC quantum yield, causing a considerable decrease in the triplet fraction. The wavelength of the laser beam should be close to the position of the absorption peak of guest molecules both for efficiently photo-exciting them and for avoiding sample heating[33].

For the case of pentacene-doped naphthalene used in the present study, the following parameters should be used. The wavelength should be set to ca. 590 nm, corresponding to the absorption peak of pentacene. Since the ISC quantum yield of pentacene is low (ca. 0.03[44]), the laser pulse width should be much longer than the natural lifetime of pentacene (ca. 30 ns[47]) and much shorter than the lifetime of the triplet state ($20 \sim 80$ μs[33]). We carried out simulations of the triplet fraction and the triplet excitation depth in pentacene-doped naphthalene for various laser pulse widths, and found the width of ~ 1 μs to be suitable for the present case. We also found that from simulations that the laser beam intensity should be much lower than 10^{11} Wm^{-2}, because otherwise the triplet fraction is considerably reduced by the non-negligible effect of the stimulated emission. The simulations also ensure that the beam intensity of $\sim 10^9$ Wm^{-1} is enough to transfer all the pentacene molecules to the triplet state in a sample with the thickness of ca. 2 mm.

More detailed treatment on the subject as to the penetration depth and the triplet excitation depth are treated in Chapter 7.

■□■ Microwave and Field sweep ■□■

In order for all the electron spin packets to participate in the polarization transfer, the field sweep width should be wide compared to the ESR line width, and the field sweep time should

be long enough so that each spin packet is swept over adiabatically. On the other hand, the field sweep should complete within the lifetime of the triplet state and the electron spin-lattice relaxation time so that the polarization transfer by ICP completes before the triplet state decays to the ground state and the electron polarization is lost. For maximizing the ICP efficiency, we experimentally examined the dependence of the initial buildup rate of ^{1}H polarization on field sweep width, field sweep time, and microwave intensity, and found the optimal conditions.

3.2 Experimental

3.2.1 Sample

Naphthalene was extensively purified by zone melting, while pentacene was used as purchased. Single crystals of pentacene-doped naphthalene were grown by the Bridgman method, from which a single crystal was cut out with a cleavage plane (*ab* plane) of 4×4 mm and a thickness of 2.2 mm. The crystal *b*-axis direction was found by inspecting birefringence, and we tried to rotate the crystal around the *b*-axis, so that the normal line to the *ab*-plane is tilted by 23° with respect to the external field.

3.2.2 Experimental setup

For the ICP buildup experiments, apparatus is necessary capable of irradiating a laser beam, applying microwave irradiation together with magnetic field sweep, and performing NMR excitation and detection. Fig. 3.2 shows a schematic diagram of the experimental setup which, with many people's help, we developed for the ICP experiments using photo-excited triplet electron spins of pentacene.

■□■ Magnet ■□■

The static magnetic field of about 0.3 T was supplied by a wide-bore superconducting

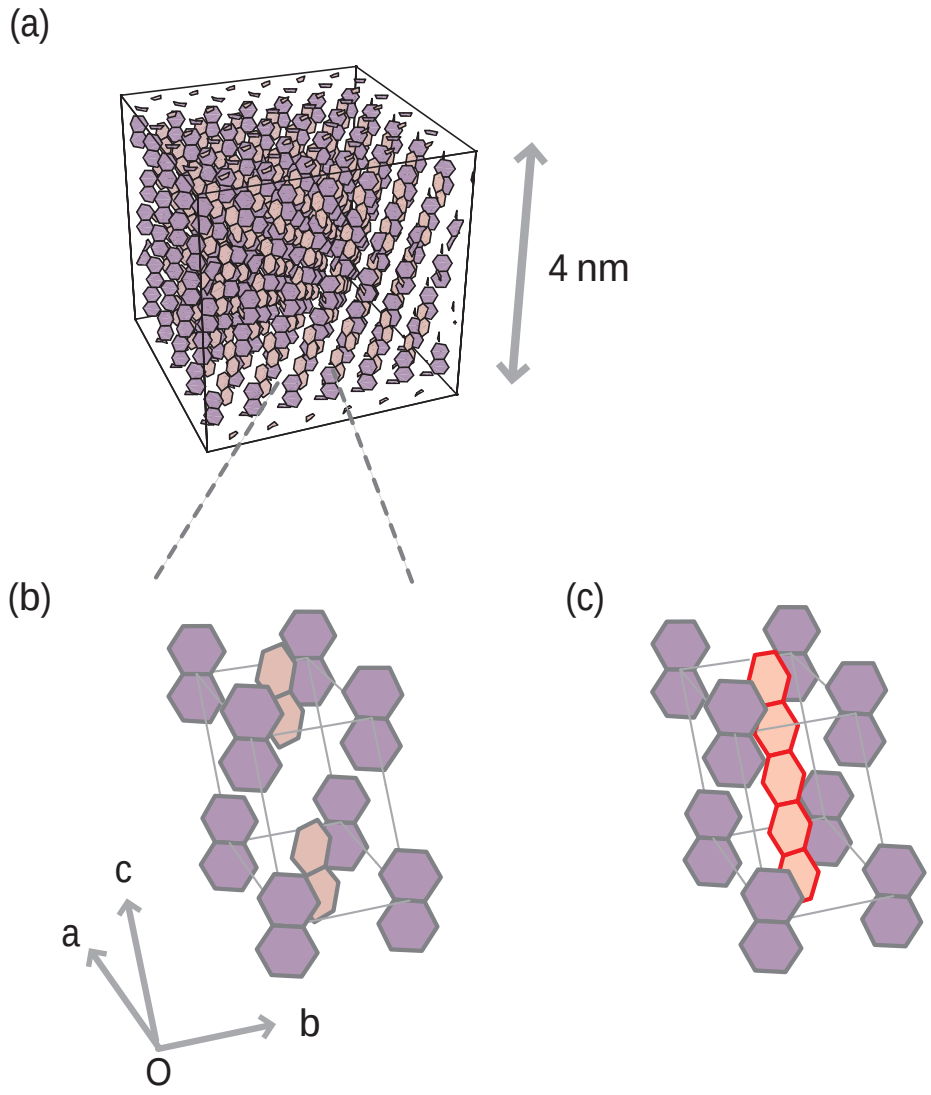

Figure 3.1: (a) Naphthalene molecules in a single crystal sample. (b) An unit cell of naphthalene, the dimensions of which are $a = 8,235$ Å, $b = 6.003$ Å, $c = 8.658$ Å, and $\angle aOc = 122°55'$[68, 69]. (c) The unit cell of naphthalene, in which two naphthalene molecules are substituted by a pentacene molecule.

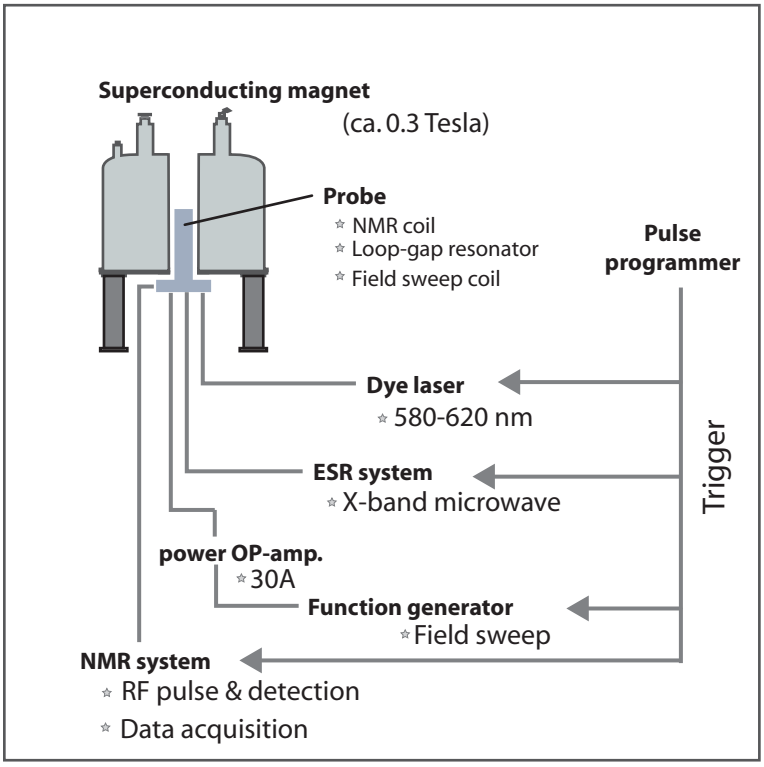

Figure 3.2: A schematic diagram of the experimental setup used for the ICP buildup experiments.

magnet. In this field, the resonance frequency of electron spins lies within X-band (∼9 GHz) region, and the ^{1}H resonance frequency is ca. 13 MHz.

■□■ Laser ■□■

For light irradiation, a flashlamp-pumped pulsed dye laser (Cynosure, LFDL-3C) was used, whose wavelength and pulse duration are 590 nm and 1 μs, respectively. The maximum energy of the laser pulse is ca. 10 mJ/pulse, and the maximum repetition rate is 50 Hz. Accordingly, the maximum repetition rate of the ICP sequence is limited to 50 Hz. The laser beam is fed into an optical fiber and guided to the sample mounted on a sample holder, where the beam diameter can be adjusted from 1 to 3 mm by a collimater lens.

■□■ Field sweep ■□■

For the field sweep, a quadrupole coil was made from a 1 mmϕ enamelled copper wire, connected to a current driving circuit via a 0.25 Ω cement resistor. The circuit diagram is shown in Fig. 3.3[70]. A triangle wave generated by a home-made function generator is amplified by a power operational amplifier PA-05 (Apex microtechnology) and sent to the the sweep coil.

■□■ Microwave ■□■

There are several candidates for an X-band microwave resonator; a microwave cavity, a loop-gap resonator (LGR), a slotted-tube resonator, and a dielectric resonator. For microwave irradiation, we developed and tested a probe based on a microwave cavity and a probe based on a LGR.

■□■ Microwave cavity-based probe ■□■

K. Fujii, an ESR engineer at JEOL Co. Ltd., kindly helped us to develop a TE102 mode cavity, whose design drawing is shown in Fig. 3.4. It resonated at 9.4 GHz, and the Q-factor was 3,000 when unloaded. When the NMR coil was inserted into the cavity (Fig. 3.5), the Q-factor was reduced to 500.

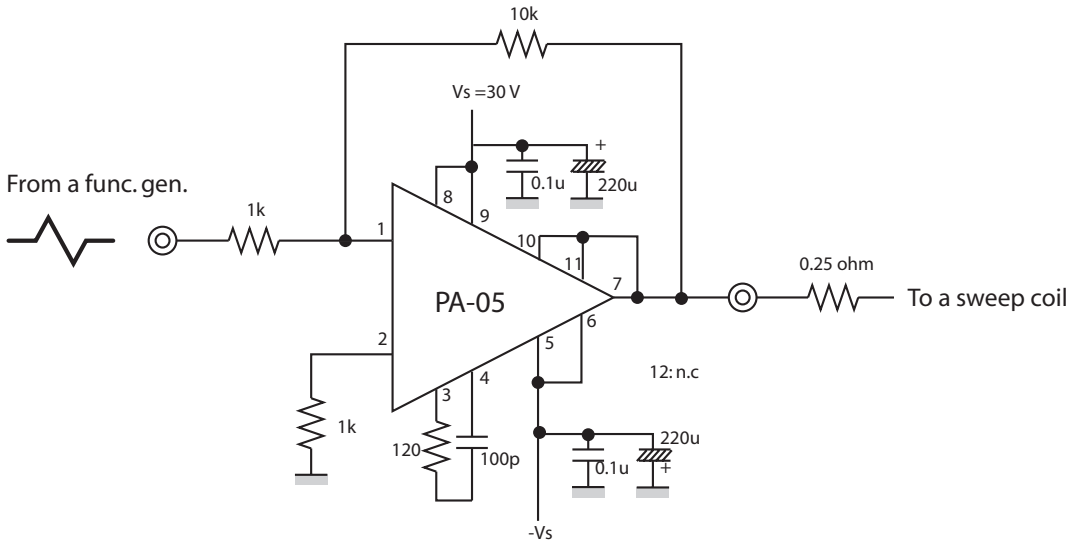

Figure 3.3: The circuit of a current driver for the field sweep.

■□■ LGR-based probe ■□■

Since we had not been satisfied with the performance of the NMR coil (Fig. 3.5), whose shape was restricted so as not to disturb the microwave fields inside the cavity, we then developed a LGR-based probe. In this system, the microwave resonator and the NMR coil are separated, between which sample can be moved (Fig. 3.7). Thus, both the microwave and the RF resonators can operate without interfering each other. The design of LGR, shown in Fig. 3.6, is based on the work by B.T. Ghim et al.[71]. G.R. Eaton and G.A. Rinard kindly provided us a computer program to calculate the LGR dimensions for the desired resonant frequency.

■□■ Experimental procedure ■□■

Following the laser pulse, the magnetic field was adiabatically swept around the $|-1\rangle \leftrightarrow |0\rangle$ transition of the ESR resonances in the photoexcited triplet state of pentacene, during which the microwave pulse was applied. The ^{1}H polarization was built up by repeating the ICP sequence with a rate of 50 Hz, after which the enhanced ^{1}H signal was observed. For various field sweep widths, field sweep times, and microwave intensities, we examined the initial buildup rate of the ^{1}H polarization in order to figure out the optimal condition that maximizes the ICP buildup efficiency.

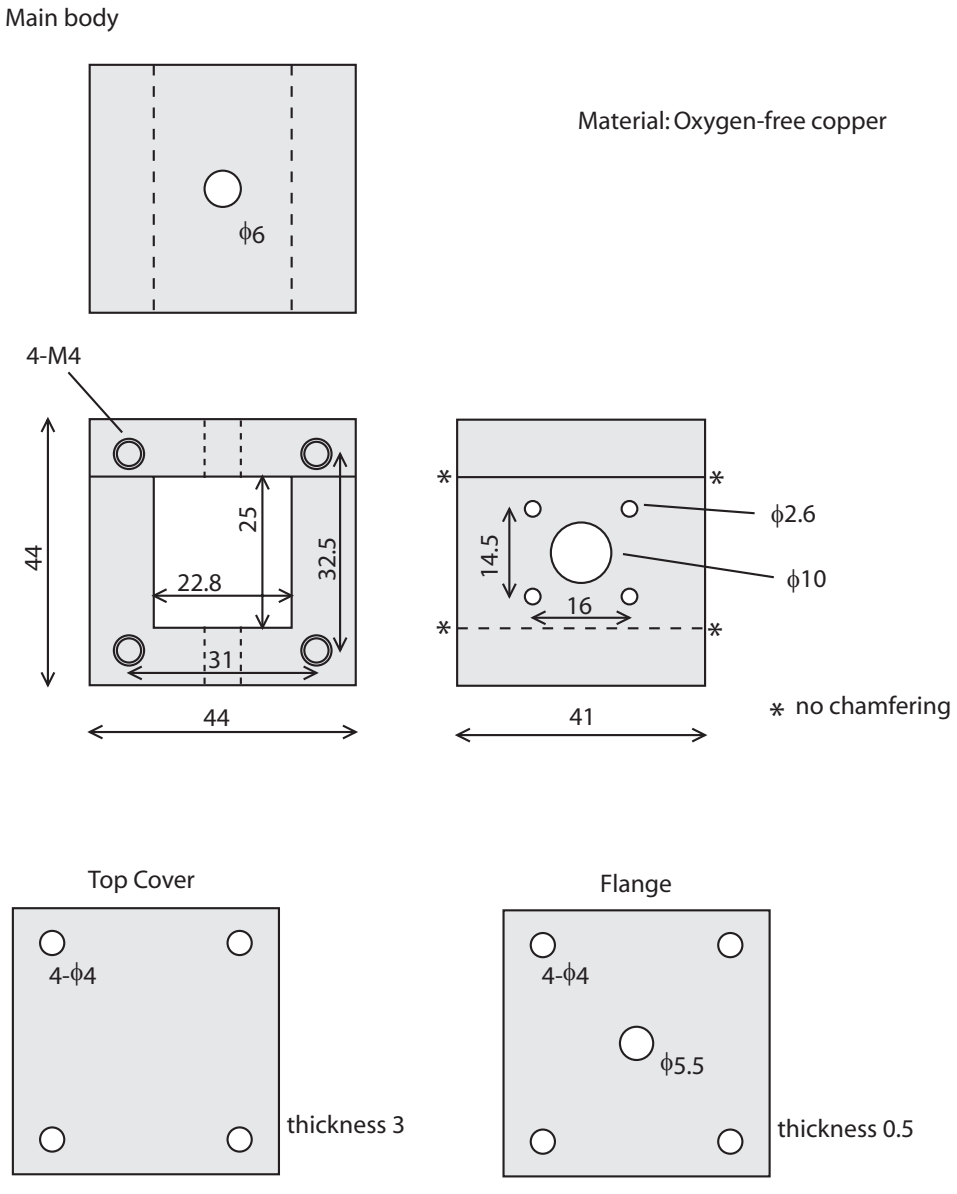

Figure 3.4: Design of a TE102 microwave cavity.

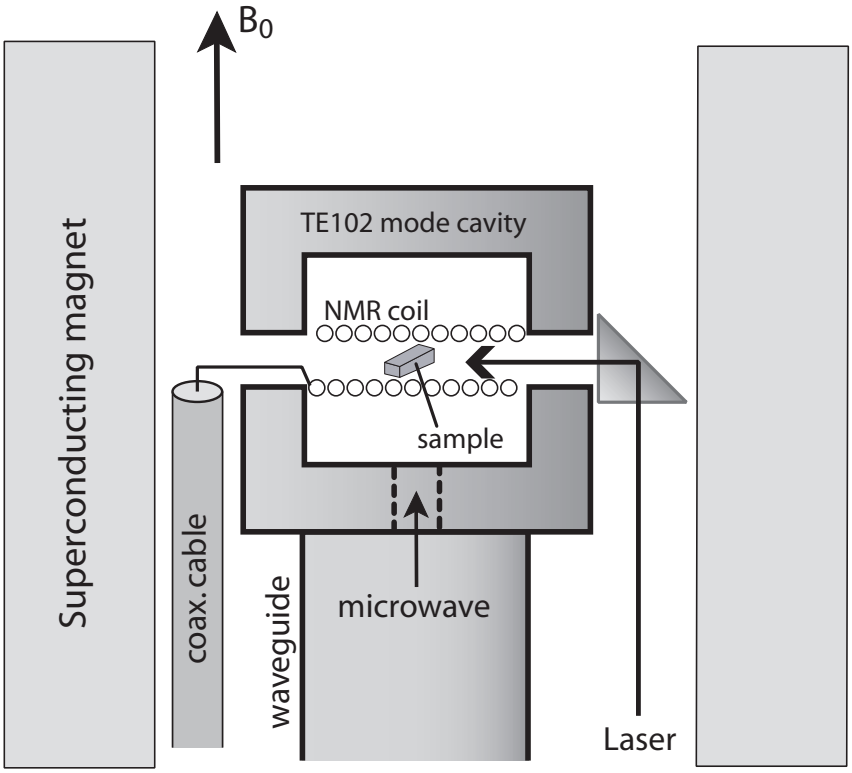

Figure 3.5: A schematic view of a microwave-cavity-based probehead for triplet DNP experiments.

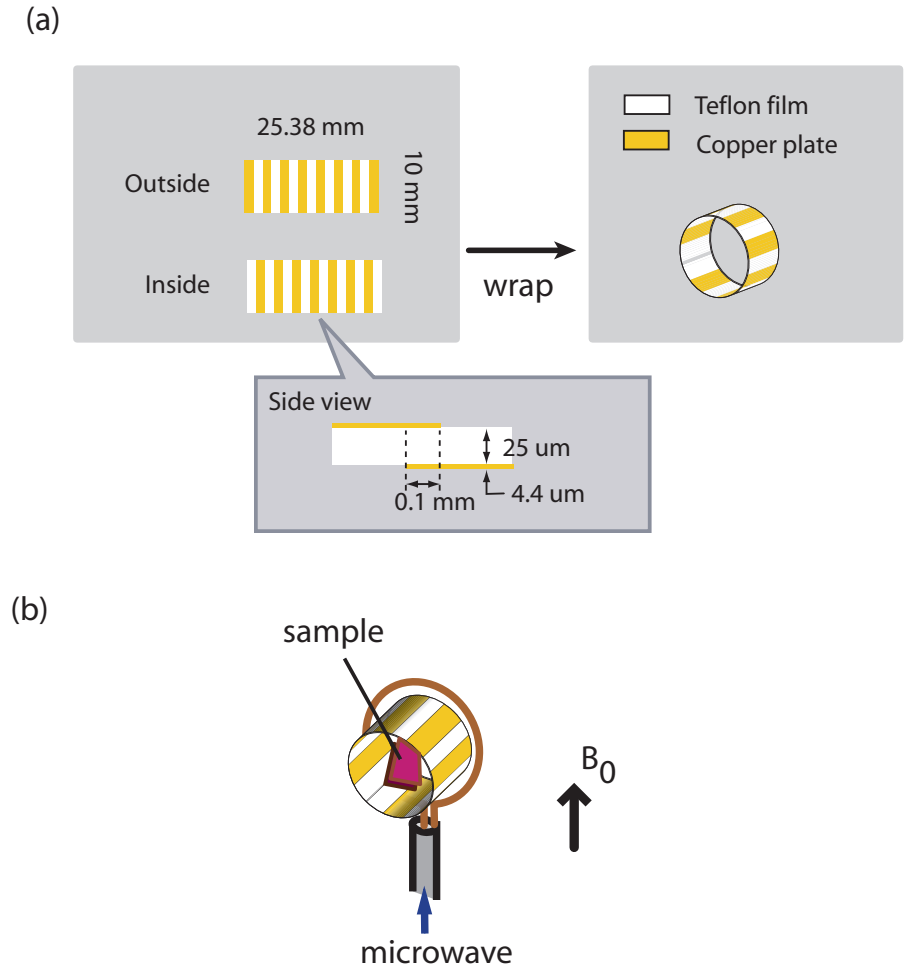

Figure 3.6: A copper-film loop-gap resonator[71].

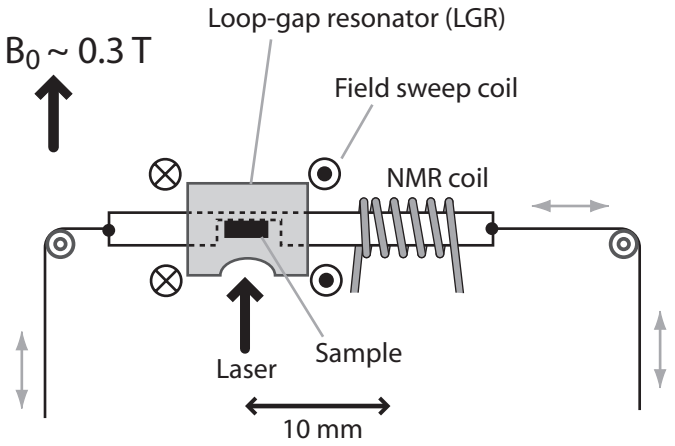

Figure 3.7: LGR-based probehead. A LGR and an NMR coil are in line, between which the sample can be moved keeping the crystal orientation.

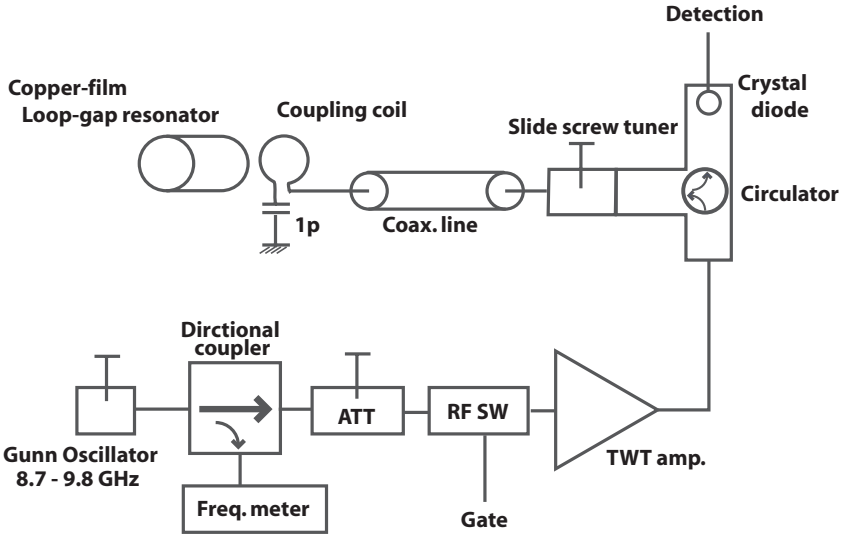

Figure 3.8: A block diagram of apparatus for X-band microwave irradiation.

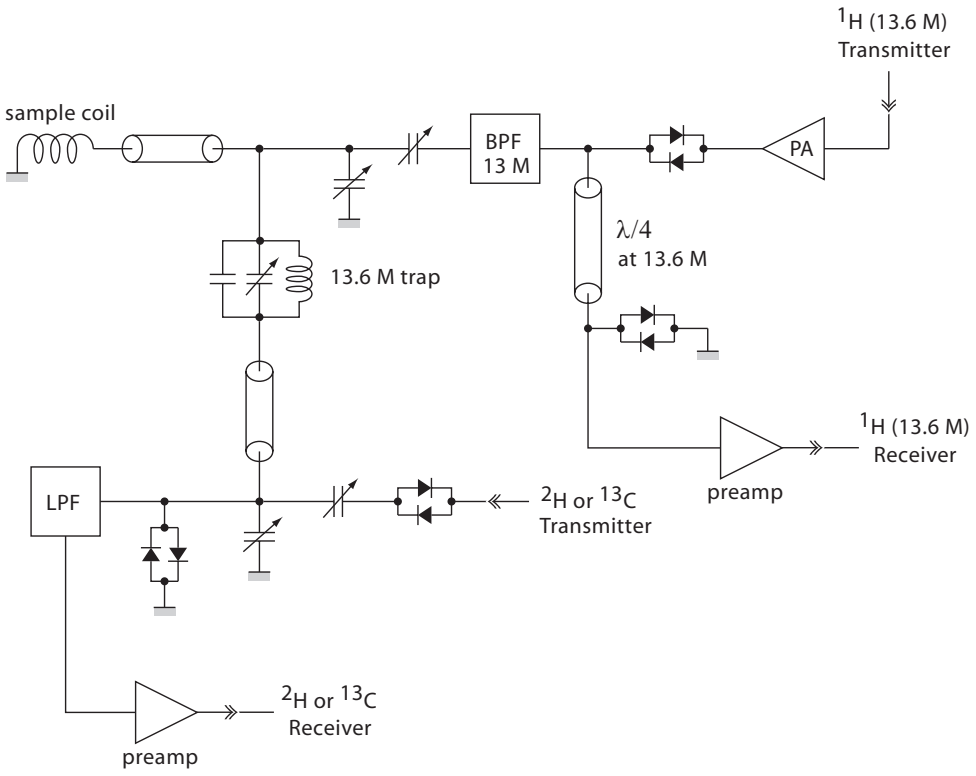

Figure 3.9: An RF circuit diagram for NMR. The sample coil is doubly-tuned for ^{1}H ($\sim$ 13.6 MHz) and ^{13}C/^{2}H ($\sim$ 3.4 MHz/$\sim$ 2.1 MHz) resonances.

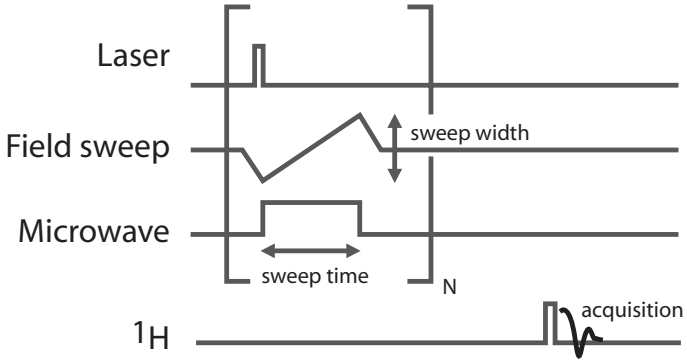

Figure 3.10: A timing sequence for ICP. Following the laser pulse, the field sweep is applied together with the microwave irradiation. The field sweep width and the sweep time should be optimized to realize efficient polarization transfer.

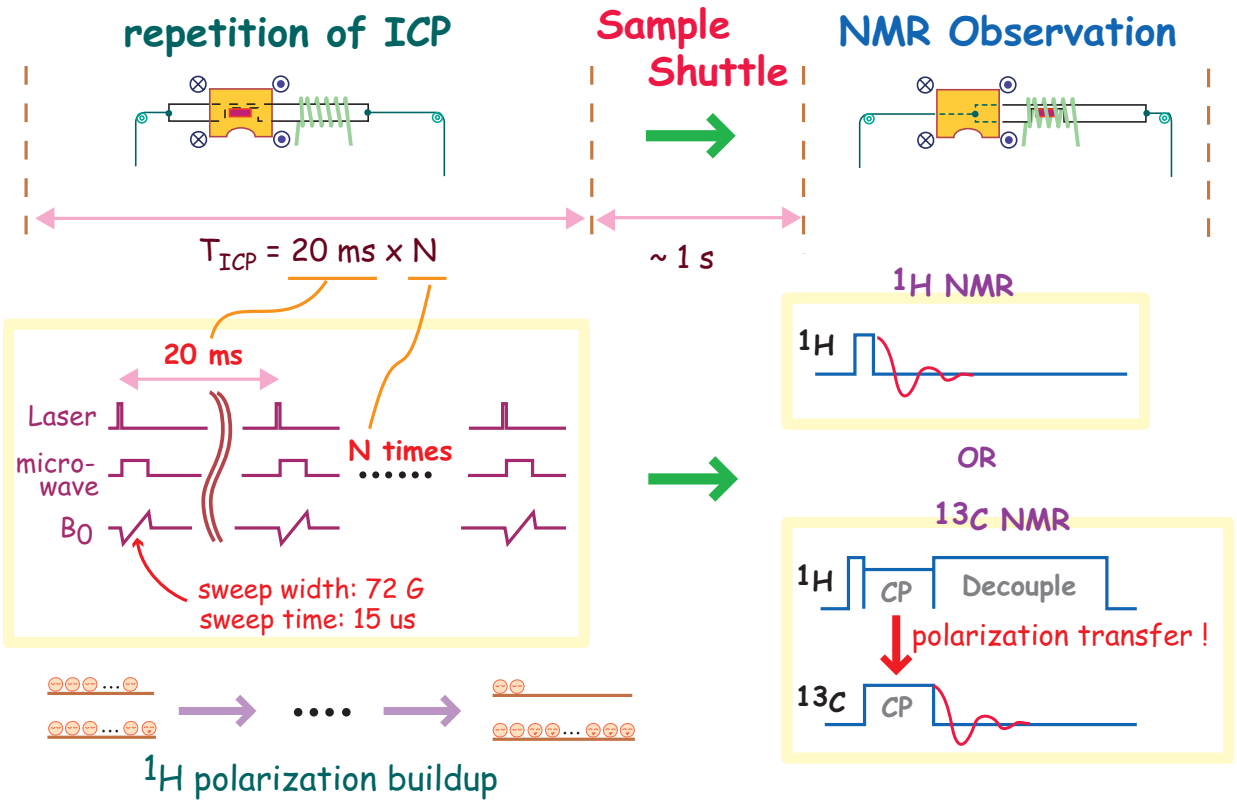

Figure 3.11: The ^{1}H polarization is built up by repeating the ICP sequences. After the buildup, the sample is moved into the NMR coil and the enhanced NMR signal is observed by applying a 90° pulse.

In order to determine the enhanced ^{1}H polarization, we first measured a ^{1}H signal in H_2O as a reference under thermal equilibrium at 298 K in the same field as used for DNP experiments. The enhancement factor Q with respect to the thermal equilibrium polarization at a temperature T is represented as

$$Q = \frac{N_{\mathrm{ref}}}{N_{\mathrm{DNP}}} \frac{T_{\mathrm{DNP}}}{T_{\mathrm{ref}}} \frac{g_{\mathrm{ref}}}{g_{\mathrm{DNP}}} \frac{E_{\mathrm{DNP}}}{E_{\mathrm{ref}}}, \tag{3.1}$$

where N is the number of ^{1}H spins, and g and E are the receiver gain and the recorded signal voltage. N_{DNP} is determined from $N_{\mathrm{DNP}} = \rho dA$, where ρ is the density of protons in naphthalene, d is the sample thickness, and A is the area of the laser beam on the sample, which was calibrated from the image of the laser spot on a photosensitive paper placed at the sample position.

Chapter 4

Results

4.1 Optimization of the experimental parameters

■□■ Crystal orientation ■□■

As mentioned in Chapter 3, we *tried* to orient the single crystal sample of pentacene-doped naphthalene so that the normal line to the *ab*-plane makes the angle of 23° with respect to the external field around the *b*-axis. In actual, however, the accurate mounting of the crystal was very difficult, and the deviation could not be removed in the axis of rotation from the crystal *b*-axis. Accordingly, we carefully examined the buildup efficiency for various angles of rotation around the goniometer axis. As shown in Fig. 4.1, there were two orientations of the sample that exhibited the maximum buildup efficiency. Each of these peaks corresponds to the crystal orientation in which the long axes of the pentacene molecules at either of the two substitution sites point in the orientation being close to that of the external field. The following buildup experiments were carried out at the crystal orientation indicated by the arrow in Fig. 4.1. A slight deviation in the direction of the pentacene long molecular axis from that of the external field does not affect the electron polarization so much, as is seen in Fig. 4.2.

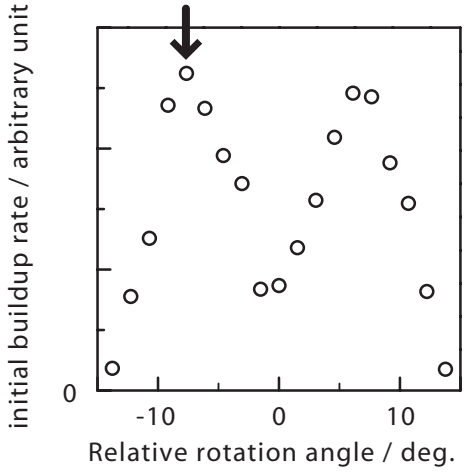

Figure 4.1: Orientational dependence of the initial buildup rate of the ^{1}H polarization in the single crystal sample of pentacene. The magnetic field was 0.3187 T, and the microwave frequency was 9.7 GHz. The appearance of two maxima indicates that the goniometer axis deviates from the crystal *b*-axis, making the pentacene molecules at the two substitution sites inequivalent.

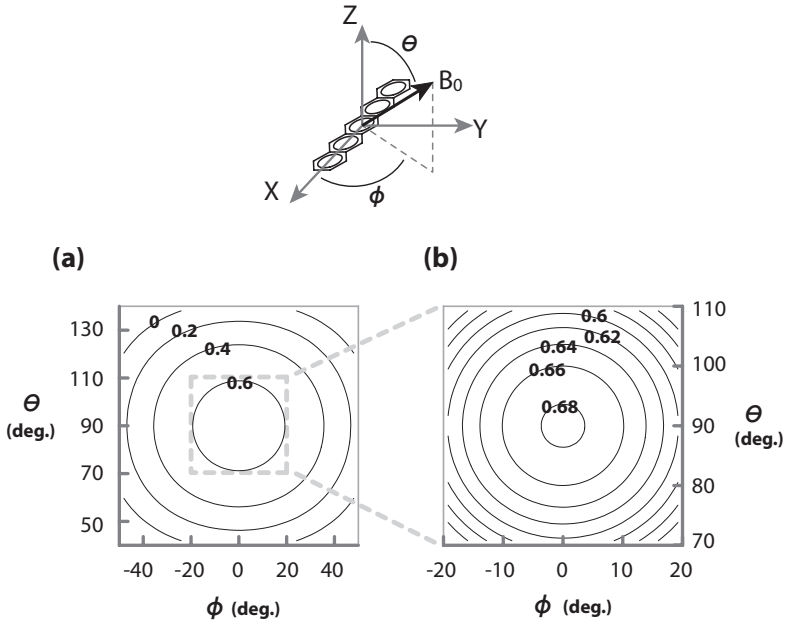

Figure 4.2: Calculated orientational dependence of the electron spin polarization of the $|-1\rangle$ and $|0\rangle$ sublevels of the photo-excited triplet state of pentacene. The polarization was obtained by calculating the high-field populations $w_\kappa(\Theta,\Phi)$ in Eq. 6.9 (page 100).

■□■ Field-sweep conditions and microwave intensity ■□■

For various field sweep widths B_s and field sweep times τ_s, we examined the initial buildup rate, and found that the condition $(B_s, \tau_s) = (7.2\ \text{mT}, 15\ \mu\text{s})$ maximized the buildup efficiency.

Microwave power dependence of the initial buildup rate of ^{1}H polarization is shown in Fig. 4.3. While we did not calibrate the microwave field intensity, it seems to have satisfied the Hartmann-Hahn condition between the electron Zeeman splitting in the rotating frame and the ^{1}H Zeeman splitting in the laboratory frame, because the enhanced signal was maximized around the microwave power of 40 W.

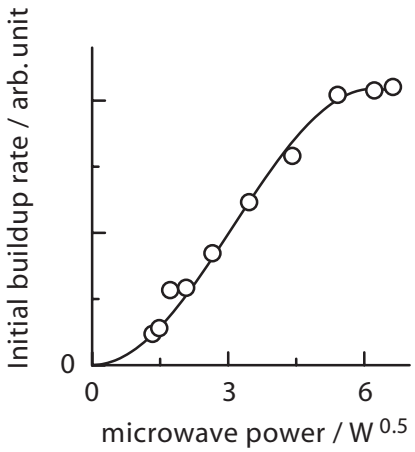

Figure 4.3: Microwave power dependence of the initial buildup rate of ^{1}H polarization.

The following experiments were carried out using these optimized experimental parameters.

4.2 Enhancement of ^{1}H polarization by ICP in pentacene-doped naphthalene

Fig. 4.4(a) shows a single scan ^{1}H spectrum obtained at room temperature after repeating the ICP sequence for 30 s, and the spectrum in Fig. 4.4(b) is obtained in a single scan at thermal equilibrium ($T_1 \sim$40 min). The two spectra obviously demonstrate that the NMR sensitivity is exceedingly enhanced by DNP. The spectrum in Fig. 4.4(a) was obtained with upfield sweep, while that in Fig. 4.4(c) was recorded with downfield sweep. The magnetization is locked parallel to the effective field in the rotating frame under the upfield sweep, while the downfield sweep locks the electron magnetization antiparallel to the effective field. This causes the phases of the spectra to be opposite to each other.

Fig. 4.5 shows the polarization buildup curve obtained at 105 K. The ^{1}H polarization is exponentially built up with a time constant of 7,890 s, and finally reaches the value of 0.70 ± 0.07, being 2.1×10^5 times as large as the thermal equilibrium polarization at 105 K. The error is due mainly to that in estimation of the laser spot size and that in the incidence angle of the laser beam with respect to the crystal cleavage plane via N in Eq. (3.1). As compared to the previous work by Iinuma et al.[33], in which the buildup time constant and the final ^{1}H polarization were 20,580 s and 0.32, respectively, about twice the ^{1}H polarization was obtained in a third of the experimental time. These improvements can be attributed to 18-fold higher concentration of pentacene molecules, to the optimization of experimental conditions on microwave and field sweep, and to the consideration of the laser beam penetration depth and the triplet excitation depth into the sample.

The maximum possible ^{1}H polarization obtainable by the present approach is given by the electron polarization averaged over the ICP sweep time τ:

$$\bar{P_e}(\tau) = \frac{1}{\tau}\int_0^\tau dt P_e(t), \tag{4.1}$$

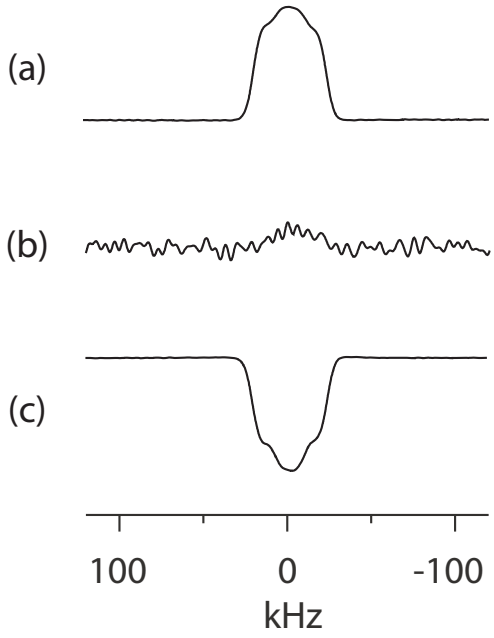

Figure 4.4: Single scan ^{1}H spectra of a single crystal sample of 0.018 mol% pentacene-doped naphthalene. (a) Enhanced by applying the ICP sequences for 30 s at a rate of 50 Hz, in which the field was swept from lower to higher value (upfield sweep). (b) Obtained under thermal equilibrium, where the sample had been kept in the magnet for 12 hours before acquisition, which is sufficiently long time for the ^{1}H spins to establish equilibrium at room temperature[67]. (c) Enhanced by the same method as (a), except that the field was swept from higher to lower value (downfield sweep). The ^{1}H resonance frequency is 13.6 MHz, and the temperature is 298 K.

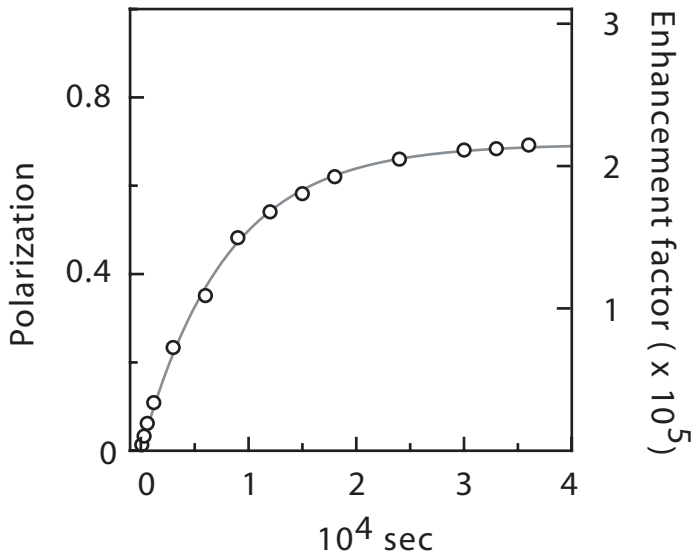

Figure 4.5: Buildup curve of the ^{1}H polarization in a single crystal sample of 0.018 mol% pentacene doped naphthalene. The ICP sequence was repeated at a rate of 50 Hz. The ^{1}H resonance frequency is 13.6 MHz, and the temperature is 105 K. The enhancement factor was calculated using Eq. (3.1).

where $P_e(t)$ is the electron polarization. $P_e(t)$ can be represented as

$$P_e(t) = \frac{N_0 e^{-k_0 t} - N_{-1} e^{-k_{-1} t}}{N_0 e^{-k_0 t} + N_{-1} e^{-k_{-1} t}}, \tag{4.2}$$

where k_0 and k_{-1} are the decay rates for the $|0\rangle$ and the $|-1\rangle$ triplet substates, and N_0 and N_{-1} are the initial populations. From ESR studies, those parameters have been measured to be $k_0 = 3.83 \times 10^4$ s^{-1} and $k_{-1} = 1.20 \times 10^4$ s^{-1}, and $N_0 = 0.729$ and $N_{-1} = 0.136$[66]. Then, from Eqs. (4.1)-(4.2), we obtain $\bar{P_e} = 0.63$ for $\tau = 15$ μs. Since this value agrees with the final ^{1}H polarization within the estimated error, we can conclude that the ^{1}H polarization was most probably built up to the ultimate value attainable by this method. The successful buildup to the ultimate value is also ascribed to the fact the ^{1}H spin-lattice relaxation time of the host naphthalene is long at 105 K[67] compared to the buildup time of the present experiment.

4.3 Polarization of dilute spins

4.3.1 Polarization of residual protons in a deuterated sample

Here, we apply this technique to single crystal and polycrystalline samples of exceedingly diluted ^{1}H spin systems. NMR of a dilute ^{1}H system attracts interest in the resonance lineshape of dilute protons, the ^{1}H distribution in a molecule, the spin diffusion among dilute protons, etc. Furthermore, dilute ^{1}H systems enable high-resolution ^{1}H solid-state NMR without application of multiple pulse spectroscopy[72], and permits long-range ^{1}H-^{1}H distance measurements[73]. Problems in these studies are the low sensitivity due to low ^{1}H concentrations and long spin-lattice relaxation times of dilute protons. Triplet DNP experiments may solve the problem and provide a ground for such NMR studies of dilute ^{1}H systems. Actually, we briefly discuss the ^{1}H lineshape and the ^{1}H distribution in deuterated naphthalene in the present study, and are currently investigating spin diffusion in ^{1}H-diluted naphthalene.

The experiments were made using a single crystal sample of 0.015 mol% pentacene-doped perdeuterated naphthalene. The residual ^{1}H abundance was determined to be 0.79% from a liquid state ^{1}H NMR spectrum by comparing the resonance line intensity with that of hydroquinone dissolved as a reference in the solvent. The single crystal orientation was adjusted in the same way as in the case of the undeuterated sample. Following the laser pulse, the magnetic field is adiabatically swept from -3.6 mT to $+3.6$ mT around the $|-1\rangle \leftrightarrow |0\rangle$ ESR resonance in the photoexcited triplet state of pentacene. The field sweep is carried out over a period of 15 μs, during which a microwave field with a power of 40 W is applied.

Fig. 4.6 shows the polarization buildup curve of the residual protons in a single crystal sample of pentacene-doped 99.21% deuterated naphthalene. The signal intensity obtained after repeating ICP for 4,000 s is 2.1×10^5 times as large as the thermal equilibrium intensity at 105 K in the magnetic field of 0.3187 T. The ^{1}H polarization finally reaches 0.71 ± 0.07, which agrees with the electron spin polarization of 0.63 in the photoexcited triplet state of pentacene; the latter

was obtained by averaging the electron spin polarization over the period of ICP[37]. Thus, the ^{1}H polarization in deuterated naphthalene has most probably been built up to the maximum possible value. The buildup time constant is 357 s, being much shorter than that (7,890 s) for undeuterated naphthalene demonstrated in Fig. 4.5. This is because the heat capacity of the ^{1}H reservoir in the deuterated host is very small, and therefore it is quickly cooled down.

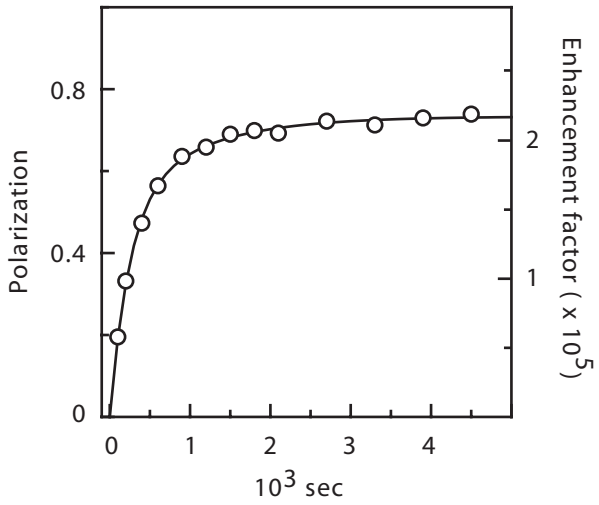

Figure 4.6: Buildup curve of the ^{1}H polarization in a single crystal sample of 99.21% deuterated naphthalene doped with 0.015 mol% pentacene. The ICP sequence was repeated at a rate of 50 Hz. The ^{1}H resonance frequency is 13.6 MHz, and the temperature is 105 K. The enhancement factor was calculated by comparing the intensity of the enhanced signal with that of the thermal ^{1}H signal obtained in checkweighed water at 298 K.

The final ^{1}H polarization can be limited by the spin-lattice relaxation, since it causes the ^{1}H spin system to be restored towards thermal equilibrium. We measured the ^{1}H spin-lattice relaxation time T_1 using the ^{1}H polarization enhanced by the present technique, and found that T_1 exceeds 10^5 s, being exceedingly longer than the buildup time. For the present case, therefore, the loss of polarization due to the spin-lattice relaxation is negligibly small as compared to the gain of polarization by ICP, so that the ^{1}H polarization is built up to the electron polarization in the triplet state.

Fig. 4.7(a) shows a ^{1}H spectrum observed for a single crystal sample of pentacene-doped 99.21% deuterated naphthalene in a single scan after the ICP time of 4,500 s. The linewidth of

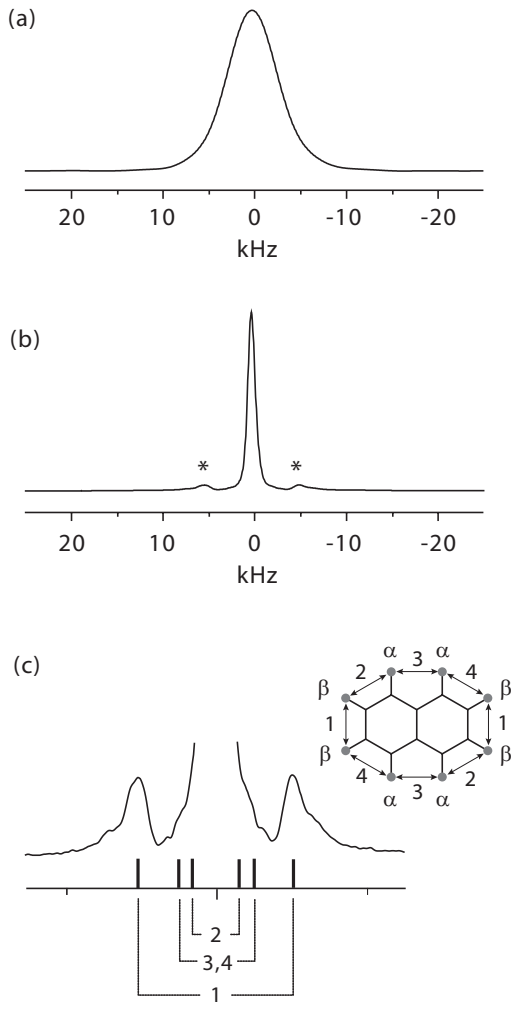

Figure 4.7: 13.6 MHz ^{1}H DNP spectra of a single crystal sample of 99.21% deuterated naphthalene doped with 0.015 mol% pentacene. Each spectrum was obtained at 105 K in a single scan after repeating the ICP sequences for 4,500 s at a rate of 50 Hz (a) without ^{2}H decoupling, (b) under double-quantum ^{2}H decoupling at 2.0855 MHz with the rf field intensity of 20 kHz. The asterisks denote the ^{1}H signals coming from the pair of isolated protons which happen to be adjacent to each other. (c) Enlarged spectrum of (b), in which the assignments of the ^{1}H-^{1}H dipolar-splitted peaks are shown. The peak positions indicated by the sticks were calculated using the crystal structure data of naphthalene[69].

ca. 7 kHz is about one sixth the ^{1}H resonance width of undeuterated naphthalene (Fig. 4.4(a)). This broadening is ascribed to the ^{1}H-^{2}H heteronuclear dipolar interactions, so that the dephasing of the free-induction decay (FID) is recovered in the form of spin echoes by applying π pulse trains, as shown in Fig. 4.8 This line broadening can be eliminated by double-quantum (DQ) ^{2}H decoupling[74], as demonstrated in Fig. 4.7(b). The spectrum has a shape close to Lorentzian, and the reduced line broadening of ca. 700 Hz certainly arises from the homonuclear dipolar interactions among dilute protons. For a system of spins distributed at random in a simple cubic lattice with a small fraction f ($f \ll 0.01$), the resonance line has theoretically been given to be Lorentzian with a linewidth

$$\delta = 10.6 f \frac{\mu_0}{4\pi} \frac{\gamma^2 \hbar}{a^3}, \tag{4.3}$$

where a is the lattice constant[75]. We replace $1/a^3$ by the density $\rho = 4.36 \times 10^{28}$ m^{-3} of the hydrogen sites in naphthalene. Then, using $f = 0.0079$, we can estimate the theoretical linewidth for the present case to be $\delta = 450$ Hz, which roughly explains the experimental linewidth (700 Hz). The difference may be ascribed to the fact that f is not much smaller than 0.01.

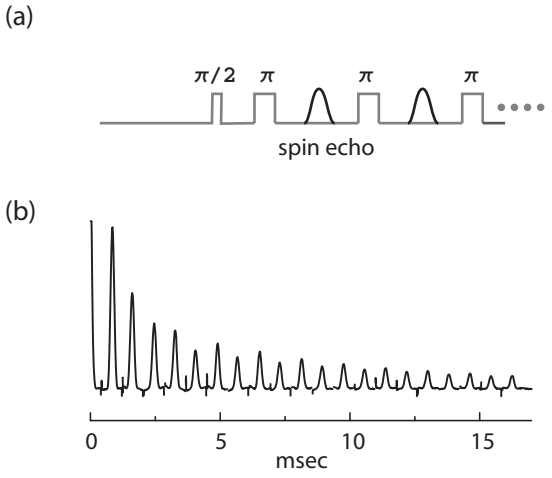

Figure 4.8: (a) A pulse sequence to produce spin echoes in spin systems having inhomogeneous dephasing of FID. (b) Observed spin echo trains of the residual ^{1}H spins in the deuterated naphthalene sample.

In the ^{2}H decoupled spectrum shown in Fig. 4.7(b), a pair of small sideband peaks is

revealed around the main peak. We attribute these to the pair of ^{1}H spins which happen to be adjacent to each other in the dilute ^{1}H system. For an isolated pair of like spins, the resonance line splitting Δ due to the dipolar interaction is given by

$$\Delta = \frac{3}{2}\frac{\mu_0}{4\pi}\frac{\gamma^2\hbar}{r^3}|1-3\cos^2\theta|, \tag{4.4}$$

where r is the internuclear distance and θ is the orientation of the internuclear vector with respect to the static field. For a given crystal orientation, Δ can be calculated using the crystal structure determined by an X-ray diffraction study[69]. Fig. 4.7(c) shows an enlarged figure of the spectrum in Fig. 4.7(b), in which the calculated dipolar splittings are depicted. The spectrum in Fig. 4.7(b) was measured by turning the crystal around the *b*-axis by 48° after the polarization buildup so that the sidebands due to the adjacent β protons (designated as the peak pair 1 in Fig. 4.7(c)) can distinctively be observed from the others. In this crystal orientation, the normal line to the crystal *ab*-plane is tilted by 71° with respect to the static field, and the peak pairs 2-4 are obscured by the strong center line due to the isolated protons. The observed positions of the peak pair 1 agree well with the calculated lines, confirming that the sidebands are assigned to the adjacent β-proton pairs remaining in a deuterated naphthalene molecule.

If we assume that the residual protons are randomly distributed with the fraction of 0.79%, the area intensity of the peak pair 1 should be 0.4% of the main peak intensity. However, as seen from Fig. 4.7(b), the observed percentage is no less than 8.6%. This rate is considerably larger than the value expected for random distribution, indicating the existence of some ordinality in the ^{1}H distribution. Naphthalene is deuterated by boiling it with deuterated sulfuric acid, by which the α positions are more easily deuterated than the β positions. By measuring a ^{1}H NMR spectrum of 99.21% deuterated naphthalene in solution, we actually found that the ^{1}H concentration at the β positions is ca. 2.55 times larger than that at the α positions. However, even if we take account of this, the ratio of the sideband intensity to the main peak intensity is calculated to be only 0.8%, still being an order of magnitude smaller than the measured value. This fact suggests that a deuterated sulfuric acid ion has a tendency to simultaneously replace two α protons in a naphthalene molecule with two deuterons.

Since the polarization is very large, the populations of the eigenstates should be exceedingly toward the ground state, making the doublet amplitudes asymmetric. This asymmetry can be observed not by a 90° pulse but by a small-tip angle pulse as pointed out by Waugh et al. in their very low temperature NMR[76]. Fig. 4.9 shows enlarged ^{1}H spectra obtained under DQ ^{2}H decoupling after the ^{1}H polarization was built up to 0.45 by ICP. When a FID is observed following a 90° pulse, the Fourier transformed spectrum shows no asymmetry as shown in Fig. 4.9(a). On the other hand, as shown in Fig. 4.9(b), the spectrum obtained from a FID following a 4.5° pulse clearly shows the polarization-induced asymmetry. The polarization obtained from this asymmetry is 0.40, which nearly agrees with the polarization (0.45) determined from the ratio of the enhanced magnetization to the thermal equilibrium magnetization.

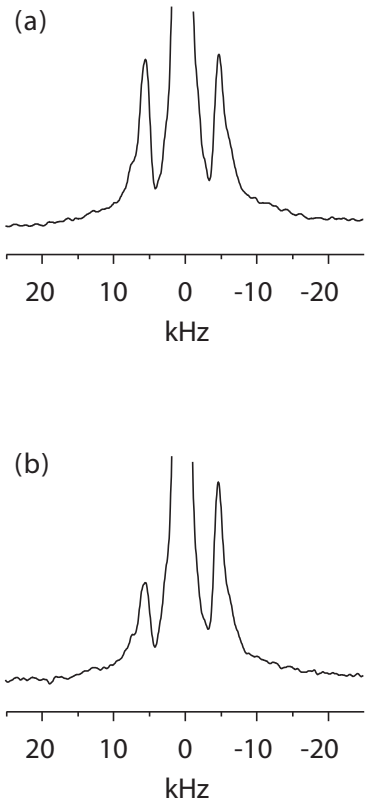

Figure 4.9: ^{2}H double-quantum decoupled ^{1}H spectra (enlarged) of a single crystal sample of 99.21% deuterated naphthalene doped with 0.015 mol% pentacene. (a) Spectrum obtained using a 90° pulse. (b) Spectrum obtained using a 4.5° pulse. The ICP was repeated at a rate of 50 Hz. The ^{1}H resonance frequency is 13.6 MHz, and the temperature is 105 K.

4.3.2 Polarization transfer from triplet electron spins to ^{13}C spins via ^{1}H spins

A ^{13}C nucleus is a spin-$\frac{1}{2}$ nucleus having a gyromagnetic ratio of about one quater that of a ^{1}H spin, and is present in organic materials with a natural abundance of ca. 1%. Here I demonstrate that the large polarization of the triplet electron spins of pentacene can be utilized to polarize the ^{13}C spins in the host molecules. This is achieved by polarizing the ^{1}H spins by ICP at first, and then by transferring the enhanced ^{1}H polarization to the ^{13}C spins by the conventional cross polarization (CP) technique[65, 64], as described in Fig. 4.10.

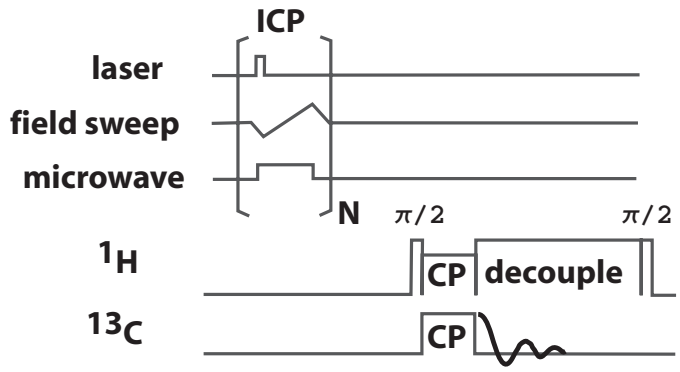

Figure 4.10: A pulse sequence for the enhanced ^{13}C signal detection, in which the ICP sequences is followed by the conventional cross polarization sequence.

Fig. 4.11(a) shows the enhanced ^{13}C signal in pentacene-doped *p*-terphenyl obtained at room temperature in 0.32 T by performing the ^{1}H polarization buildup by the ICP technique, and then by carrying out the conventional CP technique. The successful polarization transfer from the triplet electron spins to the ^{13}C spins via protons can clearly be seen. On the other hand, the thermal equilibrium signal was so weak that it was completely covered with noise (Fig. 4.11(b)). In Fig. 4.11(a) the upfield sweep was performed in the ICP buildup, while in Fig. 4.11(c) the downfield sweep was used, causing the phases of the spectra to be opposite, just as in the case of the result shown in Fig. 4.4 (page 51).

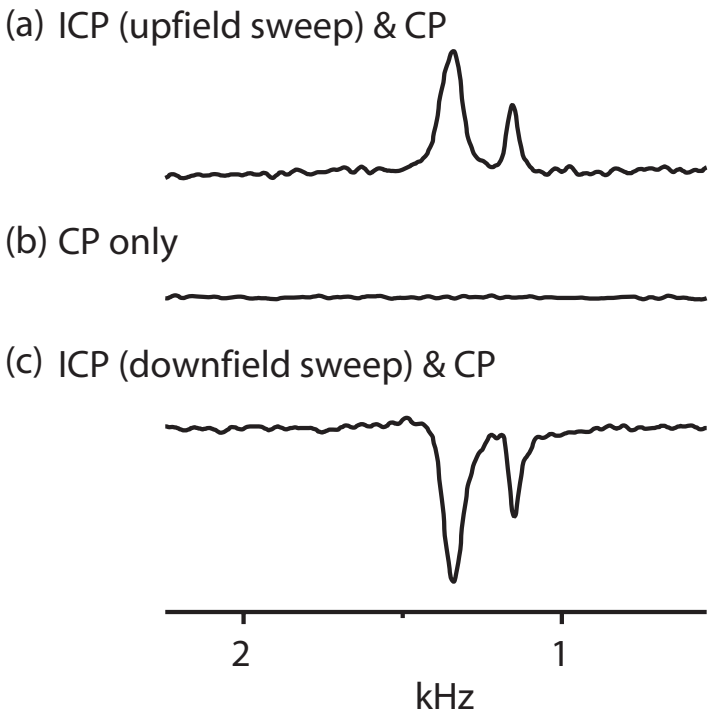

Figure 4.11: ^{13}C spectra of a single crystal sample of pentacene-doped *p*-terphenyl obtained at room temperature in 0.32 T. (a) Enhanced by applying the ICP sequences to polarize ^{1}H spins, and then by transferring the enhanced ^{1}H polarization by the conventional cross polarization (CP) technique. (b) ^{13}C CP spectrum. The ^{1}H thermal equilibrium polarization is so small that the resultant ^{13}C signal became too weak to be appreciable. (c) Enhanced by the same method as (a), except that the field was swept from higher to lower value (downfield sweep). The ^{13}C resonance frequency was 3.42 MHz.

■□■ Sample shuttling between high and low fields ■□■

In NMR experiments being popularly carried out nowadays for the characterization of chemical/biological materials, superconducting magnets are usually used capable of producing a high, stable, and homogeneous magnetic fields. NMR measurements in high magnetic field improves the resolution of spectra, since chemical shift, arising from the shielding effect of magnetic field at the position of nuclei by electrons, is proportional to the external field.

On the other hand, magnetic fields as low as ~ 0.3 T are suitable for the ICP experiments, where an appreciable microwave power suffices to satisfy the Hartmann-Hahn condition between the electron spin in the rotating frame of reference and the ^{1}H spins in the laboratory frame. In order to take advantage of both the high-resolution and the high-sensitivity, we have developed a sample shuttle system, as schematically described in Fig. 4.12. This consists of two magnets; a 4.7 T superconducting magnet for NMR measurements, and a field-variable air-core coil, in which the ^{1}H polarization is built up by ICP. The air-core coil can produce magnetic fields of up to 0.35 T and has a 10 mm gap, through which the laser beam can be irradiated at the sample. The field sweep and the microwave irradiation are performed with a quadrupole coil and a loop-gap resonator.

Fig. 4.13 shows the experimental procedure for the ICP experiment followed by the sample shuttling into the superconducting magnet and the conventional ^{1}H -^{13}C cross polarization measurement, and the enhanced high-field ^{13}C spectrum is demonstrated in Fig. 4.14(b). As compared to the low-field ^{13}C spectrum shown in Fig. 4.14(b), the resolution of the spectrum is considerably improved.

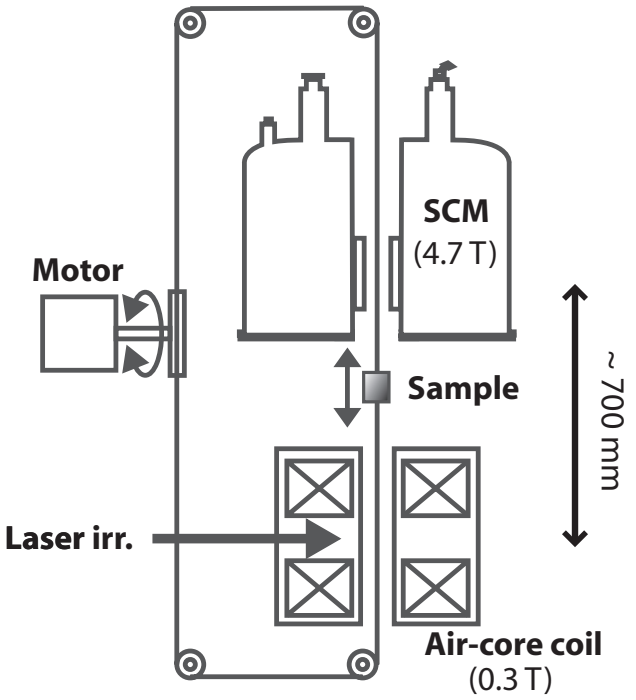

Figure 4.12: Schematic view of a sample shuttle system. This consists of a 4.7 T superconducting magnet (SCM) and a field-variable air-core magnet, between which the sample can be shuttled within $\sim$ 1 sec.

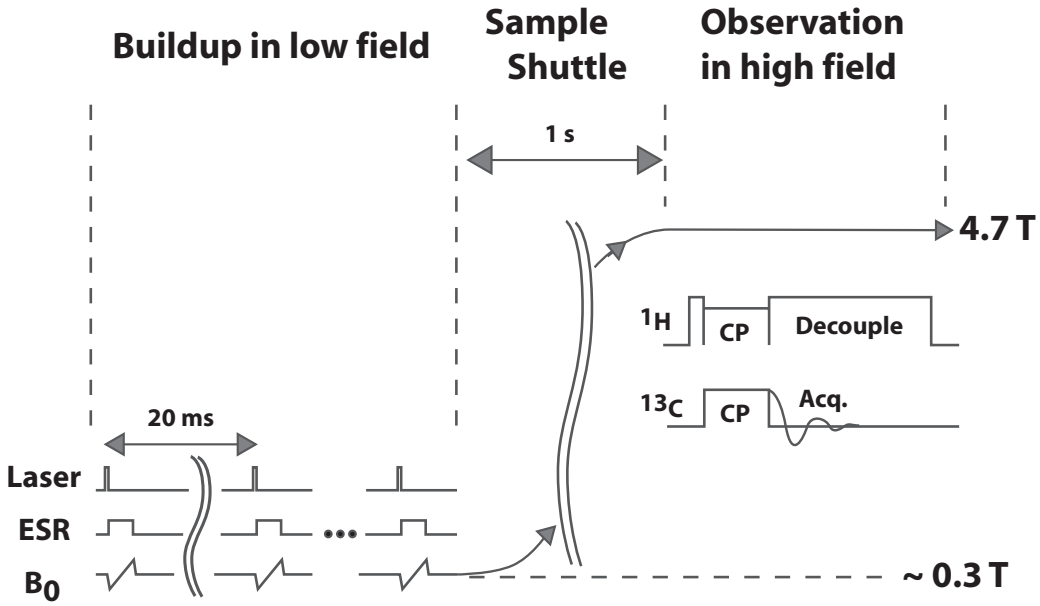

Figure 4.13: An experimental procedure for the ICP buildup in low field followed by the sample shuttling into the high field and the conventional cross polarization ^{1}H -^{13}C double resonance experiment.

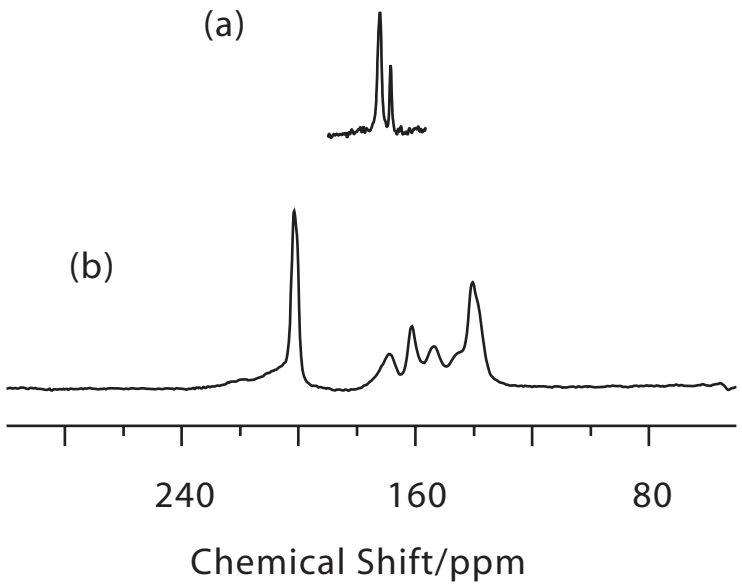

Figure 4.14: (a) ^{13}C NMR spectrum of a single crystal sample of pentacene-doped *p*-terphenyl measured in 0.3 T. (b) ^{13}C NMR spectrum of a single crystal sample of pentacene-doped naphthalene measured in 4.7 T. The NMR frequencies are 3.4 and 50 MHz for (a) and (b), respectively.

Chapter 5

Toward better understanding of DNP by photo-excited triplet electron spins

In the previous chapter, I demonstrated that the ^{1}H polarization has successfully built up to the ultimate value attainable using the triplet electron spins of pentacene. Moreover, the time required to polarize ^{1}H spins became shorter than the previous works. Thus, this result gives the answer “Yes.” to the first question (Q1) I have posed at the end of Chapter 1 (page 8). The successful buildup is ascribed to that the experimental parameters were carefully optimized so as to realize the efficient buildup of ^{1}H polarization. In this chapter, I attempt to make a quantitative account for the experimental results in order to answer the second question (Q2) on the mechanism that govern the buildup behavior. This question is closely related to the first question on the possibility of improving the buildup efficiency; once one has a firm grip on a set of the basic processes lying behind the buildup behavior, one would be able to predict the best experimental condition that maximizes the buildup efficiency.

5.1 A model for the buildup process

■□■ The first property ■□■

A proper model for the description of the buildup behavior should incorporate two properties. First, the polarization transfer by ICP should occur only between the triplet electron spin and the ^{1}H spin relatively close to each other, since the dipolar interaction, which contributes to the polarization transfer, decreases as the cube of the distance between them. With the pentacene concentrations of the samples used in this work, the most distant ^{1}H spin from the electron spin is apart by several nanometers, whereas the nearest one, belonging to the pentacene guest molecule itself, is at a distance of about only 0.1 nm. Hence, the nearer ^{1}H spins should be much more likely to be polarized than the farther ones. In the following I shall argue, with some experimental supports, that the direct polarization transfer from the triplet electron spin to the ^{1}H spins mainly takes place *within* the pentacene guest molecules.

In order to compare the efficiency of the intramolecular polarization transfer with that of the intermolecular polarization transfer, we examined how the ICP parameters (the field-sweep width and the field-sweep time) affect the initial buildup rate for three different samples: pentacene-doped naphthalene (sample A), pentacene-doped deuterated-naphthalene (sample B), and deuterated-pentacene-doped naphthalene (sample C).

As shown in Fig. 5.1(a) and 5.1(b), deuteration of the host naphthalene does not affect the optimal ICP conditions (the sweep width of 7.2 mT and the sweep time of 15 μs). This indicates that the direct polarization transfer by ICP occurs within the pentacene molecule. On the other hand, in sample C, where intramolecular electron-to-^{1}H polarization transfer is obviously impossible, the buildup of the host naphthalene was much less efficient than in sample A for the same sweep parameters (not shown). Even when the optimal sweep parameters were used for sample C (the sweep width of 2.4 mT and the sweep time of 140 μs), the initial buildup rate was still an order of magnitude smaller than that in the case of sample A.

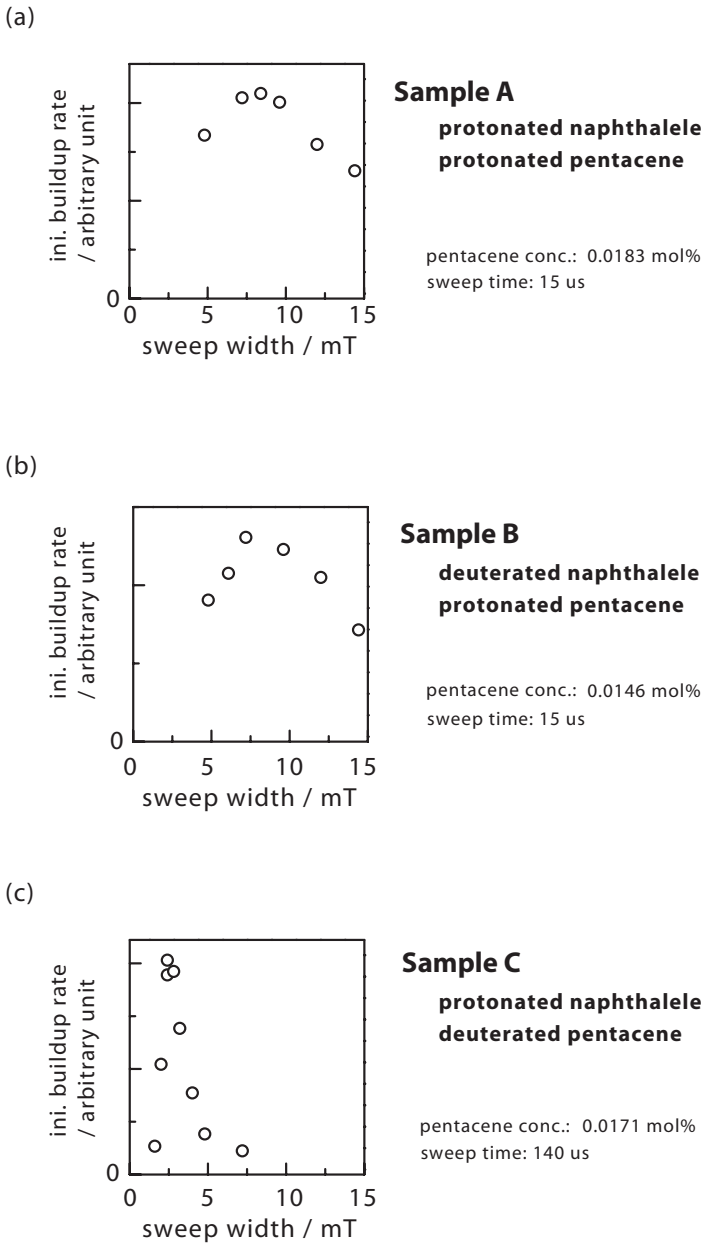

Figure 5.1: Sweep width dependence of the initial buildup rate of ^{1}H polarization for (a) sample A, (b) sample B, and (c) sample C. The optimized sweep times are 15, 15, 140 μs for sample A, B, and C, respectively

The fact that the optimal sweep conditions are the same for sample A and sample B, together with the much less efficient intermolecular polarization transfer observed in sample C, strongly supports the idea that the direct electron-to-^{1}H polarization transfer mainly takes place within the pentacene molecules during the buildup experiments.

■□■ The second property ■□■

It is not that the distant protons cannot be polarized at all; on the contrary, they can actually be polarized no less than the nearby ^{1}H spins can. It is well known that in proton-rich solids, ^{1}H polarization is transported by a mechanism called *spin diffusion*. Thus, the second feature required for a proper model is that it has to take account of the effect of spin diffusion. At first, the ^{1}H polarization created by ICP should be localized at the pentacene guest molecules. Then, it should spread over farther host naphthalene molecules by spin diffusion (Fig. 5.2). Therefore, all the ^{1}H spins, including the distant as well as the nearby ones, can be polarized simply by repeating the ICP sequences, because spin diffusion transports the ^{1}H polarization during the intervals of the ICP sequences (Fig. 5.3).

■□■ Structure of this Chapter ■□■

In order to reproduce the experimental buildup curve by simulation, I divide the problem into three parts:

- **Step 1:** In Section 5.2, I evaluate the efficiency of the intramolecular polarization transfer by ICP, focusing on a single pentacene molecule in the photo-excited triplet state, in which the triplet electron spin exchanges its polarization with the 14 protons under the action of an ICP sequence, and dealing with what happens within the field-sweep time. In this step, all the other protons on the host naphthalene molecules are ignored.

- **Step 2:** In Section 5.3, I evaluate the ^{1}H spin diffusion constants for both undeuterated and deuterated naphthalene.

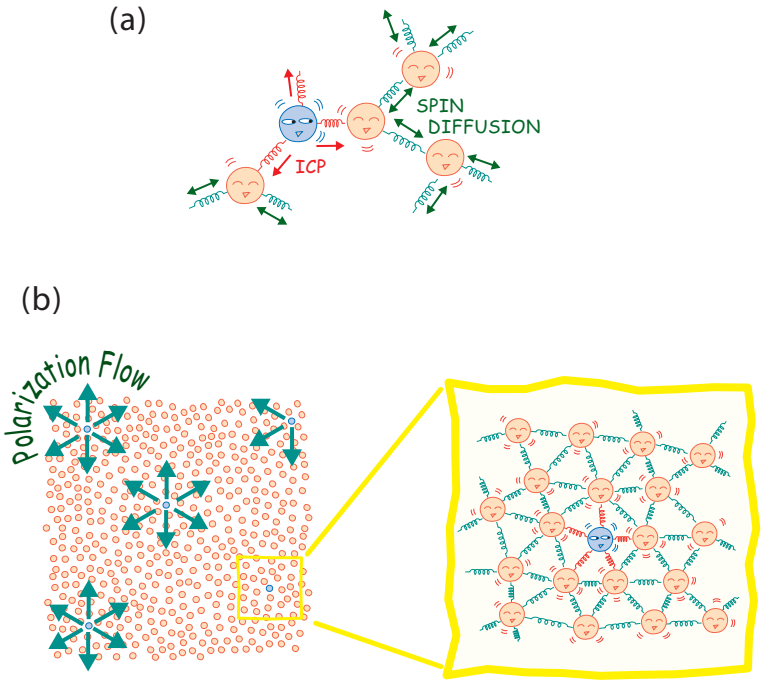

Figure 5.2: (a) The triplet electron spin, depicted schematically by a blue circle, transfers its large polarization to nearby protons (red circles) by ICP. Then, the enhanced ^{1}H polarization is further transported by spin diffusion driven by dipolar interaction among ^{1}H spins. (b) In a larger scale, spin polarization created at the electron site is diffused over the whole sample volume.

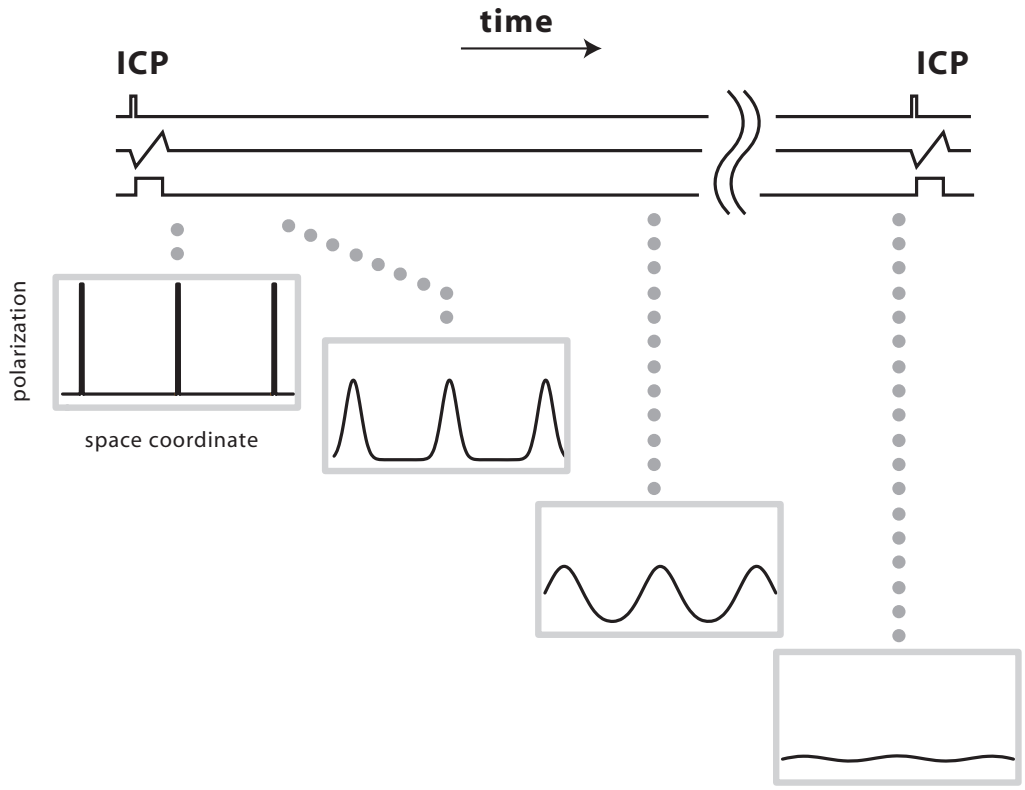

Figure 5.3: During the interval of each ICP sequence, spin diffusion smooth out the localized polarization created at near the triplet electrons. Thus all ^{1}H spins, including the distant as well as near ones, can be polarized simply by repeating the ICP sequences.

- **Step 3:** In Section 5.4, I simulate the buildup process using the parameters evaluated in Section 5.2 and 5.3, treating a long-time behavior and consider much larger volume containing sufficiently large number of pentacene molecules so that the pentacene molecules can be thought of as uniformly-distributed point sources of spin polarization, from which the polarization is diffused over the whole sample volume.

5.2 Intramolecular polarization transfer from a triplet electron spin to nuclear spins

5.2.1 Extraction of the flip-flop term that causes the polarization transfer

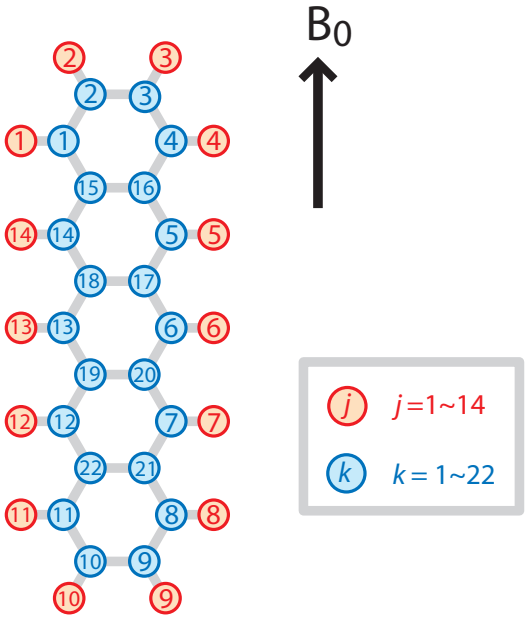

Figure 5.4: Numbering of the hydrogen atomic sites ($j = 1 \sim 14$) and the carbon atomic sites ($k = 1 \sim 22$) on a pentacene molecule.

■□■ Hamiltonian during an ICP sequence ■□■

Consider a pentacene molecule with its long molecular axis being parallel to the external magnetic field (Fig. 5.4), and suppose that microwave irradiation is applied together with a field sweep of width B_s and duration τ_s, so that the external field changes in time according to

$$B_0(t) = B_0 \pm \frac{B_s}{\tau_s}\left(t - \frac{\tau_s}{2}\right), \tag{5.1}$$

where the plus and the minus sign correspond to the upfield and downfield sweep, respectively. We are interested in what happens to a spin system consisting of an triplet electron spin S (=1) and ^{1}H spins $I^j (j = 1, 2, \cdots, 14)$ during the sweep. The time evolution of the system is driven by the Hamiltonian

$$\mathscr{H} = \mathscr{H}_{ZI} + \mathscr{H}_{ZS} + \mathscr{H}_{\rm ZFS} + \mathscr{H}_{\rm HF}^{\rm iso} + \mathscr{H}_{\rm HF}^{\rm aniso} + \mathscr{H}_{\rm mw} + \mathscr{H}_{\rm D}^{II}, \tag{5.2}$$

which includes the Zeeman interaction $\mathscr{H}_{ZI}$ and $\mathscr{H}_{ZS}$ for the I and the S spins, the ZFS interaction $\mathscr{H}_{\rm ZFS}$ (see Eq. (2.1)-(2.13) (page 14$\sim$)), the isotropic hyperfine coupling $\mathscr{H}_{\rm HF}^{\rm iso}$ (see Eq. (2.15) (page 19)), the anisotropic hyperfine coupling $\mathscr{H}_{\rm HF}^{\rm iso}$ (see Eq. (2.17) (page 20)), the interaction between the S spin and the microwave radiation $\mathscr{H}_{\rm mw}$, and the dipolar interaction $\mathscr{H}_{\rm D}^{II}$ among the ^{1}H spins. As we shall see later, the ^{1}H -^{1}H dipolar interaction has only a little effect on the evolution of the system during the field-sweep time of about 15 μs, and is neglected henceforth. When the system is viewed from the rotating frame for the S spin and from the laboratory frame for the I spins, the apparent microwave field becomes stationary for the S spin, and all the other terms that do not commute with the operator S_Z rapidly oscillate and do not affect the evolution of the system in first order. Thus, the Hamiltonian $\mathscr{H}_{\rm R}$, viewed in the rotating frame for the S spin and in the laboratory frame for the I spins, can be expressed as

$$\begin{aligned}
\mathscr{H}_{\rm R} &= -\omega_I(t)\sum_j I_Z^j - [\omega_S(t) - \omega]S_Z \\
&\quad + \omega_{\rm ZFS}\left[S_Z^2 - \frac{1}{3}S(S+1)\right] \\
&\quad + \sum_{j,k}\left[(Q_{jk} + A_{jk})I_Z^j + (C_{jk}I_+^j + C_{jk}^* I_-^j)\right]S_Z \\
&\quad + \omega_1 S_X,
\end{aligned} \tag{5.3}$$

where

$$\omega_S(t) = \gamma_S B_0(t), \tag{5.4}$$

$$\omega_I(t) = \gamma_I B_0(t), \tag{5.5}$$

$$\omega_{\mathrm{ZFS}} = \frac{1}{2}D(1-3\cos^2\Theta)+\frac{3}{2}E\sin^2\Theta\cos 2\Phi, \tag{5.6}$$

$$Q_{jk} = \delta_{jk}\rho_k\gamma_S B_{\mathrm{C}}, \tag{5.7}$$

$$A_{jk} = \rho_k d_{jk}(1-3\cos^2\theta_{jk}), \tag{5.8}$$

$$C_{jk} = -\frac{3}{2}\rho_k d_{jk}\sin\theta_{jk}\cos\theta_{jk}e^{-i\phi_{jk}}, \tag{5.9}$$

$$d_{jk} = \left(\frac{\mu_0}{4\pi}\right)\gamma_I\gamma_S\hbar r_{jk}^{-3}. \tag{5.10}$$

(Θ,Φ) is the orientation of the ZFS tensor with respect to the external field. When the long axis of the pentacene molecule aligns along the external field, $(\Theta,\Phi)=(90^\circ,0^\circ)$. r_{jk} is the distance between the kth carbon site and the jth proton site in pentacene, and θ_{jk} and ϕ_{jk} are the elevation and the azimuth of the vector connecting them. ρ_k is the spin density at the kth carbon site (see page 19)[61]. The values for r_{jk}, ρ_k, and θ_{jk} are summarized in Table 5.1-5.3.

■□■ Fictitious spin $\frac{1}{2}$ formalism ■□■

We are interested in the situation in which the microwave frequency ω is close to either of the two resonance frequencies of the triplet-electron spin. In order to focus on the two energy levels between which the transition occurs, it is convenient to use a fictitious spin $\frac{1}{2}$ formalism [64, 77] to the triplet electron spin S. For a three-level system labelled by $|1\rangle$, $|2\rangle$, and $|3\rangle$, the

	Proton site (j)													
Carbon site (k)	$j=1$	2	3	4	5	6	7	8	9	10	11	12	13	14
$k=1$	1.1	2.43	3.7	4.2	4.85	6.41	8.4	10.6	12.4	12.1	9.76	7.36	4.97	2.66
2	2.17	1.33	2.42	3.7	5.05	7.	9.18	11.5	13.5	13.3	11.1	8.68	6.32	4.06
3	3.42	2.3	1.4	2.42	4.2	6.42	8.74	11.1	13.4	13.5	11.4	9.07	6.85	4.84
4	3.9	3.59	2.42	1.4	2.8	5.05	7.41	9.8	12.1	12.4	10.5	8.25	6.22	4.59
5	4.59	5.53	4.85	2.8	1.4	2.8	5.05	7.41	9.7	10.1	8.25	6.22	4.59	3.9
6	6.22	7.74	7.27	5.05	2.8	1.4	2.8	5.05	7.27	7.74	6.22	4.59	3.9	4.59
7	8.25	10.1	9.7	7.41	5.05	2.8	1.4	2.8	4.85	5.53	4.59	3.9	4.59	6.22
8	10.5	12.4	12.1	9.8	7.41	5.05	2.8	1.4	2.42	3.59	3.9	4.59	6.22	8.25
9	11.4	13.5	13.4	11.1	8.74	6.42	4.2	2.42	1.4	2.3	3.42	4.84	6.85	9.07
10	11.1	13.3	13.5	11.5	9.18	7.	5.05	3.7	2.42	1.33	2.17	4.06	6.32	8.68
11	9.76	12.1	12.4	10.6	8.4	6.41	4.85	4.2	3.7	2.43	1.1	2.66	4.97	7.36
12	7.36	9.7	10.1	8.4	6.41	4.85	4.2	4.85	5.6	4.85	2.66	1.1	2.66	4.97
13	4.97	7.28	7.79	6.41	4.85	4.2	4.85	6.41	7.79	7.28	4.97	2.66	1.1	2.66
14	2.66	4.85	5.6	4.85	4.2	4.85	6.41	8.4	10.1	9.7	7.36	4.97	2.66	1.1
15	2.17	3.68	4.2	3.7	3.7	5.05	7.	9.18	11.1	10.9	8.68	6.32	4.06	2.17
16	3.42	4.13	3.7	2.42	2.42	4.2	6.42	8.74	10.9	11.1	9.07	6.85	4.84	3.42
17	4.84	6.37	6.1	4.2	2.42	2.42	4.2	6.42	8.51	8.71	6.85	4.84	3.42	3.42
18	4.06	6.09	6.41	5.05	3.7	3.7	5.05	7.	8.74	8.5	6.32	4.06	2.17	2.17
19	6.32	8.5	8.74	7.	5.05	3.7	3.7	5.05	6.41	6.09	4.06	2.17	2.17	4.06
20	6.85	8.71	8.51	6.42	4.2	2.42	2.42	4.2	6.1	6.37	4.84	3.42	3.42	4.84
21	9.07	11.1	10.9	8.74	6.42	4.2	2.42	2.42	3.7	4.13	3.42	3.42	4.84	6.85
22	8.68	10.9	11.1	9.18	7.	5.05	3.7	3.7	4.2	3.68	2.17	2.17	4.06	6.32

Table 5.1: The distances r_{jk} (in Å) between the jth hydrogen atomic site and the kth carbon atomic site on a pentacene molecule. It is assumed that the length of each edge of hexagonal aromaric ring is 1.4 Å, and the carbon-hydrogen bond length is 1.1 Å.

k	ρ_k	k	ρ_k
1	0.045	12	0.128
2	0.025	13	0.188
3	0.025	14	0.128
4	0.045	15	-0.015
5	0.128	16	-0.015
6	0.188	17	-0.021
7	0.128	18	-0.021
8	0.045	19	-0.021
9	0.025	20	-0.021
10	0.025	21	-0.015
11	0.045	22	-0.015

Table 5.2: Spin densities ρ_k calculated by T.-S.T. Lin et al. [61] for the triplet electron of pentacene.

fictitious spin $\frac{1}{2}$ operators are defined as

$$\begin{aligned} S_X^{r-s} &= \frac{1}{2}(|r\rangle\langle s| + |s\rangle\langle r|), \\ S_Y^{r-s} &= -\frac{i}{2}(|r\rangle\langle s| - |s\rangle\langle r|), \qquad (5.11) \\ S_Z^{r-s} &= \frac{1}{2}(|r\rangle\langle r| - |s\rangle\langle s|), \end{aligned}$$

(5.12)

where $r,s = 1,2,3$. From Eqs. (5.12), the following commutation relations are obtained.

$$\left[S_X^{r-s}, S_Y^{r-s}\right] = iS_Z^{r-s}, \quad \left[S_Y^{r-s}, S_Z^{r-s}\right] = iS_X^{r-s}, \quad \left[S_Z^{r-s}, S_X^{r-s}\right] = iS_Y^{r-s}, \qquad (5.13)$$

$$\left[S_X^{r-t}, S_X^{s-t}\right] = \left[S_Y^{r-t}, S_Y^{s-t}\right] = \frac{i}{2}S_Y^{r-s}, \qquad (5.14)$$

$$\left[S_Z^{r-t}, S_Z^{s-t}\right] = 0, \qquad (5.15)$$

$$\left[S_X^{r-t}, S_Y^{s-t}\right] = \frac{i}{2}S_X^{r-s}, \qquad (5.16)$$

$$\left[S_X^{r-t}, S_Z^{s-t}\right] = -\frac{i}{2}S_Y^{r-t}, \qquad (5.17)$$

$$\left[S_Y^{r-t}, S_Z^{s-t}\right] = \frac{i}{2}S_X^{r-t}. \qquad (5.18)$$

	Proton site (j)													
Carbon site (k)	$j=1$	2	3	4	5	6	7	8	9	10	11	12	13	14
$k=1$	90.0	3.96	50.8	90.0	122	141	152	158	167	179	174	171	167	156
2	124	30.0	64.0	111	139	152	159	164	172	178	171	168	163	154
3	111	64.0	30.0	124	154	163	168	171	178	172	164	159	152	139
4	90.0	50.8	3.96	90.0	156	167	171	174	179	167	158	152	141	122
5	58.1	30.0	1.87	24.4	90.0	156	167	171	179	164	152	141	122	90.0
6	38.8	20.7	1.22	12.8	24.4	90.0	156	167	179	159	141	122	90.0	58.1
7	28.2	15.7	0.910	8.60	12.8	24.4	90.0	156	178	150	122	90.0	58.1	38.8
8	21.9	12.6	0.724	6.47	8.60	12.8	24.4	90.0	176	129	90.0	58.1	38.8	28.2
9	16.3	8.48	2.41	9.37	12.0	16.5	26.3	56.0	150	116	69.2	41.3	27.8	20.7
10	9.37	2.41	8.48	16.3	20.7	27.8	41.3	69.2	116	150	56.0	26.3	16.5	12.0
11	6.47	0.724	12.6	21.9	28.2	38.8	58.1	90.0	129	176	90.0	24.4	12.8	8.60
12	8.60	0.910	15.7	28.2	38.8	58.1	90.0	122	150	178	156	90.0	24.4	12.8
13	12.8	1.22	20.7	38.8	58.1	90.0	122	141	159	179	167	156	90.0	24.4
14	24.4	1.87	30.0	58.1	90.0	122	141	152	164	179	171	167	156	90.0
15	56.0	9.25	30.0	69.2	111	139	152	159	170	177	168	163	154	124
16	69.2	30.0	9.25	56.0	124	154	163	168	177	170	159	152	139	111
17	41.3	18.6	5.41	26.3	56.0	124	154	163	176	167	152	139	111	69.2
18	26.3	5.41	18.6	41.3	69.2	111	139	152	167	176	163	154	124	56.0
19	16.5	3.82	13.3	27.8	41.3	69.2	111	139	161	175	154	124	56.0	26.3
20	27.8	13.3	3.82	16.5	26.3	56.0	124	154	175	161	139	111	69.2	41.3
21	20.7	10.4	2.96	12.0	16.5	26.3	56.0	124	171	150	111	69.2	41.3	27.8
22	12.0	2.96	10.4	20.7	27.8	41.3	69.2	111	150	171	124	56.0	26.3	16.5

Table 5.3: The angles θ_{jk} (in degree) of the vector connecting the jth hydrogen atomic site and the kth carbon atomic site with respect to the external field aligned along the long molecular axis of pentacene. It is assumed that the length of each edge of hexagonal aromaric ring is 1.4 Å, and the carbon-hydrogen bond length is 1.1 Å.

Using these fictitious spin $\frac{1}{2}$ operators, the spin operators S_X, S_Y, and S_Z can be expressed as

$$\begin{aligned} S_X &= \sqrt{2}(S_X^{1-2} + S_X^{2-3}), \\ S_Y &= \sqrt{2}(S_Y^{1-2} + S_Y^{2-3}), \\ S_Z &= 2(S_Z^{1-2} + S_Z^{2-3}) = 2S_Z^{1-3}. \end{aligned} \tag{5.19}$$

(5.20)

Then, the Hamiltonian $\mathscr{H}_{\mathrm{R}}$ is rewritten as

$$\begin{aligned} \mathscr{H}_{\mathrm{R}} &= 2(\omega_{\mathrm{S}}(t) - \omega)S_Z^{1-3} + \frac{2}{3}\omega_{\mathrm{ZFS}}(S_Z^{1-2} - S_Z^{2-3}) + \sqrt{2}\omega_1(S_X^{1-2} + S_Z^{2-3}) \\ &\quad + 2\sum_{j,k}\left[(Q_{jk} + A_{jk})I_Z^j + (C_{jk}I_+^j + C_{jk}^* I_-^j)\right] S_Z^{1-3} \\ &\quad + \omega_I(t)\sum_j I_Z^j. \end{aligned} \tag{5.21}$$

■□■ *Case (a):* $\omega \sim \omega_{\mathrm{S}}(t) + \omega_{\mathrm{ZFS}}$ ■□■

In this case, S_Z^{2-3} can safely be neglected because it connects the levels 2 and 3 whose energy is separated by $2\omega_{\mathrm{ZFS}}$, which is assumed to be much larger than $\sqrt{2}\omega_1$. Using the resonance offset $\Delta\omega(t) = \omega_{\mathrm{S}}(t) + \omega_{\mathrm{ZFS}} - \omega$, Eq. (5.21) is rewritten as

$$\begin{aligned} \mathscr{H}_{\mathrm{R}} &= \left[\Delta\omega(t) - \frac{4}{3}\omega_{\mathrm{ZFS}}\right](S_Z^{1-3} + S_Z^{2-3}) \\ &\quad + \Delta\omega(t)S_Z^{1-2} + \sqrt{2}\omega_1 S_X^{1-2} \\ &\quad + 2\sum_{j,k}\left[(Q_{jk} + A_{jk})I_Z^j + (C_{jk}I_+^j + C_{jk}^* I_-^j)\right] S_Z^{1-3} \\ &\quad + \omega_I\sum_j I_Z^j. \end{aligned} \tag{5.22}$$

The first term $(S_Z^{1-3} + S_Z^{2-3})$ can be dropped, since it commutes with every other terms.

Now let us consider a new reference frame in which Z-axis points in the direction of the effective field for the S spin. During an ICP sequence, the direction of the effective field changes in time as pictured in Fig. 2.12, and we have seen that the electron magnetization will be locked along the effective field if the adiabatic condition is satisfied (page 29), that is, if the rate of

the change in the direction of the effective field is sufficiently slow compared to the effective precession frequency. The transformation into the new frame is accomplished by tilting the system around the Y-axis by an angle α given by

$$\alpha(t) = \tan^{-1}\left[\frac{\sqrt{2}\omega_1}{\Delta\omega(t)}\right]. \tag{5.23}$$

In this "tilted" frame, the electron magnetization always points in the Z direction. Mathematically, the transformation of the Hamiltonian $\mathscr{H}_{\rm R}$ into the tilted frame can be expressed by the interaction representation with respect to $\alpha(t)S_Y^{1-2}$ as

$$\mathscr{H}_{\rm TR} = \exp\left[i\alpha(t)S_Y^{1-2}\right]\mathscr{H}_{\rm R}\exp\left[-i\alpha(t)S_Y^{1-2}\right], \tag{5.24}$$

which leads to

$$\begin{aligned}\mathscr{H}_{\rm TR} &= \omega_{eS}S_Z^{1-2} + \omega_I\sum_j I_Z^j \\ &\quad +2\sum_{j,k}(Q_{jk}+A_{jk})I_Z^j\left[S_Z^{1-3} + \frac{1}{2}(-1+\cos\alpha)S_Z^{1-2} - \frac{1}{2}\sin\alpha S_X^{1-2}\right] \\ &\quad +2\sum_{j,k}(C_{jk}I_+^j + C_{jk}^* I_-^j)\left[S_Z^{1-3} + \frac{1}{2}(-1+\cos\alpha)S_Z^{1-2} - \frac{1}{2}\sin\alpha S_X^{1-2}\right].\end{aligned} \tag{5.25}$$

In the above calculation, I used

$$\exp[i\alpha S_Y^{1-2}]S_Z^{1-3}\exp[-i\alpha S_Y^{1-2}] = S_Z^{1-3} + \frac{1}{2}(-1+\cos\alpha)S_Z^{1-2} - \frac{1}{2}\sin\alpha S_X^{1-2}, \tag{5.26}$$

which can be proved using the commutators (Eqs. (5.13) and (5.18)).

In order to envision the exchange of the spin states between the S and the I spins by cross polarization, further transformation is performed on $\mathscr{H}_{\rm TR}$ into the interaction representation

$\widetilde{\mathscr{H}_{\mathrm{TR}}}$ with respect to the Zeeman term $(\omega_{eS}S_Z^{1-2}+\omega_I\sum_j I_Z^j)$ in Eq. 5.25, yielding

$$\begin{aligned}
\widetilde{\mathscr{H}_{\mathrm{TR}}} &= 2\sum_{j,k}(Q_{jk}+A_{jk})I_Z^jS_Z^{1-3} \\
&\quad -(1-\cos\alpha)\sum_{j,k}(Q_{jk}+A_{jk})I_Z^jS_Z^{1-2} \\
&\quad -\frac{1}{2}\sin\alpha\sum_{j,k}(Q_{jk}+A_{jk})I_Z^j\left[\exp(i\omega_{eS}(t)t)S_+^{1-2}+\exp(-i\omega_{eS}(t)t)S_-^{1-2}\right] \\
&\quad +2\sum_{j,k}(C_{jk}\exp(i\omega_I(t)t)I_+^j+C_{jk}^*\exp(-i\omega_I(t)t)I_-^j)S_Z^{1-3} \\
&\quad -(1-\cos\alpha)\sum_{j,k}(C_{jk}\exp(i\omega_I(t)t)I_+^j+C_{jk}^*\exp(-i\omega_I(t)t)I_-^j)S_Z^{1-3} \\
&\quad -\frac{1}{2}\sin\alpha\sum_{jk}(C_{jk}\exp(i\Delta(t)t)I_+^jS_-^{1-2}+C_{jk}^*\exp(-i\Delta(t)t)I_-^jS_+^{1-2}) \\
&\quad -\frac{1}{2}\sin\alpha\sum_{jk}(C_{jk}\exp(i\Sigma(t)t)I_+^jS_+^{1-2}+C_{jk}^*\exp(-i\Sigma(t)t)I_-^jS_-^{1-2}), \qquad (5.27)
\end{aligned}$$

where

$$\Delta(t) = \omega_I(t)-\omega_{eS}(t), \qquad (5.28)$$

$$\Sigma(t) = \omega_I(t)+\omega_{eS}(t). \qquad (5.29)$$

Since the oscillating terms do not have first-order contributions to the time evolution of the system, all time-dependent terms may be dropped except for $\exp[i\Delta(t)t]$, because $\Delta(t)$ can be zero and thus $\exp[i\Delta(t)t]$ can be time-independent when the condition

$$\Delta(t)=0 \qquad \text{or} \qquad \omega_I(t)-\omega_{eS}(t)=0 \qquad (5.30)$$

is satisfied. Therefore, we arrive at the final form

$$\begin{aligned}
\widetilde{\mathscr{H}_{\mathrm{TR}}} &= 2\sum_{j,k}(Q_{jk}+A_{jk})I_Z^jS_Z^{1-3} \\
&\quad -(1-\cos\alpha)\sum_{jk}(Q_{jk}+A_{jk})I_Z^jS_Z^{1-2} \\
&\quad -\frac{1}{2}\sin\alpha\sum_{jk}(C_{jk}\exp(i\Delta(t)t)I_+^jS_-^{1-2}+C_{jk}^*\exp(-i\Delta(t)t)I_-^jS_+^{1-2}). \qquad (5.31)
\end{aligned}$$

Eq. (5.30) is the condition for the Hartmann-Hahn matching, whose intuitive explanation was given in Chapter 2 (page 23).

■□■ *Case (b):* $\omega \sim \omega_S(t) - \omega_{\rm ZFS}$ ■□■

In the case that the microwave frequency ω is close to the resonance condition between the substates $|2\rangle$ and $|3\rangle$, a similar procedure leads to the Hamiltonian in the interaction frame expressed as

$$\begin{aligned}\widetilde{\mathscr{H}_{\rm TR}} &= 2\sum_{j,k}(Q_{jk}+A_{jk})I_Z^j S_Z^{1-3} \\ &\quad -(1-\cos\alpha)\sum_{jk}(Q_{jk}+A_{jk})I_Z^j S_Z^{2-3} \\ &\quad -\frac{1}{2}\sin\alpha\sum_{jk}(C_{jk}\exp(i\Delta(t)t)I_+^j S_-^{2-3}+C_{jk}^*\exp(-i\Delta(t)t)I_-^j S_+^{2-3}), \qquad (5.32)\end{aligned}$$

where $\Delta\omega(t)$, which is implicitly included in $\omega_{eS}(t)$ and thereby $\Delta(t)$, is defined by $\Delta\omega(t) = \omega_S(t) - \omega_{\rm ZFS} - \omega$.

■□■ Which ^{1}H spins are likely to be polarized by ICP? ■□■

When the Hartmann-Hahn condition is satisfied, the exchange of the spin states, and therefore the polarization transfer from the electron to the ^{1}H spins, is driven by the flip-flop term $I_\pm^j S_\mp^{r-s}$ in Eq. (5.31) or Eq. (5.32). The efficiency of the polarization transfer is determined by the flip-flop coefficients $\sin\alpha$ and C_{jk}. Since the latter depends on j, some ^{1}H spins should be more likely to exchange polarization with the triplet electron spin. Table 5.4 summerizes the probability amplitudes $|\sum_k C_{jk}|^2$ for the flip-flop transition between the jth ^{1}H spin and the electron spin for the case of a pentacene molecule with its long molecular axis being parallel to the external field.

As we can see from Table 5.4, the flip-flop is the most efficient for the protons 2, 3, 9, 10 located at both ends of the pentacene molecule, while the transition probabilities are much smaller for the other protons. This is explained by the fact that the vectors connecting these ^{1}H spins to their nearest fractional electron spins are the right angles to the external field, so that $\sin\theta_{jj}\cos\theta_{jj}$ vanishes in Eq. (5.9).

On the other hand, the term $(Q_{jk}+A_{jk})$ in Eq. (5.31) or Eq. (5.32) do not have any

Proton site (j)													
$j=1$	2	3	4	5	6	7	8	9	10	11	12	13	14
0.0363	1.52	1.52	0.0363	0.148	0.00	0.148	0.363	1.51	1.51	0.0363	0.148	0.00	0.148

Table 5.4: Values for $|\sum_k C_{jk}|^2/(2\pi)^2$ (in MHz^2) when the long molecular axis of the pentacene molecule is parallel to the external field.

Proton site (j)													
$j=1$	2	3	4	5	6	7	8	9	10	11	12	13	14
-4.59	1.24	1.24	-4.59	-14.4	-21.9	-14.4	-4.59	1.24	1.24	-4.59	-14.4	-21.9	-14.4

Table 5.5: Values for $\sum_k (Q_{jk}+A_{jk})/(2\pi)$ (in MHz) when the long molecular axis of the pentacene molecule is parallel to the external field..

contribution to the exchange, and the only effect is to shift the resonance conditions. The shift felt by each ^{1}H spin are summarized in Table 5.5, from which the resonance shift is found to be the greatest for the protons 6,13 located at the middle of the pentacene molecule. This is mainly due to the larger triplet-electron spin densities at the carbon atomic sites 6 and 13.

5.2.2 Simulation of the polarization transfer by ICP

■□■ Procedure ■□■

Unfortunately, with one triplet-electron spin $S(=1)$ and 14 ^{1}H spins $I(=\frac{1}{2})$, the representation of the operators requires $49,152 \times 49,152$ complex matrices, being too huge to be handled by current personal computers, and accordingly I considered only four ^{1}H spins out of the 14 hydrogen sites on a pentacene molecule. (Simulations taking account of more protons are currently being worked out, but they consume a large amount of computer memory and will take a long time.) The procedure of the simulations are as follows:

- In the simulation, only the protons 3,4,5,6 (see Fig. 5.4 on page 71) were considered.

Thus, the system considered here consists of four protons (spin-$\frac{1}{2}$) and one triplet electron spin (spin-1), and the operators are represented by 48×48 complex matrices.

- The long axis of the pentacene molecule was assumed to be parallel to the external field.
- The initial populations on the sublevels $(|1\rangle, |2\rangle, |3\rangle)$ of the triplet electron were assumed to be $(0.12, 0.76, 0.12)$[40], and the decay of the triplet state and the population changes due to electron spin-lattice relaxation were ignored.
- Initially, the ^{1}H polarization was assumed to be zero for all four protons, and the ^{1}H spin-lattice relaxation was neglected.
- Setting the initial density operator ρ of the system as

$$\rho = \rho_S \otimes \rho_I, \tag{5.33}$$

$$\rho_S = 0.12|1\rangle\langle 1| + 0.76|2\rangle\langle 2| + 0.12|3\rangle\langle 3|, \tag{5.34}$$

$$\rho_I = 0.5|\tfrac{1}{2}\rangle\langle\tfrac{1}{2}| + 0.5|-\tfrac{1}{2}\rangle\langle -\tfrac{1}{2}|, \tag{5.35}$$

  the time evolution of the system was simulated according to the Liouville-von Neumann equation

$$\frac{d}{dt}\rho = i\left[\rho, \mathscr{H}_{\mathrm{R}}\right], \tag{5.36}$$

  where $\mathscr{H}_{\mathrm{R}}$ is the Hamiltonian represented in Eq. (5.3) (page 72).
- The external field, the field-sweep width, and the field-sweep time was set to $B_0 = 0.3187$ T, $B_s = 7.2$ mT, and $\tau_s = 15\mu$s, respectively (see Eq. (5.1) on page 72).
- Simulations were carried out for various microwave intensities (ω_1 in Eq. (5.3) on page 72), and the time dependences of the ^{1}H polarization and the triplet sublevels' populations were sampled during the field-sweeping time.

The program list for the simulations of the intramolecular electron-to^{1}H polarization transfer is shown in Section 9.1 (page 135$\sim$).

■□■ Results of the simulations ■□■

Fig. 5.5 shows simulated time dependences of ^{1}H polarization during an ICP sequence for various microwave intensities (B_1) with the field sweep time of 15 μs and the field sweep width of 7.2 mT. One can see that, for B_1 less than 3 Gauss, the ^{1}H polarization changes suddenly twice during the ICP sequence. These changes in the ^{1}H polarization are induced by the exchange of the spin states with the triplet electron spin at the moment when the Hartmann-Hahn condition is fulfilled, as explained earlier (see Fig. 2.13 and 2.14 (page 28)). On the other hand, when B_1 exceeds ca. 4.5 G, the ^{1}H polarization was hardly affected by the ICP sequence, as demonstrated in Fig. 5.5(e). This is because that B_1 was too large to satisfy the Hartmann-Hahn condition during the sweep.

In order to examine the contribution of the dipolar interaction among these ^{1}H spins to the result, I also carried out simulations ignoring the ^{1}H -^{1}H dipolar interaction during the sweep, and found that the results were almost the same as above (not shown). Therefore, it seems to be valid to ignore the contribution of the dipolar interactions among protons during the ICP sequence of the duration of 15 μs, as I did in Section 5.2.1 (page 71$\sim$).

As seen from Fig. 5.5(a)-(e), the ^{1}H polarization at the end of the field sweep ($t = \tau_s = 15$ μs) is strongly influenced by the irradiating microwave intensity B_1 For example, for $B_1 = 1.2$ G (Fig. 5.5(b)) the polarization transfer occurs so that the ^{1}H polarization is constructively increased. On the other hand, for $B_1 = 3.0$ G (Fig. 5.5(d)), the ^{1}H polarization is enhanced at the first Hartmann-Hahn matching, and then is returned to the triplet electron spin at the second Hartmann-Hahn matching, so that the resultant enhancement of the ^{1}H polarization enhancement becomes very small. Fig. 5.6 plots the ^{1}H polarization at the end of the ICP sequence as a function of B_1. One can see that, as B_1 is increased, the resultant ^{1}H polarization rapidly oscillates. In actual experiments using a microwave cavity or a loop-gap resonator, there would be a field inhomogeneity inside the resonator, and B_1 would be slightly fluctuating with time. Thus, it may be reasonable to imagine that the oscillatory behavior predicted by the

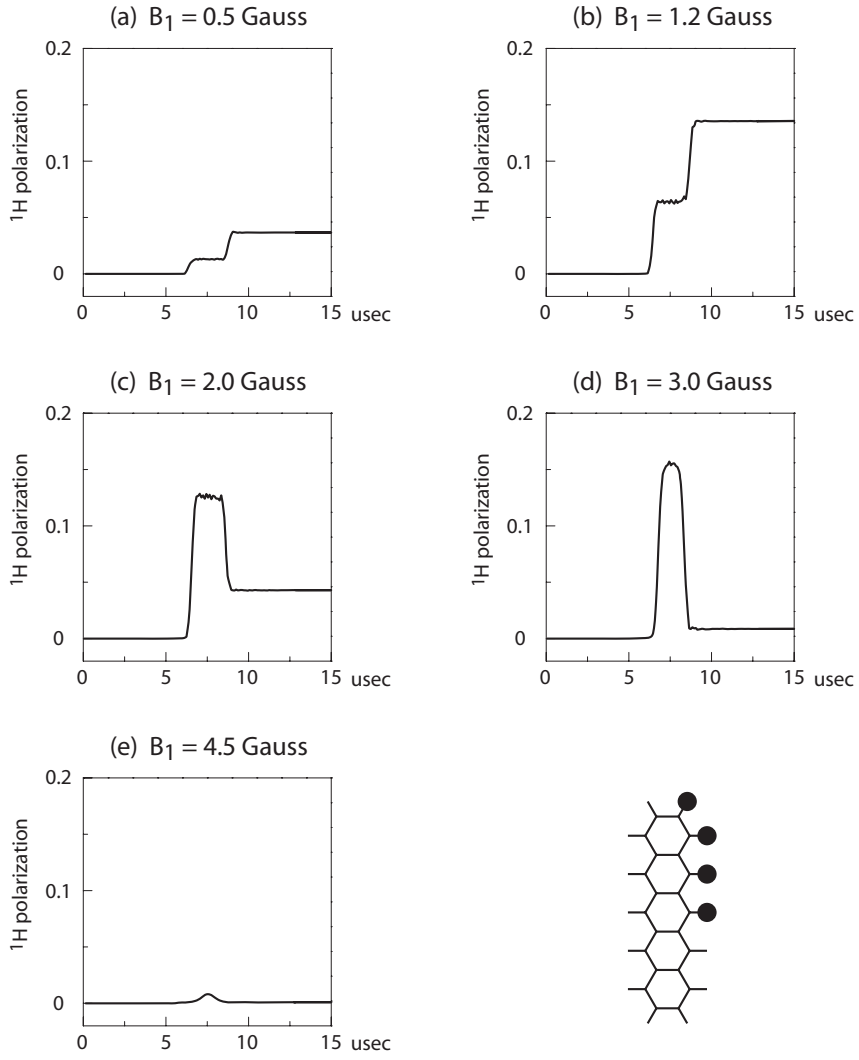

Figure 5.5: Simulated time dependences of the ^{1}H polarization during an ICP sequence with the field sweep time τ_s of 15 μs and the field sweep time B_s of 7.2 mT. The irradiating microwave intensities are (a) 0.5 G, (b) 1.2 G, (c) 2.0 G, (d) 3.0 G, and (e) 4.5 G. The long axis of the pentacene molecule was assumed to be parallel to the external field, and four ^{1}H spins (3, 4, 5, 6), marked by filled circles, were taken into account in the simulation.

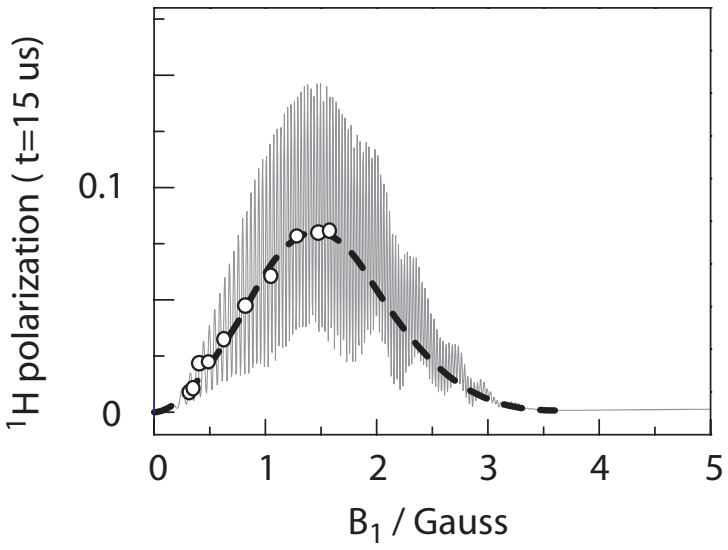

Figure 5.6: Simulated B_1 dependence of the resultant ^{1}H polarization at the end of an ICP sequence with a field sweep time of 15 μs. The simulation has taken account of four ^{1}H spins 3, 4, 5, 6 in a pentacene molecule. Circles represent the observed microwave-power dependence of the initial buildup rate (same as in Fig. 4.3)

simulation would be obscured by interference, so that the resultant B_1 dependence would be like a broken line depicted in Fig. 5.6. This is supported by the observed B_1 dependence of the initial buildup rate, as shown by circles in Fig. 5.6 (the same data shown in Fig. 4.3 (page 49)).

The reason why the resultant ^{1}H polarization has such a B_1 dependence is not clear, and further analyses are necessary. However, some hints can be found for the origin of the oscillatory behavior from simulations for various ICP field sweep times. Fig. 5.7(b) plots the simulated B_1 dependences of the resultant ^{1}H polarization with the ICP sequence of the field sweep time of 1.5 μs. The simulation predicts that, when such a short field sweep time is used, the oscillation gets fluent and the microwave intensity maximizing the polarization transfer efficiency becomes larger. This result also implys that the efficiency of the polarization transfer may further be improved, if the field-sweeping time and the microwave intensity are set to ca. 1.5 μs and ca. 3.4 G (the condition indicated by an arrow in Fig. 5.7), because the oscillation is fluent enough to prevent the B_1 fluctuation from obscuring the oscillatory behavior due to the interference. Furthermore, such a short sweep time really makes it valid to neglect the effect of the

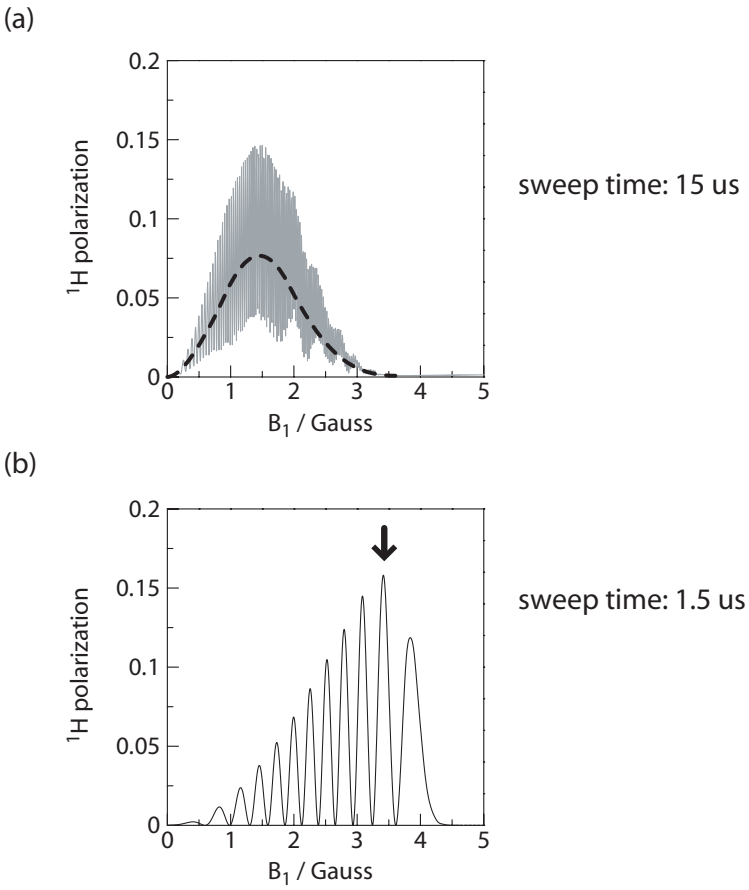

Figure 5.7: Simulated B_1 dependences of the resultant ^{1}H polarization at the end of an ICP sequence. (a) With a field sweep time of 15 μs. (b) With a field sweep time of 1.5 μs.

decay of the triplet sublevels to the ground state and the spin-lattice relaxation of the triplet electron spins, while they are tentatively ignored for the present analyses.

5.3 Evaluation of ^{1}H spin diffusion constants in naphthalene

Spin diffusion is one of the earliest concept in NMR, firstly put forward by N. Bloembergen to account for the unexpectedly fast spin-lattice relaxation rates observed in ionic crystals in the presence of paramagnetic impurities[78]. Since then a number of theories were proposed to evaluate spin diffusion constants[78, 79, 80, 81, 82, 83], and calculations were made for the ^{19}F spin diffusion constant in CaF_2, yielding similar values to each other. On the other hand, the measurement of the spin diffusion constant turned out to be extremely difficult[1], and has not been accomplished until very recently by W. Zhang and D.G. Cory using strong field-gradient pulses together with a magic-sandwich-echo technique[85]. Their measurement of spin diffusion constants confirmed these theories, and thus we can use one of them to calculate the ^{1}H spin diffusion constant for naphthalene used in the present work.

■□■ ^{1}H spin diffusion constant for undeuterated naphthalene ■□■

Here I follow the method proposed by I.J. Lowe and S. Gade[79], according to which spin diffusion constant $D_{\alpha\beta}(\alpha,\beta = x,y,z)$ is given by

$$D_{\alpha\beta} = \sum_k B_k^2 F_k x_k^\alpha x_k^\beta, \tag{5.37}$$

$$B_k = -\frac{1}{4}\left(\frac{\mu_0}{4\pi}\right)\gamma^2\hbar r_k^{-3}(1-3\cos^2\theta_k), \tag{5.38}$$

$$F_k \sim \left[\frac{2}{\pi}\sum_j (A_j - A_{kj})^2\right]^{-\frac{1}{2}}, \tag{5.39}$$

[1]This was not the case for heterogeneous solids such as polymer blends, in which individual accessibility of spins due to the chemical shift difference makes it easier to measure the spin diffusion constant[84].

where

$$A_j = -2B_j = \frac{1}{2}\left(\frac{\mu_0}{4\pi}\right)\gamma^2\hbar r_j^{-3}(1-3\cos^2\theta_k), \tag{5.40}$$

$$A_{kj} = \frac{1}{2}\left(\frac{\mu_0}{4\pi}\right)\gamma^2\hbar r_{kj}^{-3}(1-3\cos^2\theta_{kj}). \tag{5.41}$$

r_k and θ_k are the distance and the angle of elevation between the origin and the kth hydrogen atomic site. r_{jk} and θ_{jk} represent the magnitude and the orientation of the vector connecting the jth and the kth hydrogen sites. Here, the sum is supposed to be taken over all the spins in the sample under consideration. It is, however, sufficient to consider a finite number of spins, because the dipolar interaction decreases as the cube of the distance between spins and distant spins do not affect the result of the calculation.

Let us suppose that a single crystal sample of naphthalene is oriented in the same way as was in the buildup experiment, so that the normal line to the cleavage plane is tilted by 23° around the b-axis, and consider a spherical region of a certain radius in the sample. Now we want calculate the spin diffusion constant using Eq. (5.37)-(5.41) by taking a finite sum over the ^{1}H spins lying within this spherical region. Fig. 5.8 plots the calculated spin diffusion constants as a function of the radius of the spherical region considered. As we can see, the radius larger than 1 nm is sufficient for the convergence of the calculation. When the spherical volume of a radius of 2 nm is considered, the calculated values for D_{xx}, D_{yy}, and D_{zz} were 2.18×10^{-16} m^2/s, 2.17×10^{-16} m^2/s, and 1.24×10^{-15} m^2/s. The average value $\bar{D} = (D_{xx}+D_{yy}+D_{zz})/3$ is 5.58×10^{-16} m^2/s.

■□■ ^{1}H spin diffusion constant for deuterated naphthalene ■□■

The effect of deuteration of naphthalene on the residual ^{1}H spin diffusion is to reduce the diffusion constant due to dilution. For the calculation of the diffusion constant, one cannot ignore the existence of the ^{2}H spins, because they cause inhomogeneous broadening in the ^{1}H resonance line as seen in Fig. 4.7(a) (page 55), and affect the spectral overlap among the ^{1}H spin packets. In order to calculate the spin diffusion constant for the deuterated naphthalene used in this work, I devised the following procedural step based on the formula by Lowe and Gade.

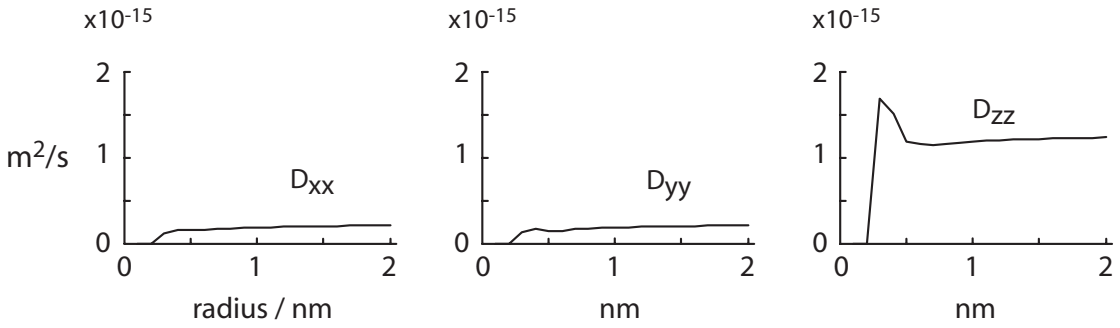

Figure 5.8: Calculated ^{1}H spin diffusion constants D_{xx}, D_{yy}, and D_{zz} for single crystal naphthalene by taking account of dipolar interaction among protons inside a spherical region. D_{xx}, D_{yy}, and D_{zz} are plotted as a function of the radius of the sphere taken into account. Calculations were done with the same crystal orientation as that set in the buildup experiment demonstrated in Chapter 4.

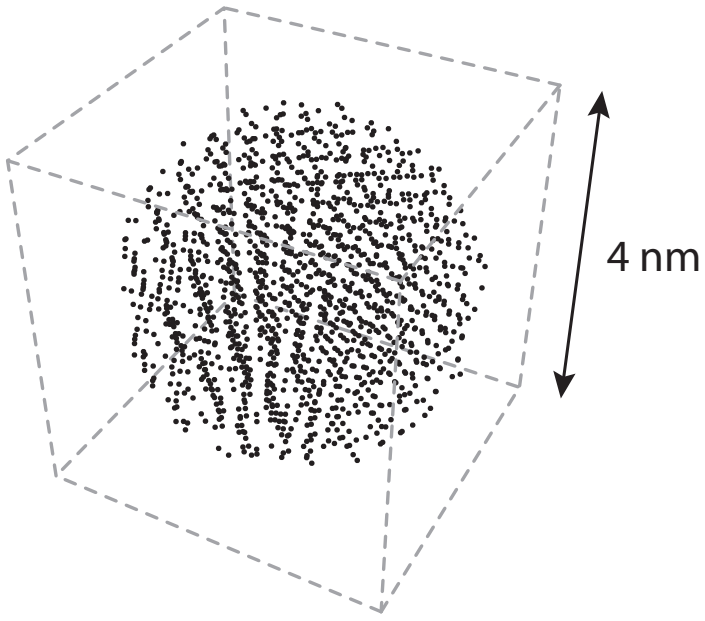

Figure 5.9: Positions of protons in naphthalene crystal. Only those protons are displayed within a spherical volume of a diameter of 4 nm. In this region 1,490 ^{1}H spins are included.

- Over the hydrogen sites depicted in Fig. 5.9 (page 89), protons were randomly distributed with a fraction of 0.0079, and all the rest of the hydrogen sites were regarded as being occupied by ^{2}H spins.

- The dipolar coupling constant $(\mu_0/4\pi)\gamma^2\hbar r_{jk}^{-3}$ in Eq. (5.41) was rewritten as $(\mu_0/4\pi)\gamma_j\gamma_k\hbar r_{jk}^{-3}$, where

$$\gamma_j = \begin{cases} \gamma_{^1H} & \text{if } j\text{th hydrogen site is occupied by } ^1\text{H}\ , \\ \gamma_{^2H} & \text{if } j\text{th hydrogen site is occupied by } ^2\text{H}. \end{cases} \tag{5.42}$$

- B_{jk} was set to zero if the jth and the kth hydrogen sites were occupied by heteronuclear spins, because B_{jk} represents the flip-flop component of the dipolar interaction, which is nonsecular for heteronuclear spins.

Following the above procedure, I calculated the residual-^{1}H spin diffusion constant in 99.21%-deuterated naphthalene by producing random numbers to assume the dilute ^{1}H distribution. Since the obtained diffusion constants differed as often as the calculations were repeated with the random ^{1}H distribution, I repeated the calculations several times and took the average value, and obtained the spin diffusion constant for the deuterated naphthalene sample to be 7.0×10^{-18} m^2/s. This is much lower than the diffusion constant for undeuterated naphthalene, because of the ^{1}H -^{1}H dipolar interactions are considerably weakened due to dilution, as is intuitively obvious from Fig. 5.10.

It must be remembered that, in order to be more precise, the calculation has to take account of the non-random ^{1}H distribution as we have seen in the previous chapter (page 55$\sim$).

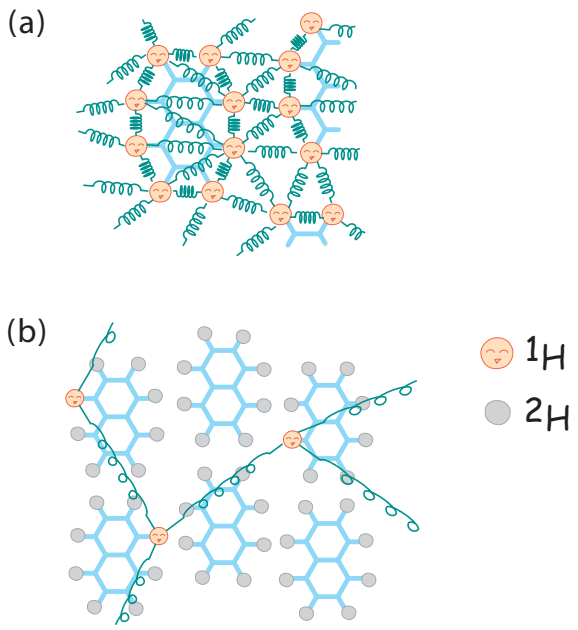

Figure 5.10: ^{1}H spin diffusion is much more efficient in undeuterated naphthalene (a) than that in heavily-deuterated naphthalene (b), because the dipolar interactions among the residual ^{1}H spins are weak.

5.4 Simulations of buildup curves

5.4.1 Simulations of the buildup behaviors

■□■ Procedure ■□■

Here I demonstrate simulations of the buildup of ^{1}H polarization by the ICP experiments. The procedure is as follows.

- A cubic region of a volume $V = L^3$ was considered within a single crystal sample of pentacene-doped naphthalene, as pictured in Fig. 5.11(a). Pentacene molecules were supposed to be distributed randomly over this cubic region, and the simulations of the buildup were made for this region.
- The cubic region was further divided into small pieces of voxels having an uniform ^{1}H

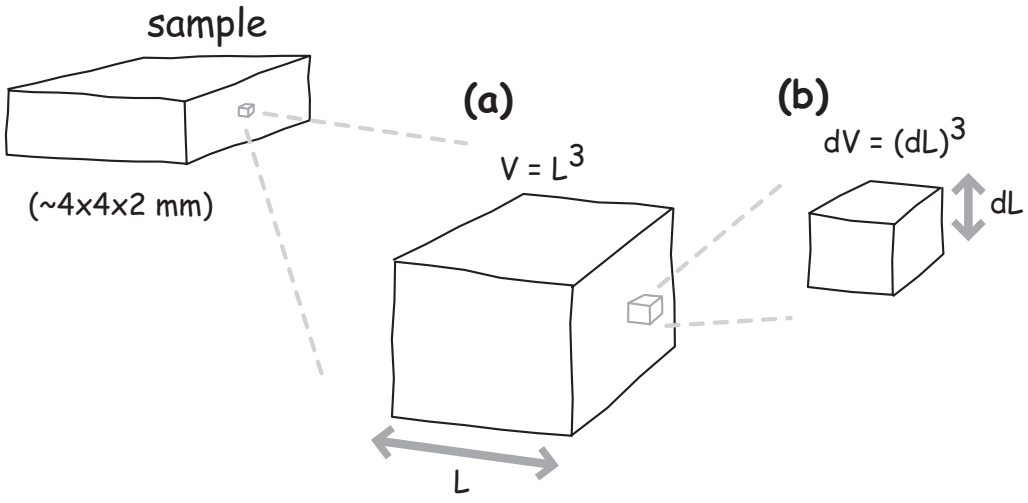

Figure 5.11: (a) The simulation of the buildup behavior of ^{1}H polarization is carried out in a cubic region of a volume $V = L^3$, assuming the periodic boundary condition. (b) In order to solve the three-dimensional diffusion equation numerically, (a) is divided into small pieces of voxels, each of which having an uniform ^{1}H polarization.

polarization (Fig. 5.11(b)). The volume $dV = (dL)^3$ of each voxel was set small enough so that it was valid to assume that every voxel contains at most one pentacene guest molecule (most voxels containing no guest molecules).

- The effect of the direct polarization transfer from the triplet electron spins to ^{1}H spins was assumed to increase the ^{1}H polarization in the voxel containing the guest molecule. Since the time scale considered here is much longer than the ICP sweep time ($\sim 15\mu$s), the polarization transfer was assumed to take place instantly at times $t = k\tau_R$, where $k = 1, 2, \ldots$ and $\tau_R = 20$ msec is the interval $(50\text{ Hz})^{-1}$ of the ICP sequences used in this study. At each moments of the ICP sequences, the ^{1}H polarization P in the guest-containing voxels was assumed to be increased by

$$\Delta P = \eta\xi\frac{1}{n}(\bar{P_e} - P), \tag{5.43}$$

$$n = \rho_{\text{naph}} dV \tag{5.44}$$

Here, ρ_{naph} denotes the density of protons in naphthalene. η is the fraction of the triplet electron spins in the $|-1\rangle$ or $|0\rangle$ substates, which is relevant to the polarization transfer.

The factor ξ was introduced to take account of the fact that the polarization of the triplet electron spins is not completely transferred to protons, as we have seen in Section 5.2.2 (page 83).

- The ^{1}H polarization $P(x,y,z;t)$ was transported according to the diffusion equation

$$\frac{d}{dt}P(x,y,z;t) = (D_{xx}\frac{\partial^2}{\partial x^2} + D_{yy}\frac{\partial^2}{\partial y^2} + D_{zz}\frac{\partial^2}{\partial z^2})P(x,y,z;t), \tag{5.45}$$

  where (D_{xx}, D_{yy}, D_{zz}) are the spin diffusion constants estimated in the previous section.

- The periodic boundary condition

$$\begin{aligned} P(x=L,y,z) &= P(x=0,y,z), \\ P(x,y=L,z) &= P(x,y=0,z), \\ P(x,y,z=L) &= P(x,y,z=0) \end{aligned} \tag{5.46}$$

  was assumed for the cubic region considered.

- ^{1}H spin-lattice relaxation was neglected, because its rate is very low in naphthalene at 105 K (the temperature at which the buildup experiments were carried out)[67].

The program list for the simulations of the buildup behavior of the ^{1}H polarization is shown in Section 9.2 (page 151∼).

5.4.2 Buildup behavior in the rapid spin diffusion limit

If the spin diffusion is so rapid that the ^{1}H polarization is smoothed out within each interval of the ICP sequences (see Fig. 5.3 (page 70)), the buildup behavior would be independent of the spin diffusion constant. Then, the time evolution of the ^{1}H polarization would be determined by the ICP repetition rate R ($\tau_R^{-1} = 50$ Hz), the fraction η of the triplet electrons in the $|-1\rangle$ or $|0\rangle$ states, and the exchange probability ξ. Therefore, we arrive at the differential equation

$$\frac{d}{dt}P = R\eta\xi\frac{\rho_e}{\rho_{\mathrm{naph}}}(\bar{P_e} - P), \tag{5.47}$$

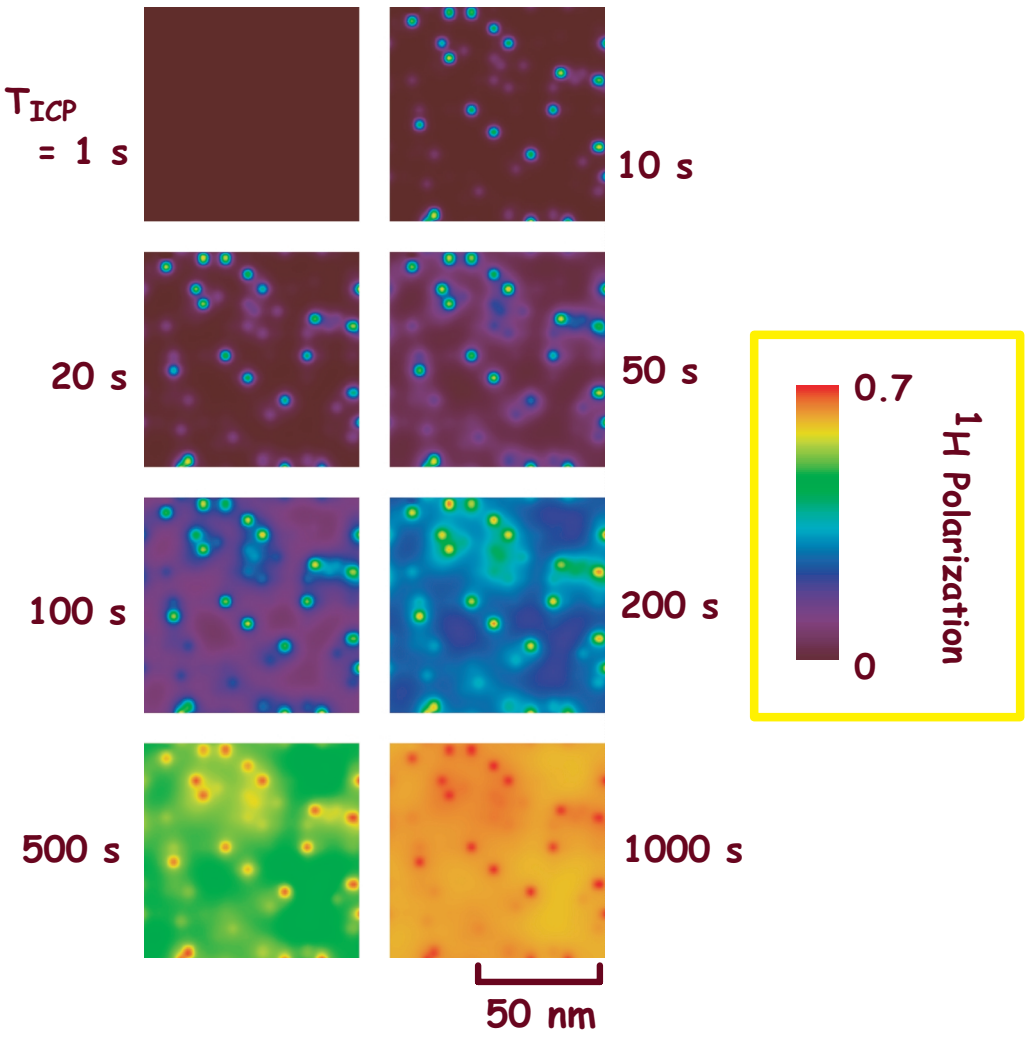

Figure 5.12: A tentative simulation of the ^{1}H polarization buildup in deuterated naphthalene.

Eq. (5.47) is solved as

$$P(t) = \bar{P_e}\left[1-\exp(-t/T_b')\right], \tag{5.48}$$

$$T_b' = \frac{\rho_{\mathrm{naph}}}{R\eta\xi\rho_e} \tag{5.49}$$

This corresponds the phenomenological description of the buildup behavior introduced by Iinuma et al.[66, 33]. If we assume that the rapid diffusion limit holds for the present study of the ^{1}H buildup experiment in the undeuterated naphthalene sample, the theoretical buildup time constant T_b' is estimated to be ca. 5000 s, which roughly explains the experimental buildup time of 7,890 s.

When the effect of ^{1}H spin-lattice relaxation cannot be neglected, the above differential equation has to be modified as

$$\frac{d}{dt}P = R\eta\xi\frac{\rho_e}{\rho_{\mathrm{naph}}}(\bar{P_e}-P)-\frac{1}{T_1}(P-P_{\mathrm{th}}) \tag{5.50}$$

$$\sim R\eta\xi\frac{\rho_e}{\rho_{\mathrm{naph}}}(\bar{P_e}-P)-\frac{1}{T_1}P, \tag{5.51}$$

whose solution is given by

$$P(t) = \frac{T_b}{T_b'}\bar{P_e}\left[1-\exp(-t/T_b)\right] \tag{5.52}$$

$$\frac{1}{T_b} = \frac{1}{T_b'}+\frac{1}{T_1}. \tag{5.53}$$

It should be noted that this phenomenological approach is valid only in the rapid spin diffusion limit. Hence, this phenomenological approach is no longer valid for analysing the buildup behavior in the deuterated naphthalene sample.

Chapter 6

Dynamic nuclear polarization by photo-excited triplet states in polycrystalline samples

6.1 Introduction

In previous chapters I presented a basic theory of DNP by photo-excited triplet electron spins, and demonstrated the attainment of high dynamic ^{1}H polarization in pentacene-doped naphthalene. All these experiments have dealt with single crystal samples, in which all the molecules in the sample align along the same direction. However, in many situations of chemical or biological interest, single crystal samples are hard to obtain. If we could apply this approach to polycrystalline samples, the sphere of its application would greatly expanded. In polycrystalline samples, however, the ESR spectrum is extremely broadened by the anisotropy of the ZFS interaction, and it is not obvious whether the optical DNP technique, presented in previous chapters, is also applicable to polycrystalline samples. In this chapter I demonstrate that DNP experiments by photo-excited triplet electron spins are possible even in polycrystalline samples

by limiting the sweep range of the magnetic field to a partial area of the broad ESR spectrum. I firstly describe how to calculate the ESR powder pattern of the photo-excited triplet electron spin from ZFS parameters and the initial population distribution on each triplet sublevel. Then I show a simulated powder ESR spectrum of the photo-excited triplet electron spins in pentacene molecules that are randomly-oriented with respect to the external magnetic field. The simulated ESR spectrum is helpful for the choice of the experimental conditions such as the static field strength, the microwave frequency, and the ICP field sweep width. Finally I show experimental results, which demonstrate the successful buildup of ^{1}H polarization in a polycrystalline sample, and discuss the efficiency of the buildup compared to experiments performed in single crystal samples.

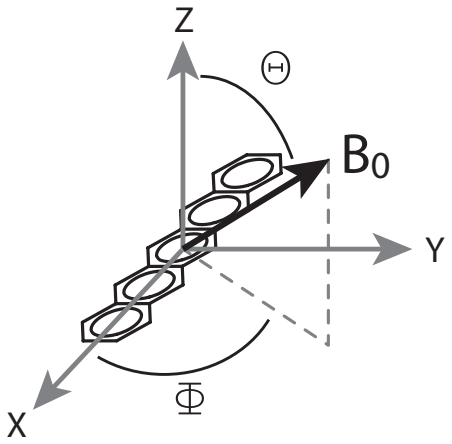

Figure 6.1: The principal axes of the ZFS interaction of the photo-excited triplet state of pentacene are oriented in the direction of the molecular symmetry axes.

6.2 Calculation of ESR powder spectra

Consider an electron spin in the triplet state, and suppose for a moment that no external magnetic field is applied. As we have seen in Section 2.2 (page 13), the energy levels are determined only

by the ZFS interaction $\mathscr{H}_{\mathrm{ZFS}}$, which can be represented using the ZFS parameters D and E as

$$\mathscr{H}_{\mathrm{ZFS}} = D\left(S_Z^2 - \frac{2}{3}\right) + E\left(S_X^2 - S_Y^2\right). \tag{6.1}$$

Let us introduce the basis set $\{|X\rangle, |Y\rangle, |Z\rangle\}$ defined by

$$\begin{aligned} |X\rangle &= \frac{1}{\sqrt{2}}(|-1\rangle - |1\rangle), \\ |Y\rangle &= \frac{i}{\sqrt{2}}(|-1\rangle + |1\rangle), \qquad (6.2) \\ |Z\rangle &= |0\rangle. \qquad (6.3) \end{aligned}$$

This basis set diagonalizes $\mathscr{H}_{\mathrm{ZFS}}$, providing the energy levels of the triplet state in zero field:

$$\begin{aligned} X &= \frac{1}{3}D + E, \\ Y &= \frac{1}{3}D - E, \qquad (6.4) \\ Z &= -\frac{2}{3}D. \qquad (6.5) \end{aligned}$$

On the other hand, in the presence of the external magnetic field, the total Hamiltonian is given by

$$\begin{aligned} \mathscr{H} &= \mathscr{H}_{\mathrm{Z}} + \mathscr{H}_{\mathrm{ZFS}}, \qquad (6.6) \\ \mathscr{H}_{\mathrm{Z}} &= \omega_0 S_Z. \qquad (6.7) \end{aligned}$$

Here, $\mathscr{H}_{\mathrm{Z}}$ represents the Zeeman interaction with the electron resonance frequency ω_0. Using the $\{|X\rangle, |Y\rangle, |Z\rangle\}$ basis set, the total Hamiltonian in Eq. (6.6) can be expressed in a matrix form as

$$\mathscr{H} = \begin{pmatrix} X & -i\omega_0\cos\Theta & i\omega_0\sin\Theta\sin\Phi \\ i\omega_0\cos\Theta & Y & -i\omega_0\sin\Theta\cos\Phi \\ -i\omega_0\sin\Theta\sin\Phi & i\omega_0\sin\Theta\cos\Phi & Z \end{pmatrix}, \tag{6.8}$$

where Θ and Φ represent the orientation of the external field with respect to the principal axis system of the ZFS tensor (Fig. 6.1). The diagonalization of the Hamiltonian for given Θ and Φ provides the eigenvalues $\{E_{-1}, E_0, E_{+1}\}$ and therefore the two ESR frequencies $\nu_- = E_0 - E_{-1}$ and $\nu_+ = E_{+1} - E_0$.

In order to calculate an ESR powder spectrum, one must take account of the non-equilibrium population distribution over the triplet sublevels which is caused by intersystem crossing. If the populations (w_X, w_Y, w_Z) of the zero-field levels are known, the populations (w_1, w_0, w_{-1}) of the high-field levels can be obtained as

$$w_\kappa(\Theta,\Phi) = \sum_\lambda |c_{\kappa\lambda}(\Theta,\Phi)|^2 w_\lambda \qquad (\kappa = 1,0,-1; \lambda = X,Y,Z), \tag{6.9}$$

where $c_{\kappa\lambda}$ denotes the $\kappa\lambda$ element of the unitary matrix which diagonalizes the Hamiltonian in Eq. (6.8). In a single crystal, the transition intensities for ν_- and ν_+ have to be weighted by $w_- = w_0 - w_{-1}$ and $w_+ = w_{+1} - w_0$, respectively. Therefore, the ESR spectrum for a single crystal with given Θ and Φ is represented by

$$S(\nu;\Theta,\Phi) = \frac{1}{2}\sum_{s=+,-} w_s(\Theta,\Phi)\delta(\nu - \nu_s(\Theta,\Phi)). \tag{6.10}$$

For a polycrystalline sample, the ESR spectrum is given by

$$S(\nu) = \frac{1}{4\pi}\int_0^{2\pi} d\Phi \int_0^{\pi} d\Theta \sin\Theta S(\nu;\Theta,\Phi). \tag{6.11}$$

For the lowest triplet state of pentacene, the zero-field energy levels and the zero-field populations w_λ have been determined by ESR studies as $(X,Y,Z) = (503, 418, -921)$ MHz and $(0.76, 0.16, 0.08)$, respectively[53, 40, 54]. Using these values and Eqs. (6.8)-(6.11), we calculated the ESR spectrum for the triplet state of pentacene at a frequency of 9.65 GHz, which is shown in Fig. 6.2. The linewidth is no less than 0.1 T due to the large ZFS interaction, and the total area intensity is zero as seen in Fig. 6.2, so that the ESR spectrum cannot thoroughly be excited. Therefore, in the present experiments we limited the sweep range to the peak width indicated in Fig. 6.2. The peak area is ascribed to the crystallites in which the long axes of pentacene molecules are nearly parallel to the magnetic field.

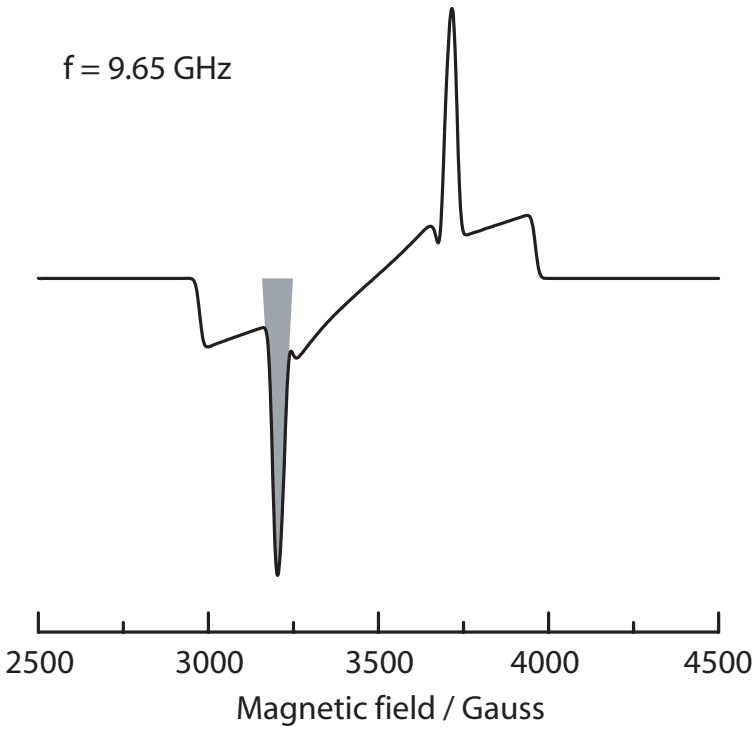

Figure 6.2: Calculated powder ESR spectrum of the photo-excited triplet electron spins of pentacene.

6.3 Result and discussion

Fig. 6.3 shows the buildup curve of the ^{1}H polarization obtained by applying the ICP sequence in a polycrystalline sample of 0.018 mol% pentacene-doped naphthalene. The ^{1}H polarization is built up exponentially with a time constant of 3,730 s. The final polarization reaches 1.02×10^{-2}, which is 3,200 times as large as the ^{1}H thermal equilibrium polarization at 105 K in the field of 0.3187 T. Fig. 6.4(a) shows a spectrum observed in a single scan after the ICP time

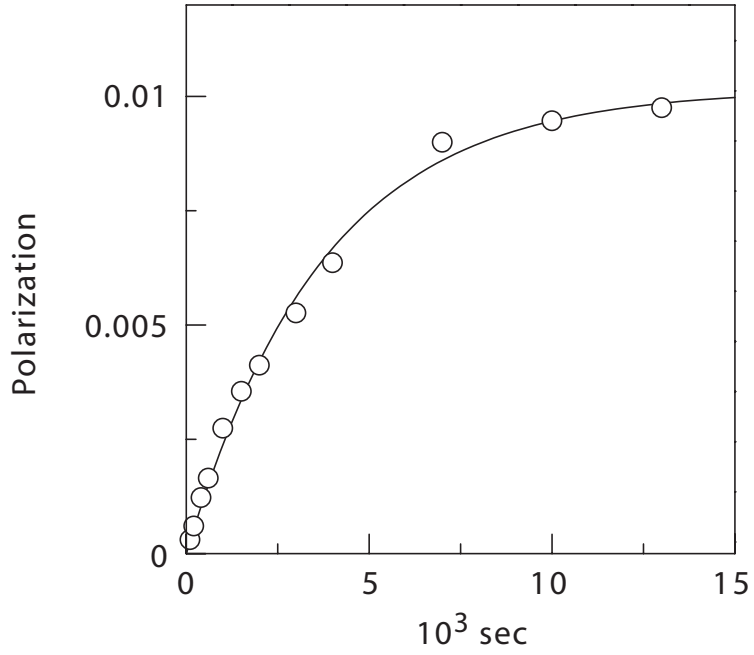

Figure 6.3: Buildup curve of the ^{1}H polarization in a polycrystalline sample of 0.018 mol% pentacene-doped naphthalene by the ICP experiment with a repetition rate of 50 Hz.

of 10,000 s. For comparison, a spectrum obtained in a single scan at 300 K without applying the DNP technique is shown in Fig. 6.4(b). These results show that large polarization and high sensitivity can be realized even in a powder sample by the present DNP technique.

Using a pentacene-doped naphthalene single crystal, Iinuma et al. have achieved the ^{1}H polarization of 0.32 at 77 K in the field of 0.3 T[33]; our result in a polycrystalline sample is 1/32 as large as theirs. This difference is partially ascribed to the fact that in the present

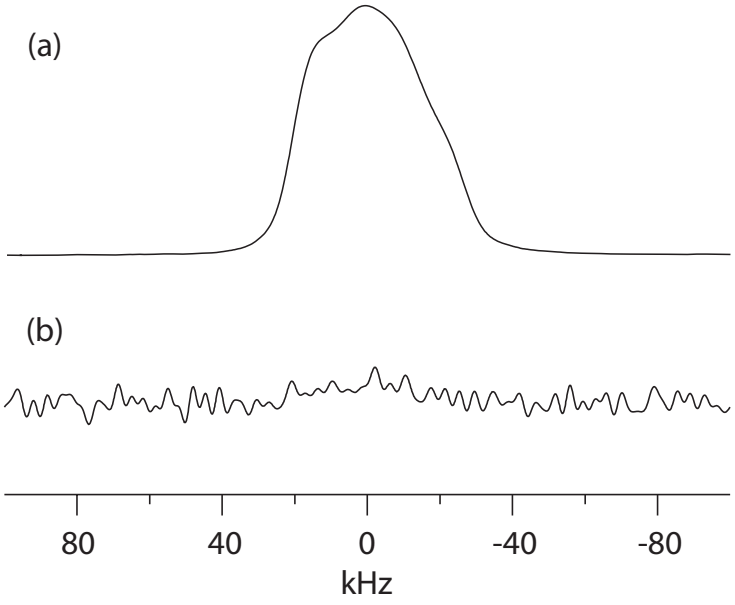

Figure 6.4: 13.6 MHz ^{1}H spectra of a polycrystalline sample of 0.018 mol% pentacene-doped naphthalene. (a) Enhanced by repeating ICP for 10,000 s at a rate of 50 Hz at 105 K (single scan). (b) In thermal equilibrium at room temperature (single scan).

experiment only a part of the electron spin packets have been used as mentioned above. The above polarization ratio is still too small compared to the ratio of the excited part to the whole ESR spectrum, suggesting the presence of any other cause. In the following, we discuss the possibility that the proton relaxation or the sample thickness causes the low polarization.

The final ^{1}H polarization can be limited by the ^{1}H spin lattice relaxation, which may prevent the ^{1}H polarization from reaching the electron polarization. We measured the ^{1}H spin lattice relaxation times at 105 K in polycrystalline and single crystal samples 0.018 mol% pentacene-doped naphthalene. The T_1 values obtained are 4,000 s and 29,100 s for the polycrystalline and single crystal samples, respectively. These results indicate that the pulverization of crystals shortens the relaxation time exceedingly. We found by ESR that our polycrystalline sample includes oxygen molecules, which are conceived to be adsorbed on the surfaces of the crystallites during the grind of the crystals in a mortar. The paramagnetism of oxygen molecules can contribute to shortening the relaxation time. However, even though we prepared an oxygen-free polycrystalline sample in the nitrogen atmosphere, the relaxation behavior was the same. Hence, the adsorption of oxygen molecules can be excluded from candidates for the cause of the low polarization. Another possibility is that radicals are produced by a mechanochemical effect: the grind of crystals can break chemical bonds of naphthalene molecules at the surfaces of crystallites. There is every possibility of its causing the fast relaxation and hence the low polarization in the polycrystalline sample.

■□■ Polycrystalline sample of a dilute ^{1}H system ■□■

We have also carried out the buildup experiment in a polycrystalline sample of pentacene-doped deuterated naphthalene. Fig. 6.5(a) shows the buildup curve obtained with the field sweep width of 12 mT. The final ^{1}H polarization is 0.033, again being considerably smaller than that obtained for the single crystal sample. Nevertheless, we could observe the ^{1}H spectrum with high sensitivity in a single scan even in the polycrystalline sample of 99.21% deuterated naphthalene as shown in Fig. 6.5(b). The thermal equilibrium ^{1}H signal cannot be observed,

being completely covered with noise.

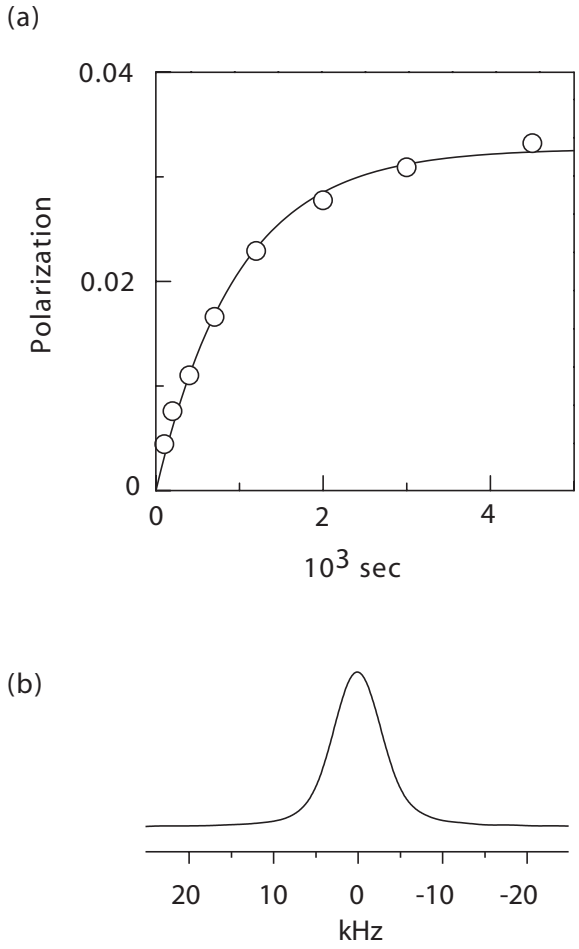

Figure 6.5: Experimental results for a polycrystalline sample of 99.21% deuterated naphthalene doped with 0.015 mol% pentacene. The ICP was repeated at a rate of 50 Hz. The ^{1}H resonance frequency is 13.6 MHz, and the temperature is 105 K. (a) Buildup curve of the ^{1}H polarization. (b) ^{1}H spectrum obtained in a single scan. The ICP sequence was repeated for 4,500 s.

Chapter 7

Study of light penetration into single crystal and polycrystalline material doped with molecules photoexcitable to the triplet state via intersystem crossing

This chapter presents a theory, simulations, and experiments as to the light penetration into both single crystal and polycrystalline material doped with the molecule whose electronic state can be excited by photo-absorption from the ground state to the excited singlet state, and transferred by intersystem crossing (ISC) into the triplet state. Propagation of light in media has extensively been studied and its theoretical framework has been well established for the two energy-level system consisting of the ground state S_0 and the excited state S_1, in which the transitions between them cause absorption and emission of photons[86]. In the weak light intensity limit where the population in the S_1 state is much lower than that in the S_0 state, the steady-state transmission is given by the Lambert-Beer law, i.e., the transmission decreases exponentially with the depth of the media[86]. On the other hand, when the light becomes so intense that the

population of the S_1 states begins to saturate, the steady state transmission is known to decrease linearly with the depth[86].

Here we treat the light penetration in a more complicated situation, in which an additional energy level of the lowest triplet state T_1 is present and the transition occurs from the S_1 state to the T_1 state through ISC induced by the spin-orbit coupling. One often encounters this three-level system in many kinds of molecules such as aromatic hydrocarbons, heterocyclics, amino acids, nucleic acids, porphyrins, and so on[87].

In general, the T_1 state has a long lifetime ranging from several microseconds to a few hours, whereas the S_1 state lifetime is of tens of nanoseconds. In the absence of the triplet-triplet absorption[1], photons pass through the molecules in the T_1 state, which is called photo-bleaching. Due to these characteristic features of in the T_1 state, the light penetration process in this kind of materials is expected to exceedingly differ from that in the S_0-S_1 two-level system, while no theoretical study on this subject has been reported so far. We present a theory

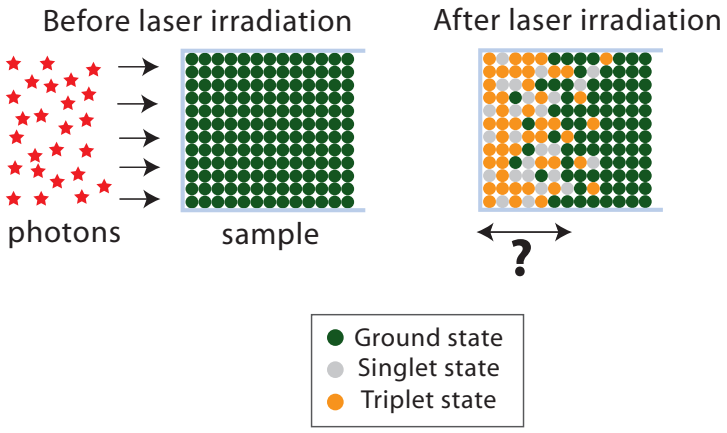

Figure 7.1: Statement of the problem: How far the light beam can penetrate through the sample, and how much the fraction of the photo-excited triplet state is?

to estimate the penetration depth in the three-level system for given conditions such as guest

[1]For the case of pentacene, the triplet-triplet absorption does not induced by light irradiation of the wavelength longer than 490 nm[88]

concentration and light intensity.

The T_1 state has an important feature of causing electron paramagnetism, which can be observed by electron spin resonance (ESR) measurements. We demonstrate that information on light penetration can be extracted from measurements of the ESR signal amplitudes for various sample thicknesses, and experimentally verify the theory by ESR measurements of the photo-excited triplet state of pentacene doped in single crystal or polycrystalline samples of *p*-terphenyl or naphthalene. The experiments are performed in the absence of an external magnetic field at room temperature. Even in zero field, the degeneracy of the triplet energy levels is lifted up by the zero-field splitting (ZFS) interaction, so that the ESR signal can be observed. Zero field measurements has an advantage that the anisotropy of the ZFS interaction is absent, which means that even in polycrystalline samples the ESR signal can be observed with appreciable sensitivity; high field observation is impractical for the polycrystalline samples, since the resonance line broadening would become no less than 0.1 Tesla.

Knowledge of the penetration depth is important, since it poses a crucial limitation on the sample volume which can be photo-excited and thus can be used for NMR sensitivity enhancement by the triplet DNP techniques. It is also possible to extract information as to the penetration depth by NMR imaging experiments, in which a field gradient pulse is applied during the signal acquisition (Fig. 7.2). Fig. 7.3 demonstrates one-dimensional NMR imaging of

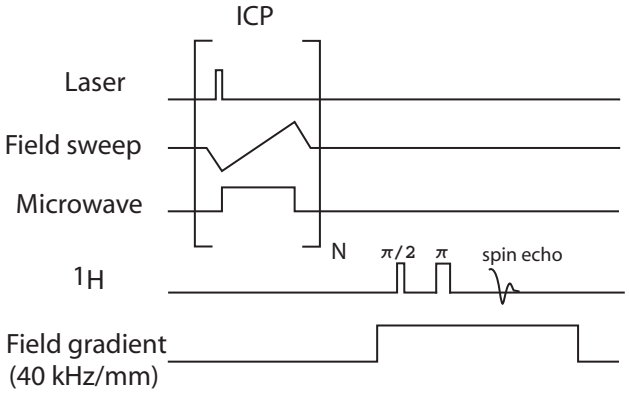

Figure 7.2: NMR imaging of ^{1}H polarization.

^{1}H polarization in a single crystal sample of 98%-deuterated *p*-terphenyl doped with pentacene, in which the polarization of the residual dilute ^{1}H spins was built by the ICP technique, and a field gradient pulse is applied along the laser beam irradiation during the acquisition. It is clearly demonstrated that the experiment with the higher laser power results in the broader resonance line, which means that the light penetrates deeper region in the sample, where the buildup of ^{1}H polarization occurs. However, this imaging experiments has a number of drawbacks. First, special hardware is required both to carry out the triplet DNP experiment and to apply the field gradient pulse. Second, spatial resolution is severely limited by the resonance linewidth due to dipolar interactions. NMR imaging experiments of a non-diluted ^{1}H system, which is the usual case and has much larger dipolar broadening, require much larger field gradient and are practically formidable.

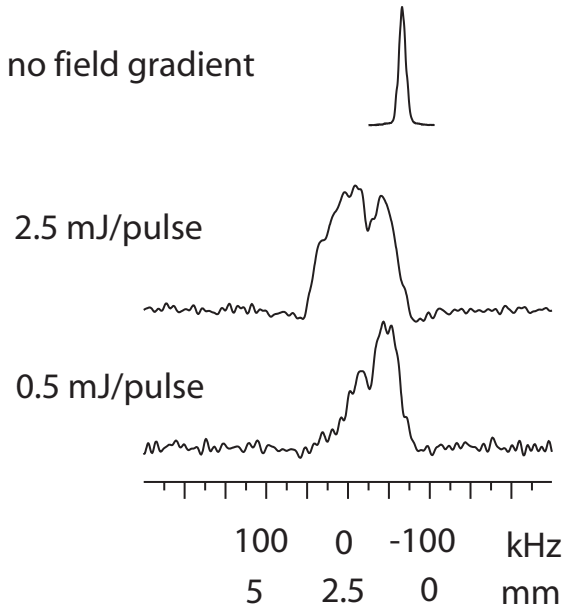

Figure 7.3: NMR imaging of ^{1}H polarization.

On the other hand, the zero-field ESR experiments, which will be shown below, are easy to carry out, and its signal intensity informs us the amount of molecules being excited to the photo-excited triplet state, which is the matter of concern here. The study presented in this

chapter might be helpful for choosing the sample size, the specification of the light source, etc. in DNP experiments and others.

7.1 Theory

This section is devoted to derive differential equations with which we can calculate the penetration behavior of a laser beam in single crystal or polycrystalline material doped with molecules photoexcitable to the triplet state via ISC. The radiative and the radiationless transitions in a three-level system are schematically displayed in Fig. 7.4. We consider that the doped molecules are homogeneously distributed in the material with density ρ_0, and suppose that the laser irradiation starts at $t = 0$ along the z axis. We treat the propagation of the laser beam as a one-dimensional problem.

While all the guest molecules are initially in the S_0 state, they can be photo-excited into the S_1 state at $t > 0$ by absorbing photons. Using the spectral density $u(\omega)$ of the laser beam, the $S_0 \rightarrow S_1$ transition rate W can be written as

$$W = B \int_{-\infty}^{\infty} F(\omega) u(\omega) d\omega. \tag{7.1}$$

Here, B is the Einstein B coefficient and $F(\omega)$ is the normalized absorption function. $u(\omega)$ is related to the beam intensity $I(\omega)d\omega$ through $cu(\omega) = \eta I(\omega)$, where c is the light velocity and η is the refractive index of the material. We approximate $u(\omega)$ by a square function with an average spectral density $\bar{u}$ as

$$u(\omega) = \begin{cases} 0, & |\omega - \omega_0| > \Delta\omega/2, \\ \bar{u}, & |\omega - \omega_0| \leq \Delta\omega/2, \end{cases} \tag{7.2}$$

where ω_0 is the center frequency of the spectrum and $\Delta\omega$ is the spectral width of the radiation. Correspondingly, we represent $I(\omega)$ as

$$I(\omega) = \begin{cases} 0, & |\omega - \omega_0| > \Delta\omega/2, \\ \bar{I} = (c/\eta)\bar{u}, & |\omega - \omega_0| \leq \Delta\omega/2. \end{cases} \tag{7.3}$$

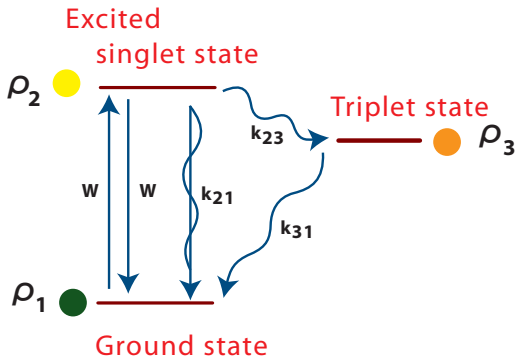

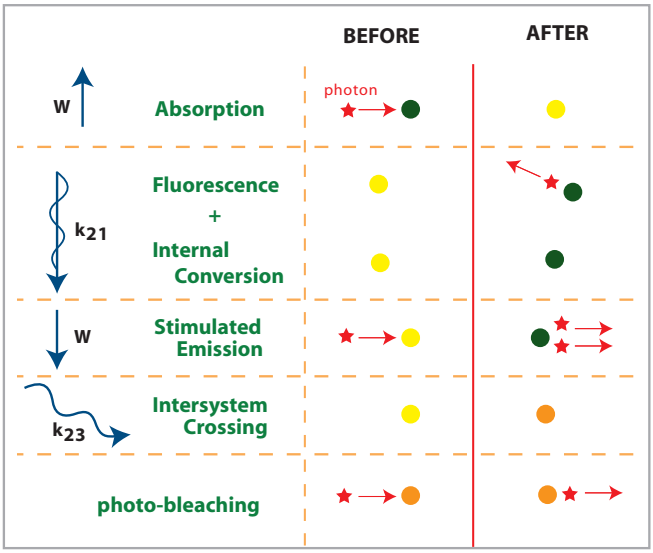

Figure 7.4: Three energy level system. The straight and the wavy arrows indicate the radiative and the radiationless transitions, respectively. The meaning of the kinetic parameters are discussed in the text.

The transition rate W can then be rewritten as

$$W = \frac{\eta}{c} B \bar{I} \int_{\omega_0 - \Delta\omega/2}^{\omega_0 + \Delta\omega/2} F(\omega) d\omega. \tag{7.4}$$

We now assume that the spectral width $\Delta\omega$ of the radiation is much smaller than that of the absorption function $F(\omega)$, so that the integral in Eq.(7.4) can be approximated to $F(\omega_0)\Delta\omega$. W is then given by

$$W = \frac{\eta B \bar{I} F(\omega_0)\Delta\omega}{c}. \tag{7.5}$$

A molecule in the S_1 state either undergoes ISC to the T_1 state with a rate constant k_{23}, or returns to the S_0 state with a transition rate k_{21}; the rate k_{21} is given by the sum of the three contributions due to stimulated emission, spontaneous emission, and internal conversion (IC). The rate constant for the stimulated emission is the same with W for the absorption, and the transition rate for the spontaneous emission is given by the Einstein A coefficient. We represent the transition rate for the internal conversion by k_{IC}. Then, the transition rate k_{21} can be written as $W + A + k_{\mathrm{IC}}$. We represent k_{21} and k_{23} in terms of the fluorescence lifetime τ_{F} and the ISC quantum yield Φ_{ISC}, which are the quantity that can experimentally be obtained. The fluorescence lifetime τ_{F} is defined as the lifetime of the radiation of the spontaneous emission in the presence of IC and ISC but in the absence of the stimulated emission, and is written as

$$\tau_{\mathrm{F}} = \frac{1}{A + k_{\mathrm{IC}} + k_{23}}, \tag{7.6}$$

and the ISC quantum yield Φ_{ISC} is represented as

$$\Phi_{\mathrm{ISC}} = \frac{k_{23}}{A + k_{\mathrm{IC}} + k_{23}}. \tag{7.7}$$

From Eqs. (7.6) and (7.7), the rate constants k_{21} and k_{23} can be represented as

$$k_{21} = W + \frac{1 - \Phi_{\mathrm{ISC}}}{\tau_{\mathrm{F}}}, \tag{7.8}$$

$$k_{23} = \frac{\Phi_{\mathrm{ISC}}}{\tau_{\mathrm{F}}}. \tag{7.9}$$

For a given depth z from the sample surface, the densities ρ_1, ρ_2, and ρ_3 of the S_0, the S_1, and the T_1 states, respectively, for a given z value, depend on time according to

$$\frac{\partial}{\partial t}\begin{pmatrix}\rho_1\\ \rho_2\\ \rho_3\end{pmatrix} = \begin{pmatrix}-W & k_{21} & k_{31}\\ W & -k_{21}-k_{23} & 0\\ 0 & k_{23} & -k_{31}\end{pmatrix}\begin{pmatrix}\rho_1\\ \rho_2\\ \rho_3\end{pmatrix}, \tag{7.10}$$

with the conditions

$$\rho_1(t=0)=\rho_0, \quad \rho_2(t=0)=\rho_3(t=0)=0, \tag{7.11}$$

$$\rho_1(t)+\rho_2(t)+\rho_3(t)=\rho_0. \tag{7.12}$$

The beam intensity $\bar{I}\Delta\omega$, which is implicitly included in Eq. (7.10) through W, also depends on t and z. In order to derive a differential equation to describe the variation of $\bar{I}$, we calculate the loss of the beam intensity $-d\bar{I}'\Delta\omega$ due to absorption in a volume $dV = adz$ during a time interval $dt = \eta dz/c$, where a represents the area of the beam spot. We firstly consider the case of a single crystal, in which the loss of the beam intensity due to scattering is negligible. The decrease $-d\bar{u}'\Delta\omega$ in the spectral density is given by

$$-d\bar{u}'\Delta\omega = -\frac{\hbar\omega dn'}{dV} \tag{7.13}$$

where dn' is the number of the photons absorbed in dV. The loss $-d\bar{I}'\Delta\omega$ can then be represented as

$$\begin{aligned} -d\bar{I}'\Delta\omega &= -(c/\eta)d\bar{u}'\Delta\omega \\ &= -\frac{c\hbar\omega dn'}{\eta dV}. \end{aligned} \tag{7.14}$$

Since dn' is equal to the number of the molecules photo-excited from the S_0 state to the S_1 state, dn' is obtained as

$$\begin{aligned} dn' &= \rho_1 dVW dt \\ &= \frac{\rho_1 dV\eta^2 B\bar{I}F(\omega_0)\Delta\omega dz}{c^2}. \end{aligned} \tag{7.15}$$

Therefore, $-d\bar{I}'\Delta\omega$ due to dn' is obtained as

$$-d\bar{I}'\Delta\omega = \frac{\rho_1\eta\hbar\omega B\bar{I}F(\omega)\Delta\omega dz}{c}. \tag{7.16}$$

We neglect the radiation due to the spontaneous emission, because its direction is random and therefore the radiation dissipates. On the other hand, the stimulated emission, whose radiation has the same direction and phase with the incident beam, restores the beam intensity lost by absorption. The beam intensity $d\bar{I}''\Delta\omega$ recovered due to the stimulated emission can similarly be obtained as

$$d\bar{I}''\Delta\omega = \frac{\rho_2\eta\hbar\omega B\bar{I}F(\omega)\Delta\omega dz}{c}. \tag{7.17}$$

The total change in the beam intensity during its travel from z to $z+dz$ is therefore given by

$$\begin{aligned}\bar{I}(z+dz,t+\eta dz/c)-\bar{I}(z,t) &= d\bar{I}'+d\bar{I}'' \\ &= \frac{(-\rho_1+\rho_2)\eta\hbar\omega B\bar{I}F(\omega)dz}{c},\end{aligned} \tag{7.18}$$

which leads to a differential equation

$$\left(\frac{\partial}{\partial z}+\frac{\eta}{c}\frac{\partial}{\partial t}\right)\bar{I}=\left[(-\rho_1+\rho_2)\frac{\eta\hbar\omega BF(\omega)}{c}\right]\bar{I}, \tag{7.19}$$

with the boundary conditions

$$\bar{I}(z,t<0)=0 \quad \text{and} \quad \bar{I}(z=0,t\geq 0)=\bar{I}_0. \tag{7.20}$$

Now we consider the case of polycrystalline samples, in which the laser beam is expected to be attenuated due to scattering at the boundaries of crystallites. In a random scattering medium, the transmission of a light beam is known to decrease exponentially with z, if z is shorter than the transport mean free path z_t, at which the direction of the incident light beam is completely randomized[89]. The exponential decay constant z_d of the light transmission in a random scattering medium is called the scattering mean free path. We assume that the exponential attenuation holds even in the case of multiple scattering at crystallite boundaries, and restrict depth z to the region of $z \leq z_d$ in the analysis. Consequently, we rewrite Eq. (7.19) for polycrystalline samples as

$$\left(\frac{\partial}{\partial z}+\frac{\eta}{c}\frac{\partial}{\partial t}\right)\bar{I}=\left[(-\rho_1+\rho_2)\frac{\eta\hbar\omega BF(\omega)}{c}-\frac{1}{z_d}\right]\bar{I}. \tag{7.21}$$

Thus, we have derived the simultaneous differential equations with which we can calculate the penetration behavior of a laser beam in material doped with molecules photoexcitable to the triplet state via ISC: numerically solving Eqs. (7.10) and (7.19) for a single crystal sample and Eqs. (7.10) and (7.21) for a polycrystalline sample, one can obtain the z dependence of both $\bar{I}$ and ρ_3 just after the laser pulse.

7.2 Experimental

Naphthalene and *p*-terphenyl were extensively purified by zone melting. Pentacene was used as purchased. Single crystals of pentacene-doped naphthalene and pentacene-doped *p*-terphenyl were grown up by the Bridgman method. The *p*-terphenyl crystal was cleaved along the *ab* plane, and was sliced with various thicknesses with a size of 5×5 mm. Polycrystalline samples were prepared by elaborately crushing the crystals into fine powder with a ceramic pestle and mortar, and then pressing into a tablet in a stainless cylinder under a pressure of ca. 1,800 kg/cm^2. The diameter of the polycrystalline samples was 6 mm.

For the photoexcitation of pentacene, a flashlamp-pumped dye laser was used, whose wavelength, spectral width, and pulse width are 590 nm, 20 nm, and 1 μs, respectively. The laser beam is unpolarized and has a diameter of 4 mm. The sample was placed in a solenoid coil tuned with a series and a parallel capacitors at 85 MHz, which is matched with the $|X\rangle \longleftrightarrow |Y\rangle$ transition frequency in the photo-excited triplet sublevels in zero external field[53]. Since both the electronic and the ESR transitions have orientational dependence, the samples of varying thickness were carefully oriented in the same way with respect to one another; the sample surface was set perpendicular to both the coil axis and the laser beam propagation. ESR of the photo-excited triplet electron spins in pentacene was detected just after the laser pulse with the Q-meter method[5]. All the experiments have been carried out at room temperature. Fig. 7.6(a) and (b) show examples of zero-field ESR signals of the photo-excited triplet electron spins of pentacene doped in polycrystalline samples of naphthalene obtained using the same laser beam

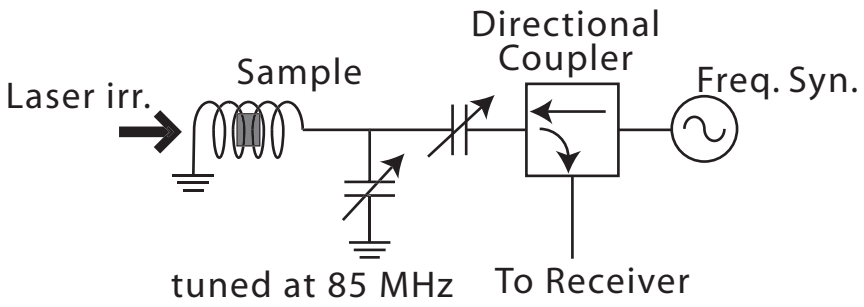

Figure 7.5: Experimental setup for the zero-field ESR measurements of photo-excited triplet state of pentacene.

intensity. The fact that the signal intensity in (a) is smaller than that in (b) indicates that the laser beam penetrated through the sample to the depth of at least 1.35 mm. Thus, by measuring the zero-field ESR signal intensities for various sample thicknesses, one can extract information as to the penetration depth and the triplet excitation depth.

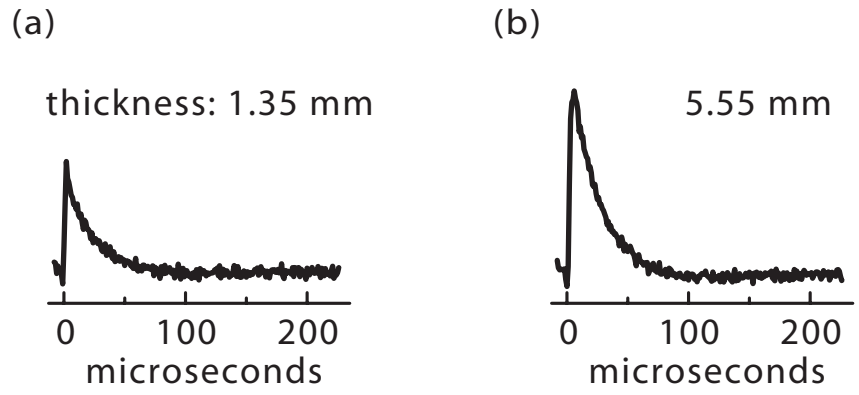

Figure 7.6: Zero-field ESR signals of the photo-excited triplet state of pentacene doped in polycrystalline naphthalene samples. The sample thicknesses are (a) 1.35 mm and (b) 5.55 mm, respectively.

7.3 Results and discussion

7.3.1 Single crystal samples of *p*-terphenyl doped with pentacene

Fig. 7.7 shows the sample thickness dependence of zero-field ESR signal amplitude of pentacene in the photo-excited triplet state in single crystals of 0.053 mol% pentacene-doped *p*-terphenyl for the three laser-beam intensities. The signal amplitude for the laser beam with the

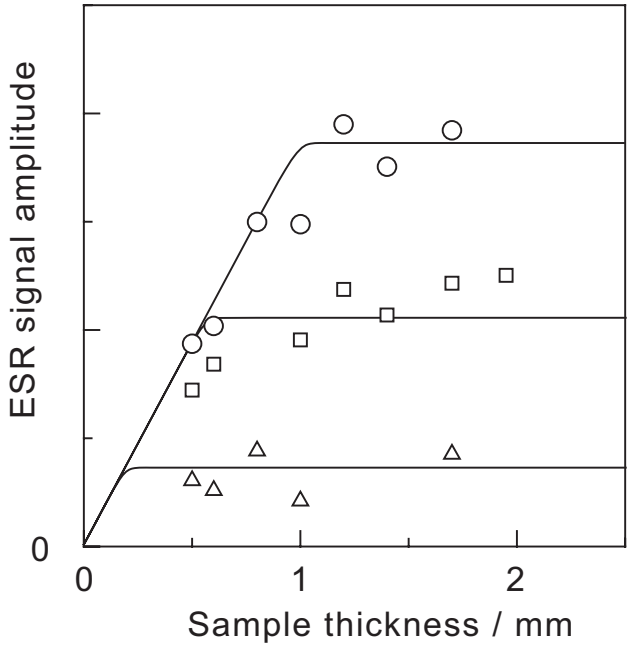

Figure 7.7: Sample thickness dependence of the zero-field ESR signal amplitude of photo-excited triplet electron spins in single crystals of 0.053 mol% pentacene-doped *p*-terphenyl with the incident laser beam intensities of 9.2×10^8 Wm^{-2} (circles), 5.2×10^8 Wm^{-2} (squares), and 1.8×10^8 Wm^{-2} (triangles). The solid lines show the calculated signal amplitudes as a function of the thickness.

highest intensity of $\bar{I}\Delta\omega = 9.2\times10^8$ Wm^{-2} increases with increasing sample thickness, until it reaches a plateau. This indicates that when the sample is sufficiently thin, the laser beam penetrates through the sample, maintaining the intensity sufficient to induce photo-excitation further. If the sample thickness is more than 1 mm, however, the laser beam loses its intensity so much that it can photo-excite no more remaining pentacene molecules. The sample thick-

ness at which the ESR signal amplitude begins saturating for increasing thickness can thus be regarded as the limit depth to which the pentacene molecules undergo the transition to the T_1 state. We call this thickness as the triplet excitation depth, which is ca. 1 mm for the laser beam intensity of 9.2 $\times 10^8$ Wm^{-2}. On the other hand, the triplet excitation depth is less than 1 mm for the lower intensities of 5.2×10^8 Wm^{-2} and 1.8×10^8 Wm^{-2}.

Here, we calculate the sample thickness (d) dependence of the zero-field ESR signal amplitude S of photo-excited triplet electron spins in pentacene in order to verify the theory described in the former section by comparing the experimental results with the calculations. Since the ESR signal amplitude is proportional to the number of the pentacene molecules in the T_1 state, the ESR signal amplitude $S(d)$ can be obtained as

$$S(d) = C\int_0^d dz\rho_3(z;t=t_p), \tag{7.22}$$

where t_p is the laser pulse width. The constant of proportionality C, which depends on the detection system, the laser beam area, and the orientation of the ESR transition moment with respect to the coil axis, is determined to fit the calculated dependences to the experimental data points.

In calculating the ESR signal amplitude according to Eqs. (7.10), (7.19), and (7.22), we used the refractive index $\eta = 1.61$[44], and neglected k_{31}, because the lifetime of the T_1 state (tens of microseconds) is much longer than the laser pulse width of 1 μs. Inspecting the absorption spectrum of pentacene, we set $F(\omega_0)\Delta\omega = 0.5$, since about a half area of the absorption peak is covered by the laser spectral width of 20 nm. The Einstein B coefficient was evaluated as follows. For random orientation of molecules, one can derive $B = (\pi\mu^2)/(3\varepsilon\hbar^2)$[86], where ε is the permittivity and μ is the magnitude of the $S_0 \rightarrow S_1$ transition dipole moment. In single crystal samples, the correct expression for B is $(\pi\mu^2\cos^2\theta)/(\varepsilon\hbar^2)$[44], where θ is the angle between the transition dipole moment and the electric field vector of radiation. For pentacene in *p*-terphenyl, the $S_0 \rightarrow S_1$ transition is known to be strongly *b*-axis polarized[90, 47]. Since the *b*-axis lies on the cleavage plane set perpendicular to the laser beam propagation, and since the laser beam used in the present work is unpolarized, the average over the possible θ val-

ues yields $B = (\pi\mu^2)/(2\varepsilon\bar{h}^2)$, which is 1.5 times as large as the B coefficient for the isotropic case. On the other hand, B is related to the radiative lifetime τ_0 through $B = (\pi^2c^3/\bar{h}\omega^3)A = (\pi^2c^3/\bar{h}\omega^3)\tau_0^{-1}$. τ_0 of the pentacene $S_0 \leftarrow S_1$ transition has been given for liquid solution to be 30 ns[91], which leads to $B = 2.58 \times 10^{21}\mathrm{J}^{-1}\mathrm{s}^{-2}\mathrm{m}^3$. By multiplying the factor 1.5, we obtained $B = 3.87 \times 10^{21}\mathrm{J}^{-1}\mathrm{s}^{-2}\mathrm{m}^3$ for the single crystal samples of the present case. The fluorescence lifetime τ_F and the ISC yield Φ_{ISC} for pentacene doped in *p*-terphenyl have been measured at 1.8 K to be 22.5 ns and 0.43%, respectively, for the crystal substitution sites O_1/O_2, and 9.3 ns and 62.5%, respectively, for the other sites O_3/O_4[47]. At room temperature the fluorescence lifetime has the same value of ca. 9 ns for all the sites[47], suggesting that the ISC yield has the same value of 62.5% for all the sites. Assuming that Φ_{ISC}=62.5% and τ_F=9 ns, we calculated the z dependence of the density ρ_3 of the pentacene molecule in the T_1 state, and thereby the ESR signal amplitude according to Eq. (7.22). As shown in Fig. 7.7, the calculations, without any adjustable parameters except for the coefficient C in Eq. (7.22), agree well with the experimental results.

The beam intensity $\bar{I}(z;t=t_p)$ as well as the T_1 density $\rho_3(z;t=t_p)$ can also be calculated on the above assumptions, which are shown in Fig. 7.8 for the pulse width of 1 μs. Note that all the pentacene molecules within the penetration depth are in the T_1 state at the end of the laser pulse as shown in Fig. 7.8(b). The reason is as follows: The laser pulse width is much longer than the lifetime (9 ns) of the S_1 state of pentacene[47], so that the $S_0 \rightarrow S_1$ excitation can be repeated many times during the period of 1 μs or the $S_1 \rightarrow T_1$ ISC takes place. Moreover, the ISC yield is no less than 62.5%, so that almost all the pentacene molecules within the penetration depth are excited to the T_1 state in 1 μs. Therefore, for the efficient generation of the T_1 state, the laser pulse width is desired to be long as far as it is much shorter than the lifetime of the T_1 state. Once the transition has occured from the S_1 state to the the T_1 state, the laser beam penetrates through the molecule by photo-bleaching, because there is no triplet-triplet absorption in pentacene at 590 nm[41]. As the laser beam intensity increases, the number of the pentacene molecules transferred to the T_1 state increases, and therefore the laser beam penetrates deeper, as shown in Fig. 7.8. However, the laser beam intensity should not be too

intense for obtaining a high ρ_3 fraction, that is, the stimulated emission rate should be much lower than the ISC rate (see below).

In general, $\bar{I}$ should not necessarily have the same z dependence as that in ρ_3; in other words, the light penetration depth may be different from the triplet excitation depth. However, the results of the above calculations revealed that for the incident beam intensities ranging from 1.8×10^8 to 9.2×10^8 Wm^{-2} both $\bar{I}$ and ρ_3 remain constant with increasing z until they suddenly drop to zero at the same depth as shown in Fig. 7.8. This coincidence arises when the stimulated emission rate can be ignored compared to the ISC rate. Then, photo-bleaching is the optical process for the laser beam to penetrate through the pentacene molecules. Since photo-bleaching takes place for the pentacene molecule in the T_1 state, $\bar{I}$ and ρ_3 show the z dependence similar to each other, and therefore the penetration depth accords with the triplet excitation depth. We carried out the same calculation, except that the stimulated emission was not taken into account, and found that the result is practically the same as in Fig. 7.8 (not shown), in agreement with the above discussion.

For comparison, we calculated the z dependences of $\bar{I}$ and ρ_3 for the hundredfold intenser laser beam intensities and the hundredth pulse width without changing the laser energies per pulse, which are shown in Fig. 7.9. In comparison with the results shown in Fig. 7.8, both of the laser beam intensity and the ρ_3 fraction extend to the longer depth with decreasing gradually. However, the ρ_3 fraction at $z = 0$ for the pulse width of 10 ns (Fig. 7.9(b)) is much smaller than that for 1 μs (Fig. 7.8(b)). In such strong laser beam intensities, the rate constant W for the stimulated emission becomes two orders of magnitude larger than the ISC rate k_{23}, so that the ISC is hard to occur, while the laser beam is hard to lose its intensity. In order to obtain a high ρ_3 fraction, the laser pulse width should be long as noted above.

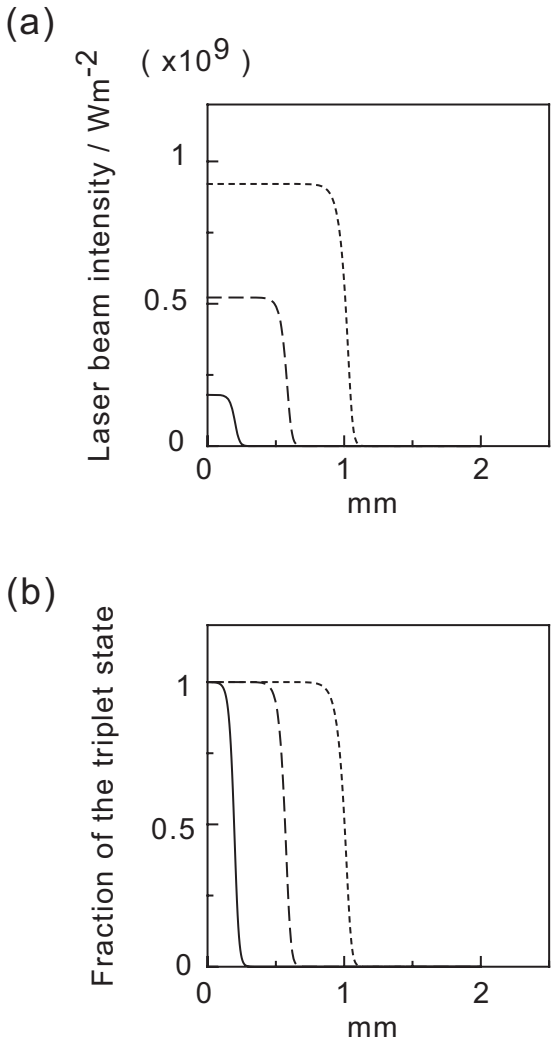

Figure 7.8: Calculated sample thickness dependence of (a) the laser beam intensity and (b) the fraction of the T_1 state, at the end of the laser pulse with the pulse width of 1μs in a single crystal sample of 0.053 mol% pentacene-doped *p*-terphenyl. The incident beam intensities are 1.8×10^8 Wm^{-2} (solid line), 5.2×10^8 Wm^{-2} (dashed line), and 9.2×10^8 Wm^{-2} (dotted line).

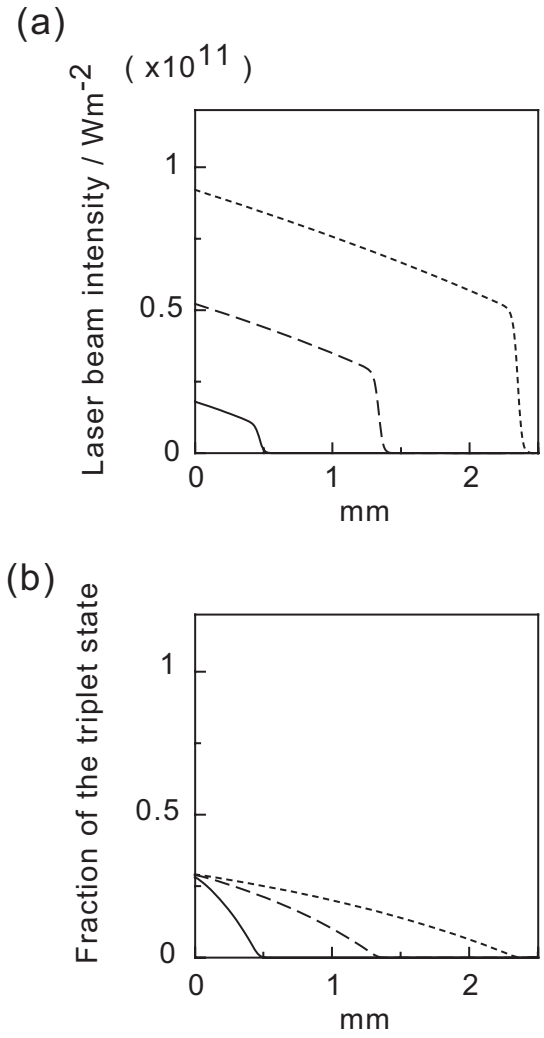

Figure 7.9: Calculated sample thickness dependence of (a) the laser beam intensity and (b) the fraction of the T_1 state, at the end of the laser pulse with the pulse width of 10 ns in a single crystal sample of 0.053 mol% pentacene-doped *p*-terphenyl. The incident beam intensities are 1.8×10^{10} Wm^{-2} (solid line), 5.2×10^{10} Wm^{-2} (dashed line), and 9.2×10^{10} Wm^{-2} (dotted line).

7.3.2 Polycrystalline samples of *p*-terphenyl and naphthalene doped with pentacene

The sample thickness dependence of the ESR signal amplitude in polycrystalline samples of 0.099 mol% pentacene-doped *p*-terphenyl is shown in Fig. 7.10. The profile is similar to that in the single crystals, but the triplet excitation depth is shorter, which may be attributed to the laser beam attenuation due to the scattering at the crystallite boundaries. We carried out the

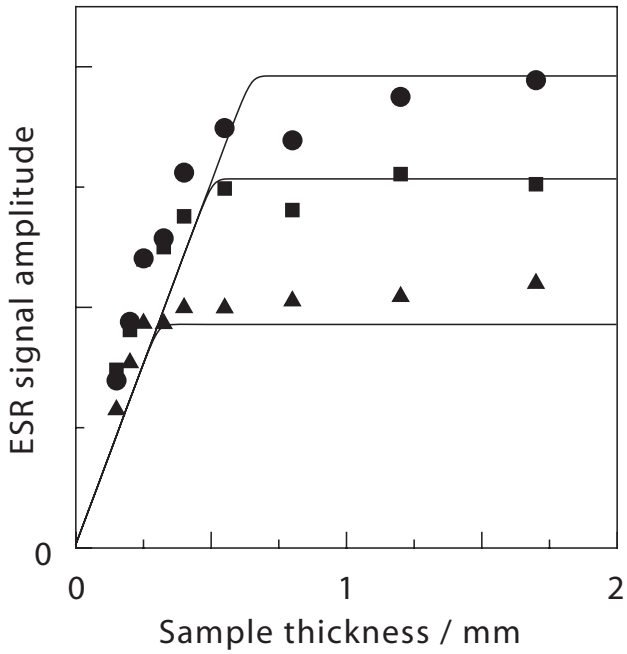

Figure 7.10: Sample thickness dependence of the zero-field ESR signal amplitude of photo-excited triplet electron spins in polycrystalline samples of 0.099 mol% pentacene-doped *p*-terphenyl. The incident beam intensities are 2.9×10^9 Wm^{-2} (filled circles), 1.8×10^9 Wm^{-2} (filled squares), and 8.1×10^8 Wm^{-2} (filled triangles). The solid lines show the calculated signal amplitudes.

calculation according to Eqs. (7.10) and (7.21) with various scattering mean free paths z_d as an adjustable parameters, and found that z_d of 0.4 mm well reproduces the experimental results as shown in Fig. 7.10, using the B value for the isotropic case and the same kinetic parameters Φ_{ISC} and τ_{F} as used in the calculations for the single crystals.

The thickness dependence of the ESR signal amplitude for pressed polycrystalline naphthalene samples with a pentacene concentration of 0.0092 mol% is also shown in Fig. 7.11. For comparison, the results for the polycrystalline *p*-terphenyl (the same as Fig. 7.10) are also shown in the figure. For pentacene doped in naphthalene, the fluorescence lifetime τ_F and the ISC quantum yield Φ_{ISC} have been measured only below 2 K. Therefore, in the calculations we treated Φ_{ISC} as well as z_d as adjustable parameters, and assumed the fluorescence lifetime τ_F to be 9 ns equally to that in *p*-terphenyl. For the refractive index η the reported value of 1.72 was used[44]. We found that the calculations using Φ_{ISC}=40% and z_d=1.5 mm agree well with the experimental data as shown in Fig. 7.11, in which we used a common value for C in Eq. (7.22) for both naphthalene and *p*-terphenyl polycrystalline samples. The ISC yield obtained in the

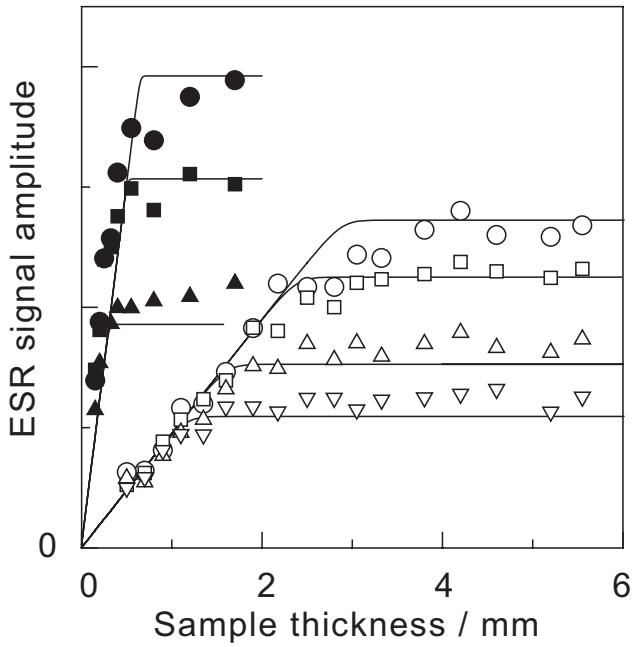

Figure 7.11: Sample thickness dependence of the zero-field ESR signal amplitude of photo-excited triplet electron spins in polycrystalline samples of 0.099 mol% pentacene-doped *p*-terphenyl and 0.0092 mol% pentacene-doped naphthalene. The incident beam intensities are 2.9×10^9 Wm^{-2} (filled circles), 1.8×10^9 Wm^{-2} (filled squares), and 8.1×10^8 Wm^{-2} (filled triangles) for the *p*-terphenyl host samples, and 3.7×10^9 Wm^{-2} (open circles), 2.5×10^9 Wm^{-2} (open squares), 1.2×10^9 Wm^{-2} (open triangles), and 7.5×10^8 Wm^{-2} (reversed triangles) for the naphthalene host samples. The solid lines show the calculated signal amplitudes.

present work at room temperature is an order of magnitude larger than the reported value of

Φ_{ISC}=2.8% at 1.4 K for pentacene-doped in naphthalene[44]. In pentacene-doped *p*-terphenyl, the pentacene molecule shows a much smaller ISC yield in the substitution sites O_1/O_2 than in the other sites O_3/O_4 at 2 K. This fact was explained as follows[48]: In the former sites the S_1 energy level is slightly lower than a triplet energy level so that ISC is unlikely to occur, whereas in the latter sites the S_1 energy level is slightly higher than a triplet energy level so that ISC can easily take place. As the temperature is raised, however, the former sites show a gradual increase in the ISC quantum yield, while the ISC quantum yield in the latter sites remains unchanged. This was explained by considering that the deficiency of energy for ISC in the former sites is supplied by thermal vibrational energy[47]. The increase in the ISC quantum yield in pentacene-doped naphthalene which was observed in the present work may also be caused by the same reason.

Fig. 7.11 also demonstrates that the laser beam penetrates deeper in naphthalene than in *p*-terphenyl, partly because that the naphthalene sample has the lower pentacene concentration. The longer penetration depth is also due to the longer scattering mean free path z_d of 1.5 mm in the naphthalene sample than that of 0.4 mm in the *p*-terphenyl sample. Since the granular variation and the space among crystallites would have a considerable effect on the light scattering, z_d depends on the mechanical properties such as hardness and plasticity of the material as well as the method of pulverization and compression. We have measured the density of our polycrystalline sample of *p*-terphenyl to be 1.11 g/cm^3, which is 10% smaller than that of 1.24 g/cm^3 in the single crystal. On the other hand, in the polycrystalline naphthalene prepared in the same way, the density was 1.16 g/cm^3, which agrees with that in the single crystal within the experimental error of $\pm$0.5%. Furthermore, the scanning electron microscope image of the polycrystalline naphthalene sample revealed the surface to be very smooth, while that in *p*-terphenyl showed a rough surface (Fig. 7.12).

These facts mean that in the naphthalene sample there is hardly any space between crystallites, whereas in the *p*-terphenyl sample the space between crystallites causes light scattering considerably. Hence, the decay length is expected to be longer for the polycrystalline naphtha-

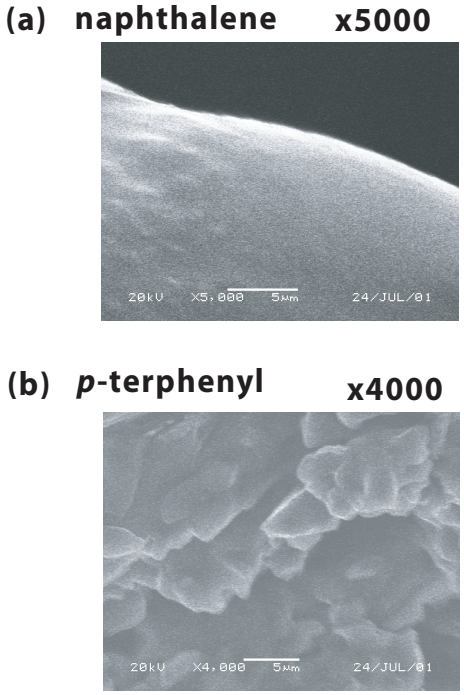

Figure 7.12: Scanning electron microscope (SEM) images of pressed polycrystalline samples of (a) naphthalene and (b) *p*-terphenyl used in this study.

lene than for the polycrystalline *p*-terphenyl, in accordance with the above results.

7.4 Summary of this chapter

In this work we presented a theory on the penetration of a laser beam into both single crystal and polycrystalline samples doped with molecules photoexcitable to the T_1 state via ISC, and measured the triplet excitation depth from the sample thickness dependence of the zero-field ESR signal amplitude of the photo-excited triplet electron spins. Experiments were performed by the laser irradiation with a pulse width of 1 μs and beam intensities of $1.8 \times 10^8 \sim 3.7 \times 10^9$ Wm^{-2}. For a single crystal of pentacene-doped *p*-terphenyl, both of the experiments and the calculations indicate that the triplet excitation depth coincides with the penetration depth of the laser beam under the above conditions. Calculations showed that the following two conditions are necessary for obtaining both of large fraction of pentacene molecules in the triplet state and a long triplet excitation depth; (i) the laser pulse width should be long as far as it is much shorter than the lifetime of the triplet state. (ii) the laser beam should be intense as far as the stimulated emission rate is lower than the ISC rate.

Zero-field ESR measurements also revealed that the laser beam penetrates even into polycrystalline samples of pentacene-doped *p*-terphenyl and naphthalene similarly to the single crystals, except for the light attenuation due to multiple scattering at the boundaries of the crystallites. The scattering mean free path z_d was determined to be 0.4 mm for a *p*-terphenyl sample and 1.5 mm for a naphthalene sample, indicating that the naphthalene sample has much narrower spaces among the crystallites than the *p*-terphenyl sample. Index matching may be effective in the improvement of penetration depth for *p*-terphenyl.

So far it has not been obvious how deeply light can penetrate through single crystal or polycrystalline material doped with molecules photoexcitable to the T_1 state. We have shown that the penetration depth of light into them can theoretically be predicted for various conditions.

The theory can be utilized for choosing the sample size, the guest concentration, the specification of the light source, and so on, for example in dynamic nuclear polarization experiments by photo-excited triplet electron spins.

Chapter 8

Conclusion

In this work, I demonstrated the attainment of a high dynamic ^{1}H polarization of 0.7 at 105 K in 0.32 T by the ICP technique using electron spins in the photoexcited triplet state. In a single crystal sample of 0.018 mol% pentacene-doped naphthalene, the ^{1}H polarization is built to the ultimate value attainable by this approach, corresponding to a 2.1×10^5-fold enhancement of ^{1}H polarization as compared to the thermal equilibrium polarization. There found to be two distinct processes behind the buildup behavior of the ^{1}H polarization, that is,

- firstly, the large triplet-electron spin polarization of pentacene, created by the highly-selective intersystem crossing from the excited singlet state, is transferred to the ^{1}H spins *within* the pentacene molecule by the ICP technique.

- Then, the enhanced ^{1}H polarization in pentacene is transported to the naphthalene host molecules by *spin diffusion*, which arises from the dipolar interactions among ^{1}H spins.

I also demonstrated that significant enhancement of nuclear polarization is possible in dilute spin systems, such as a diluted ^{1}H system in heavily deuterated naphthalene and a natural-abundance ^{13}C spin system. And moreover, the triplet DNP technique could be applied to

polarize nuclear spins in polycrystalline samples as well as single crystal samples, opening a way to enhance nuclear polarization in many systems of interest whose single crystals are hard to obtain.

The ^{1}H polarization of 0.7 attained in pentacene-doped naphthalene is, to our knowledge, the highest value ever realized above 4.2 K. As compared to the previous work by Iinuma et al.[33], in which the buildup time constant and the final ^{1}H polarization were 20,580 s and 0.32, respectively, about twice the ^{1}H polarization was obtained in a third of the experimental time. These improvements can be attributed particularly to the following factors. First, we have doped pentacene molecules with 18-fold higher concentration than in their work. As a consequence, it became easier to cool down the ^{1}H Zeeman reservoir by the larger amount of the triplet electron spins. Second, we have simulated the laser beam intensity dependence of the triplet excitation depth and the triplet fraction, and estimated the beam intensity with which all the pentacene molecules in the sample with a sample depth of 2.2 mm can be transferred to the triplet state after the laser pulse. And the last, we have carefully optimized the experimental conditions such as crystal orientation, ICP field sweep width, sweep time, and microwave intensity.

For some purposes, ^{1}H polarization even larger than 0.7 may be required. In such cases, it is necessary to use molecules whose triplet states have even larger electron polarizations. For example, the triplet state of Zn porphin is known to be completely polarized[92, 93]. Thus, the maximum possible ^{1}H polarization attainable using this molecule can be 1. However, in order to strategize to attain the ultimate ^{1}H polarization using such a material, many factors have to be checked with great care as we have discussed above. It may also be necessary to seek suitable molecules whose inherent characteristics meet those criteria.

For other purposes, it may be necessary to polarize the ^{1}H spins of a sample with a larger thickness or area compared with the sample used in the present study. For this purpose, a high-power laser with appropriate beam intensity and pulse width must be equipped, and if necessary, the microwave resonator should be redesigned and/or the magnetic field should be lowered to treat a larger sample. Nevertheless, there is always the maximum possible sample thickness for

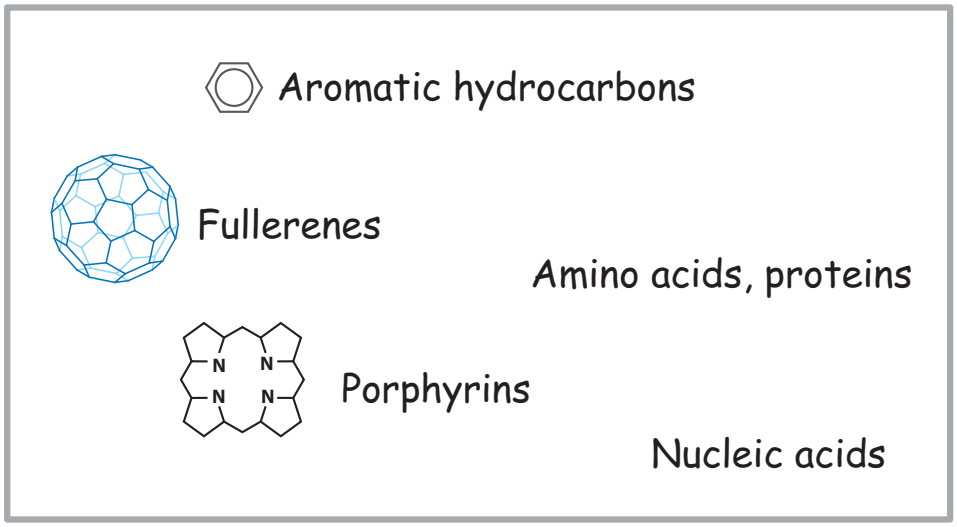

Figure 8.1: Molecules photo-excitable to the triplet state via ISC.

a given set of the kinetic parameters and the amount of doped molecules, however intense the laser beam is. This is because the very intense laser beam causes stimulated emission, which reduces the triplet fraction.

The high nuclear-spin polarization obtained in the present study can be used in some fields. Particularly in particle beam experiments, the capability of polarizing ^{1}H spins at a "high" temperature makes naphthalene a radiation-resistant target material, because the radiation damage due to the particle beam is self-recovered in naphthalene above 77 K[66]. In this respect, ^{1}H-polarized naphthalene is advantageous over the conventional targets prepared at very low temperatures, in which depolarization inevitably occurs due to the spin-lattice relaxation accelerated by the irrecoverable radiation damage[94].

In order to apply the triplet DNP technique to various systems of chemical/biological interest or materials suitable for NMR quantum computation, we consider the following two approaches. The first one is application to interesting systems which can be transferred to the triplet states. For instance, the electronic states of such amino acids as tryptophan, tyrosine, and phenylalanine are known to be photo-excitable to the triplet state[95, 96, 97]. They may be used

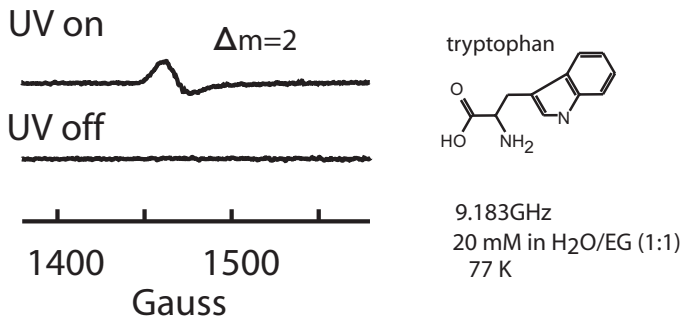

Figure 8.2: ESR spectrum of photo-excited triplet state of tryptophan in frozen water/ethylene-glycol mixture.

to enhance the sensitivity in peptides and proteins. The other way is transfer of the large polarization created in such a system as pentacene-doped naphthalene to an initially unpolarized interesting system by some way. For example, in a system in which molecules are adsorbed on or synthesized with a solid surface, nuclear spin polarization can be exchanged between the molecule and the surface through cross polarization[98] or spin-induced nuclear Overhauser effect (SPINOE)[99]. Thus, the signal of the molecule on the surface would become observable by contacting it with the ^{1}H-polarized single crystal. Another possibility is to perform DNP experiments in a microscopic mixture of pentacene-doped naphthalene and interesting molecules, in which spin diffusion transports the enhanced ^{1}H polarization in naphthalene to the molecules of interest. Such a mixture would be prepared by melt quenching or solution freezing. Moreover, spin-polarized liquids can also be realized by rapidly dissolving polarized naphthalene into solvent. We plan to polarize nuclear spins in other systems than naphthalene using some one of these approaches.

Chapter 9

Appendix

9.1 Program list for the simulation of the intramolecular polarization transfer by ICP

This C++ program requires the GAMMA library[1][100].

```
 #include <gamma.h>
#include <iostream.h>
#include <fstream.h>
#include <string.h>
#include <stdlib.h>

#define AROMATIC_CC 1.4
#define AROMATIC_CH 1.1

#define PROTONGAMMA -2*PI*4.26E7 // rad s^-1 T^-1
#define GFACTOR 2.0
#define BOHRMAGNETON 1.399E10   // s^-1 T^-1
#define ELECTRONGAMMA 2*PI*GFACTOR*BOHRMAGNETON // rad s^-1 T^-1
#define PLANCKHBAR 1.054E-34 // J s rad^-1

#define D_HH 7.5513E5
         // rad s^-1 A^3
#define D_EH 4.9687E8
         // rad s^-1 A^3
#define FERMI -4.04E8
         // rad s^-1   (rho*-23 Gauss = rho*-4.04E8 rad s^-1)
#define PENTACENE_NH 14
#define PENTACENE_NC 22
```

[1] http://gamma.magnet.fsu.edu/

```
#define BOLTZMANNCONST 1.38E-23

//  Default orientation
//   (X//long axis, Y//short axis, Z//out of plane)
col_vector pentaceneHydrogenSite(int);
col_vector pentaceneCarbonSite(int);
double distanceHH(int, int);
double distanceCH(int, int);
double distanceCC(int, int);
col_vector vectorCH(int, int);   // CH vector
col_vector n_vectorCH(int, int); // normalized CH vector
col_vector vectorHH(int, int);   // HH vector
col_vector n_vectorHH(int, int); // normalized HH vector
col_vector vectorCC(int,int);    // CC vector
col_vector n_vectorCC(int,int);  // normalized CC vector

//
//
matrix eulerZYZ_RAD(double a, double b, double g);
matrix eulerZYZ_DEG(double a, double b, double g);
//
//
col_vector pentaceneHydrogenSite(double, double, double, int);
col_vector pentaceneCarbonSite(double, double, double, int);
col_vector vectorCH(double, double, double, int, int);   // CH vector
col_vector n_vectorCH(double, double, double, int, int); // normalized CH vector
col_vector vectorHH(double, double, double, int, int);   // HH vector
col_vector n_vectorHH(double, double, double, int, int); // normalized HH vector
col_vector vectorCC(double, double, double, int,int);    // CC vector
col_vector n_vectorCC(double, double, double, int,int);  // normalized CC vector


double cosThetaCH(double a, double b, double g, int i, int j);
double sinThetaCH(double a, double b, double g, int i, int j);
double thetaAngleCH(double a, double b, double g, int i, int j);
double cosThetaHH(double a, double b, double g, int i, int j);
double sinThetaHH(double a, double b, double g, int i, int j);
double thetaAngleHH(double a, double b, double g, int i, int j);
double cosThetaCC(double a, double b, double g, int i, int j);
double sinThetaCC(double a, double b, double g, int i, int j);
double thetaAngleCC(double a, double b, double g, int i, int j);
double cosPhiCH(double a, double b, double g, int i, int j);
double sinPhiCH(double a, double b, double g, int i, int j);
double phiAngleCH(double a, double b, double g, int i, int j);
double cosPhiHH(double a, double b, double g, int i, int j);
double sinPhiHH(double a, double b, double g, int i, int j);
double phiAngleHH(double a, double b, double g, int i, int j);
double cosPhiCC(double a, double b, double g, int i, int j);
double sinPhiCC(double a, double b, double g, int i, int j);
double phiAngleCC(double a, double b, double g, int i, int j);

//****  dipolar alphabet (H-H) ****
double dHH(int, int);
complex d_A_HH(double a, double b, double g, int i, int j);
complex d_B_HH(double a, double b, double g, int i, int j);
complex d_C_HH(double a, double b, double g, int i, int j);
complex d_D_HH(double a, double b, double g, int i, int j);
complex d_E_HH(double a, double b, double g, int i, int j);
complex d_F_HH(double a, double b, double g, int i, int j);

//****  dipolar alphabet (ELECTRON-H) ****
double dEH(int, int);
complex d_A_EH(double a, double b, double g, int i, int j);
complex d_B_EH(double a, double b, double g, int i, int j);
complex d_C_EH(double a, double b, double g, int i, int j);
complex d_D_EH(double a, double b, double g, int i, int j);
complex d_E_EH(double a, double b, double g, int i, int j);
complex d_F_EH(double a, double b, double g, int i, int j);

double spinDensity(int k);
double fermiContact(int k);
complex hyperfineGz(double a, double b, double g, int k);
                              // k: index for proton spins
complex hyperfineGPlus(double a, double b, double g, int k);
```

```
complex hyperfineGMinus(double a, double b, double g, int k);

double inverseSpinTemperature(double T);
double protonOmega(double b0);
double electronOmega(double b0);

spin_op h_Z(spin_sys &sys, double b0, int k_spin);
spin_op zeemanHamiltonian(spin_sys &sys, double b0);
spin_op h_dHH(spin_sys &sys, double a, double b, double g, int i_space, int j_space,
                                                        int i_spin, int j_spin);
spin_op dipolarHamiltonian_HH(spin_sys &sys, double a, double b, double g, col_vector &po);

spin_op rho_k(spin_sys &sys, double b0, double temp, int k);

double protonPolarization(spin_sys &sys, gen_op &rho);
double protonPolarization(spin_sys &sys, gen_op &rho, int k);
spin_op thermalProtonDensityOperator(spin_sys &sys, double b0, double temp);
spin_op initialDensityOperator(spin_sys &sys, double b0, double temp, double pol1, double pol2, double pol3);

void setDefaultPosition(col_vector &po);
int pentaceneNumbering(int k);


double icpSweepOffset_inGauss(double width_inGauss, double tau, double time);
     // symmetric sweep
double icpSweepOffset_inGauss(double bi_inGauss, double bf_inGauss, double tau, double time);
     // asymmetric sweep
//
//-----------------------------------------------
//
matrix eulerZYZ_DEG(double a, double b, double g)
  return eulerZYZ_RAD(a*PI/180,b*PI/180,g*PI/180);

//
//-----------------------------------------------
//
matrix eulerZYZ_RAD(double a, double b, double g)
  matrix result(3,3);
  result.put(cos(a)*cos(b)*cos(g) - sin(a)*sin(g),0,0);
  result.put(cos(b)*cos(g)*sin(a) + cos(a)*sin(g),0,1);
  result.put(-cos(g)*sin(b),0,2);
  result.put(-cos(g)*sin(a) - cos(a)*cos(b)*sin(g),1,0);
  result.put(cos(a)*cos(g) - cos(b)*sin(a)*sin(g),1,1);
  result.put(sin(b)*sin(g),1,2);
  result.put(cos(a)*sin(b),2,0);
  result.put(sin(a)*sin(b),2,1);
  result.put(cos(b),2,2);
  return result;

//
//-----------------------------------------------
//
col_vector n_vectorCH(int i, int j)  // normalized CH vector
   return vectorCH(i,j)/distanceCH(i,j);

col_vector n_vectorCH(double a, double b, double g, int i, int j)
   return vectorCH(a,b,g,i,j)/distanceCH(i,j);

//
//-----------------------------------------------
//
col_vector vectorCH(int i, int j)  // CH vector
  return pentaceneHydrogenSite(j)-pentaceneCarbonSite(i);

col_vector vectorCH(double a, double b, double g, int i, int j)
  return pentaceneHydrogenSite(a,b,g,j)-pentaceneCarbonSite(a,b,g,i);

//
//-----------------------------------------------
//
col_vector n_vectorHH(int i, int j)  // normalized HH vector
   if (i!=j) return vectorHH(i,j)/distanceHH(i,j);
   else return col_vector(3,0);
```

```
col_vector n_vectorHH(double a, double b, double g, int i, int j)
   if (i!=j) return vectorHH(a,b,g,i,j)/distanceHH(i,j);
   else return col_vector(3,0);

//
//-----------------------------------------------
//
col_vector vectorHH(int i, int j)  // HH vector
  return pentaceneHydrogenSite(j)-pentaceneHydrogenSite(i);

col_vector vectorHH(double a, double b, double g, int i, int j)
  return pentaceneHydrogenSite(a,b,g,j)-pentaceneHydrogenSite(a,b,g,i);

//
//-----------------------------------------------
//
col_vector n_vectorCC(int i, int j)  // normalized HH vector
   if (i!=j) return vectorCC(i,j)/distanceCC(i,j);
   else return col_vector(3,0);

col_vector n_vectorCC(double a, double b, double g, int i, int j)
   if (i!=j) return vectorCC(a,b,g,i,j)/distanceCC(i,j);
   else return col_vector(3,0);

//
//-----------------------------------------------
//
col_vector vectorCC(int i, int j)  // HH vector
  return pentaceneCarbonSite(j)-pentaceneCarbonSite(i);

col_vector vectorCC(double a, double b, double g, int i, int j)
  return pentaceneCarbonSite(a,b,g,j)-pentaceneCarbonSite(a,b,g,i);

//
//-----------------------------------------------
//
double cosThetaCH(double a, double b, double g, int i, int j)
  return Re(n_vectorCH(a,b,g,i,j)(2));

double sinThetaCH(double a, double b, double g, int i, int j)
  double c=cosThetaCH(a,b,g,i,j);
  return sqrt(1.0-c*c);

double thetaAngleCH(double a, double b, double g, int i, int j)
  double c=cosThetaCH(a,b,g,i,j);
  return acos(c)*180/PI;

double cosThetaHH(double a, double b, double g, int i, int j)
  return Re(n_vectorHH(a,b,g,i,j)(2));

double sinThetaHH(double a, double b, double g, int i, int j)
  double c=cosThetaHH(a,b,g,i,j);
  return sqrt(1.0-c*c);

double thetaAngleHH(double a, double b, double g, int i, int j)
  double c=cosThetaHH(a,b,g,i,j);
  return acos(c)*180/PI;

double cosThetaCC(double a, double b, double g, int i, int j)
  return Re(n_vectorCC(a,b,g,i,j)(2));

double sinThetaCC(double a, double b, double g, int i, int j)
  double c=cosThetaCC(a,b,g,i,j);
  return sqrt(1.0-c*c);

double thetaAngleCC(double a, double b, double g, int i, int j)
  double c=cosThetaCC(a,b,g,i,j);
  return acos(c)*180/PI;

//
//-----------------------------------------------
//
double cosPhiCH(double a, double b, double g, int i, int j)
  double ex=Re(vectorCH(a,b,g,i,j)(0)), ey=Re(vectorCH(a,b,g,i,j)(1));
```

```
  if(ex==0 && ey==0) return 1.0;
  else if(ex==0 && ey!=0) return 0.0;
  else if(ex>0 && ey==0) return 1.0;
  else if(ex<0 && ey==0) return -1.0;
  else  //ex!=0 && ey!=0
    double ta=ey/ex, sgn;
    if(ta>0) sgn=1.0; else sgn=-1.0;
   return sgn*sqrt(1/(1+ta*ta));


double sinPhiCH(double a, double b, double g, int i, int j)
  double ex=Re(vectorCH(a,b,g,i,j)(0)), ey=Re(vectorCH(a,b,g,i,j)(1));
  if(ex==0 && ey==0) return 0.0;
  else if(ex==0 && ey>0) return 1.0;
  else if(ex==0 && ey<0) return -1.0;
  else  // ex!=0 && ey!=0
    double ta=ey/ex, sgn;
    if(ey>0) sgn=1.0; else sgn=-1.0;
  return sgn*sqrt(ta*ta/(1+ta*ta));


double phiAngleCH(double a, double b, double g, int i, int j)
  double c=cosPhiCH(a,b,g,i,j), s=sinPhiCH(a,b,g,i,j);
  if(c==0 && s==0) return 0;
  else if(c==0 && s>0) return 90.0;
  else if(c==0 && s<0) return 270.0;
  else if(c>0  && s==0) return 0.0;
  else if(c<0  && s==0) return 180.0;
  else return atan(s/c)*180/PI;

//
//-------------------------------------------------
//
double cosPhiHH(double a, double b, double g, int i, int j)
  double ex=Re(vectorHH(a,b,g,i,j)(0)), ey=Re(vectorHH(a,b,g,i,j)(1));
  if(ex==0 && ey==0) return 1.0;
  else if(ex==0 && ey!=0) return 0.0;
  else if(ex>0 && ey==0) return 1.0;
  else if(ex<0 && ey==0) return -1.0;
  else  //ex!=0 && ey!=0
    double ta=ey/ex, sgn;
    if(ta>0) sgn=1.0; else sgn=-1.0;
   return sgn*sqrt(1/(1+ta*ta));


double sinPhiHH(double a, double b, double g, int i, int j)
  double ex=Re(vectorHH(a,b,g,i,j)(0)), ey=Re(vectorHH(a,b,g,i,j)(1));
  if(ex==0 && ey==0) return 0.0;
  else if(ex==0 && ey>0) return 1.0;
  else if(ex==0 && ey<0) return -1.0;
  else  // ex!=0 && ey!=0
    double ta=ey/ex, sgn;
    if(ey>0) sgn=1.0; else sgn=-1.0;
  return sgn*sqrt(ta*ta/(1+ta*ta));


double phiAngleHH(double a, double b, double g, int i, int j)
  double c=cosPhiHH(a,b,g,i,j), s=sinPhiHH(a,b,g,i,j);
  if(c==0 && s==0) return 0;
  else if(c==0 && s>0) return 90.0;
  else if(c==0 && s<0) return 270.0;
  else if(c>0  && s==0) return 0.0;
  else if(c<0  && s==0) return 180.0;
  else return atan(s/c)*180/PI;

//
//-------------------------------------------------
//
double cosPhiCC(double a, double b, double g, int i, int j)
  double ex=Re(vectorCC(a,b,g,i,j)(0)), ey=Re(vectorCC(a,b,g,i,j)(1));
  if(ex==0 && ey==0) return 1.0;
  else if(ex==0 && ey!=0) return 0.0;
  else if(ex>0 && ey==0) return 1.0;
  else if(ex<0 && ey==0) return -1.0;
```

```
  else  //ex!=0 && ey!=0
    double ta=ey/ex, sgn;
    if(ta>0) sgn=1.0; else sgn=-1.0;
   return sgn*sqrt(1/(1+ta*ta));


double sinPhiCC(double a, double b, double g, int i, int j)
  double ex=Re(vectorCC(a,b,g,i,j)(0)), ey=Re(vectorCC(a,b,g,i,j)(1));
  if(ex==0 && ey==0) return 0.0;
  else if(ex==0 && ey>0) return 1.0;
  else if(ex==0 && ey<0) return -1.0;
  else  // ex!=0 && ey!=0
    double ta=ey/ex, sgn;
    if(ey>0) sgn=1.0; else sgn=-1.0;
  return sgn*sqrt(ta*ta/(1+ta*ta));


double phiAngleCC(double a, double b, double g, int i, int j)
  double c=cosPhiCC(a,b,g,i,j), s=sinPhiCC(a,b,g,i,j);
  if(c==0 && s==0) return 0;
  else if(c==0 && s>0) return 90.0;
  else if(c==0 && s<0) return 270.0;
  else if(c>0  && s==0) return 0.0;
  else if(c<0  && s==0) return 180.0;
  else return atan(s/c)*180/PI;

//
//-------------------------------------------------
//
double spinDensity(int k)
  if( k==1 || k==4 || k==8 || k==11 ) return 0.045;
  else if( k==2 || k==3 || k==9 || k==10 ) return 0.025;
  else if( k==5 || k==7 || k==12 || k==14 ) return 0.128;
  else if( k==6 || k==13) return 0.188;
  else if( k==15 || k==16 || k==21 || k==22 ) return -0.015;
  else if( k==17 || k==18 || k==19 || k==20 ) return -0.021;
  else return 0.0;

//
//-------------------------------------------------
//
col_vector pentaceneHydrogenSite(int k)
  double x,y,z;
  col_vector result(3);
  double a=AROMATIC_CC;
  double b=AROMATIC_CH;
  switch (k)
    case 1: x=2*sqrt(3)*a;     y=a+b;      z=0; break;
    case 2: x=(5*sqrt(3)*a/2)
             +(sqrt(3)*b/2);   y=(a+b)/2;  z=0; break;
    case 3: x=(5*sqrt(3)*a/2)
             +(sqrt(3)*b/2);   y=-(a+b)/2; z=0; break;
    case 4: x=2*sqrt(3)*a;     y=-a-b;     z=0; break;
    case 5: x=sqrt(3)*a;       y=-a-b;     z=0; break;
    case 6: x=0;               y=-a-b;     z=0; break;
    case 7: x=-sqrt(3)*a;      y=-a-b;     z=0; break;
    case 8: x=-2*sqrt(3)*a;    y=-a-b;     z=0; break;
    case 9: x=-(5*sqrt(3)*a/2)
              -(sqrt(3)*b/2);  y=-(a+b)/2; z=0; break;
    case 10: x=-(5*sqrt(3)*a/2)
               -(sqrt(3)*b/2); y=(a+b)/2;  z=0; break;
    case 11: x=-2*sqrt(3)*a;   y=a+b;      z=0; break;
    case 12: x=-sqrt(3)*a;     y=a+b;      z=0; break;
    case 13: x=0;              y=a+b;      z=0; break;
    case 14: x=sqrt(3)*a;      y=a+b;      z=0; break;
    default: x=0;              y=0;        z=0; break;
  //switch
  result.put(x,0); result.put(y,1); result.put(z,2);
  return result;

//
//-------------------------------------------------
//
col_vector pentaceneCarbonSite(int k)
```

```
  double x,y,z;
  col_vector result(3, complex(1,0));
  double a=AROMATIC_CC;
    switch (k)
      case 1: x=2*sqrt(3)*a;    y=a;      z=0; break;
      case 2: x=5*sqrt(3)*a/2;  y=a/2;    z=0; break;
      case 3: x=5*sqrt(3)*a/2;  y=-a/2;   z=0; break;
      case 4: x=2*sqrt(3)*a;    y=-a;     z=0; break;
      case 5: x=sqrt(3)*a;      y=-a;     z=0; break;
      case 6: x=0;              y=-a;     z=0; break;
      case 7: x=-sqrt(3)*a;     y=-a;     z=0; break;
      case 8: x=-2*sqrt(3)*a;   y=-a;     z=0; break;
      case 9: x=-5*sqrt(3)*a/2;  y=-a/2;  z=0; break;
      case 10: x=-5*sqrt(3)*a/2; y=a/2;   z=0; break;
      case 11: x=-2*sqrt(3)*a;   y=a;     z=0; break;
      case 12: x=-sqrt(3)*a;     y=a;     z=0; break;
      case 13: x=0;              y=a;     z=0; break;
      case 14: x=sqrt(3)*a;      y=a;     z=0; break;
      case 15: x=3*sqrt(3)*a/2;  y=a/2;   z=0; break;
      case 16: x=3*sqrt(3)*a/2;  y=-a/2;  z=0; break;
      case 17: x=sqrt(3)*a/2;    y=-a/2;  z=0; break;
      case 18: x=sqrt(3)*a/2;    y=a/2;   z=0; break;
      case 19: x=-sqrt(3)*a/2;   y=a/2;   z=0; break;
      case 20: x=-sqrt(3)*a/2;   y=-a/2;  z=0; break;
      case 21: x=-3*sqrt(3)*a/2; y=-a/2;  z=0; break;
      case 22: x=-3*sqrt(3)*a/2; y=a/2;   z=0; break;
      default: x=0.0;            y=0.0;   z=0.0;
  //switch
  result.put(x,0); result.put(y,1); result.put(z,2);
  return result;

//
//-------------------------------------------------
//
col_vector pentaceneHydrogenSite(double a, double b, double g, int i)
  return eulerZYZ_DEG(a,b,g)*pentaceneHydrogenSite(i);

//
//-------------------------------------------------
//
col_vector pentaceneCarbonSite(double a, double b, double g, int i)
  return eulerZYZ_DEG(a,b,g)*pentaceneCarbonSite(i);

//
//-------------------------------------------------
//
double distanceHH(int i, int j)
col_vector r1(3),r2(3);
double dx,dy,dz;
  if(i==j) return 0.0;
  else
    r1=pentaceneHydrogenSite(i); r2=pentaceneHydrogenSite(j);
    dx=Re(r1(0))-Re(r2(0));
    dy=Re(r1(1))-Re(r2(1));
    dz=Re(r1(2))-Re(r2(2));
    return sqrt(dx*dx + dy*dy + dz*dz);
   // else

//
//-------------------------------------------------
//
double distanceCH(int i, int j)
col_vector r1(3),r2(3);
double dx,dy,dz;
    r1=pentaceneCarbonSite(i); r2=pentaceneHydrogenSite(j);
    dx=Re(r1(0))-Re(r2(0));
    dy=Re(r1(1))-Re(r2(1));
    dz=Re(r1(2))-Re(r2(2));
    return sqrt(dx*dx + dy*dy + dz*dz);

//
//-------------------------------------------------
//
double distanceCC(int i, int j)
```

```
col_vector r1(3),r2(3);
double dx,dy,dz;
  if(i==j) return 0.0;
  else
    r1=pentaceneCarbonSite(i); r2=pentaceneCarbonSite(j);
    dx=Re(r1(0))-Re(r2(0));
    dy=Re(r1(1))-Re(r2(1));
    dz=Re(r1(2))-Re(r2(2));
    return sqrt(dx*dx + dy*dy + dz*dz);
   // else

//
//-------------------------------------------------
//
double dHH(int i, int j)
   double r=distanceHH(i,j);
   if (r==0) return 0;
   return D_HH/(r*r*r);   // rad s^-1

complex d_A_HH(double a, double b, double g, int i, int j)
  double d=dHH(i,j), ct=cosThetaHH(a,b,g,i,j);
  return d*complex(1-3*ct*ct, 0);

complex d_B_HH(double a, double b, double g, int i, int j)
  return -0.25*d_A_HH(a,b,g,i,j);

complex d_C_HH(double a, double b, double g, int i, int j)
  double d=dHH(i,j),
         ct=cosThetaHH(a,b,g,i,j), st=sinThetaHH(a,b,g,i,j),
         cp=cosPhiHH(a,b,g,i,j),  sp=sinPhiHH(a,b,g,i,j);
  return -1.5*d*st*ct*complex(cp,-sp);

complex d_D_HH(double a, double b, double g, int i, int j)
  return conj(d_C_HH(a,b,g,i,j));

complex d_E_HH(double a, double b, double g, int i, int j)
  double d=dHH(i,j),
         st=sinThetaHH(a,b,g,i,j),
         cp2=2*cosPhiHH(a,b,g,i,j),  sp2=2*sinPhiHH(a,b,g,i,j);
  return -0.75*d*st*st*complex(cp2,-sp2);

complex d_F_HH(double a, double b, double g, int i, int j)
  return conj(d_E_HH(a,b,g,i,j));


//
//-------------------------------------------------
//
double dEH(int i, int j)
   double r=distanceCH(i,j);
   return spinDensity(i)*D_EH/(r*r*r);   // rad s^-1

complex d_A_EH(double a, double b, double g, int i, int j)
  double d=dEH(i,j), ct=cosThetaCH(a,b,g,i,j);
  return d*complex(1-3*ct*ct, 0);

complex d_B_EH(double a, double b, double g, int i, int j)
  return -0.25*d_A_EH(a,b,g,i,j);

complex d_C_EH(double a, double b, double g, int i, int j)
  double d=dEH(i,j),
         ct=cosThetaCH(a,b,g,i,j), st=sinThetaCH(a,b,g,i,j),
         cp=cosPhiCH(a,b,g,i,j),  sp=sinPhiCH(a,b,g,i,j);
  return -1.5*d*st*ct*complex(cp,-sp);

complex d_D_EH(double a, double b, double g, int i, int j)
  return conj(d_C_EH(a,b,g,i,j));

complex d_E_EH(double a, double b, double g, int i, int j)
  double d=dEH(i,j),
         st=sinThetaCH(a,b,g,i,j),
         cp2=2*cosPhiCH(a,b,g,i,j),  sp2=2*sinPhiCH(a,b,g,i,j);
  return -0.75*d*st*st*complex(cp2,-sp2);
```

```
complex d_F_EH(double a, double b, double g, int i, int j)
  return conj(d_E_EH(a,b,g,i,j));


//
//-------------------------------------------------
//
double fermiContact(int k)
  return FERMI*spinDensity(k);

//
//-------------------------------------------------
//
complex hyperfineGz(double a, double b, double g, int k)
                                  // k: index for proton spins
  int i;
  complex result=0;
  for(i=1; i<=PENTACENE_NC; i++) result += d_A_EH(a,b,g,i,k);
  result += fermiContact(k);
  return result;

//
//-------------------------------------------------
//
complex hyperfineGPlus(double a, double b, double g, int k)
                                  // k: index for proton spins
  int i;
  complex result=0;
  for(i=1; i<=PENTACENE_NC; i++) result += d_C_EH(a,b,g,i,k);
  return result;

//
//-------------------------------------------------
//
complex hyperfineGMinus(double a, double b, double g, int k)
                                  // k: index for proton spins
  int i;
  complex result=0;
  for(i=1; i<=PENTACENE_NC; i++) result += d_D_EH(a,b,g,i,k);
  return result;

//
//-------------------------------------------------
//
spin_op rho_k(spin_sys &sys, double b0, double temp, int k)
  spin_op a;
  double b=PLANCKHBAR*protonOmega(b0)*inverseSpinTemperature(temp);
  a=exp(-b*Fz(sys,k));
  return a/trace(a);

//
//-------------------------------------------------
//
int pentaceneNumbering(int k)
  int result;
  switch(k)
    case 1: result=2; break;
    case 2: result=3; break;
    case 3: result=9; break;
    case 4: result=10; break;
    case 5: result=1; break;
    case 6: result=4; break;
    case 7: result=8; break;
    case 8: result=11; break;
    case 9: result=5; break;
    case 10: result=7; break;
    case 11: result=12; break;
    case 12: result=14; break;
    case 13: result=6; break;
    case 14: result=13; break;
    default: result=2;

  return result;
```

```
//
//------------------------------------------------
//
void setDefaultPosition(col_vector &po)
  for(int k=1; k<=PENTACENE_NH; k++)
    po(k) = pentaceneNumbering(k);


//
//------------------------------------------------
//
double protonOmega(double b0)   // in Tesla
  return PROTONGAMMA*b0;

//
//------------------------------------------------
//
double electronOmega(double b0) // in Tesla
  return ELECTRONGAMMA*b0;

//
//------------------------------------------------
//
double inverseSpinTemperature(double T)
   return 1/(BOLTZMANNCONST*T);

//
//------------------------------------------------
//
//
double protonPolarization(spin_sys &sys, gen_op &rho)
  int nProton=sys.spins()-1;  // don't count the 0th spin (electron)
  double result=0.0;
  for(int k=1; k<=nProton; k++)
    result += protonPolarization(sys,rho,k);
    result = result/nProton;
  return result;

double protonPolarization(spin_sys &sys, gen_op &rho, int k)
  int nProton=sys.spins()-1;   // don't count the 0th spin (electron)
  if (k>nProton) return 0.0;
  spin_op pol_op=2*Fz(sys,k);
  return Re(trace(rho,pol_op));

//
//------------------------------------------------
//
double tripletPopulation1(spin_sys &sys, gen_op &rho)
  spin_op pol_op = 0.5*(Iz(sys,0)+(Iz(sys,0)*Iz(sys,0))); // diag(1,0,0);
  return Re(trace(rho,pol_op));

double tripletPopulation2(spin_sys &sys, gen_op &rho)
  spin_op pol_op = (Ie(sys,0)-(Iz(sys,0)*Iz(sys,0)));  // diag(0,1,0)
  return Re(trace(rho,pol_op));

double tripletPopulation3(spin_sys &sys, gen_op &rho)
  spin_op pol_op = 0.5*((Iz(sys,0)*Iz(sys,0))-Iz(sys,0)); // diag(0,0,1);
  return Re(trace(rho,pol_op));

//
//------------------------------------------------
//
spin_op thermalProtonDensityOperator(spin_sys &sys, double b0, double temp)
  int nProton=sys.spins();
  spin_op result;
  result = rho_k(sys,0,temp,0);
  for(int k=1; k<nProton; k++) result *= rho_k(sys,b0,temp,k);
  result = result*3*pow(2,(nProton-1)*nProton)/2;
  return result;

//
//------------------------------------------------
//
spin_op initialDensityOperator(spin_sys &sys, double b0, double temp, double pol1, double pol2, double pol3)
```

```
  spin_op res;
  res  = pol1*0.5*(Iz(sys,0)+(Iz(sys,0)*Iz(sys,0))); // diag(1,0,0)
  res += pol2*(Ie(sys,0)-(Iz(sys,0)*Iz(sys,0)));     // diag(0,1,0)
  res += pol3*0.5*((Iz(sys,0)*Iz(sys,0))-Iz(sys,0)); // diag(0,0,1)
  res *= thermalProtonDensityOperator(sys,b0,temp);
  res = res/trace(res); // normalization
  return res;

//
//-------------------------------------------------
//
spin_op h_dHH(spin_sys &sys, double a, double b, double g, int i_space, int j_space, int i_spin, int j_spin)
   return d_A_HH(a,b,g,i_space,j_space)*Fz(sys,i_spin)*Fz(sys,j_spin)
         + d_B_HH(a,b,g,i_space,j_space)*(Fp(sys,i_spin)*Fm(sys,j_spin)
                                         +Fm(sys,i_spin)*Fp(sys,j_spin));

//
//-------------------------------------------------
//
spin_op dipolarHamiltonian_HH(spin_sys &sys, double a, double b, double g, col_vector &po)
  int i,j,k,l;
  int nProton=sys.spins()-1;  // uncount the 0th (electron) spin
  spin_op dHH;
  for(i=1;i<=nProton;i++)  for(j=i+1; j<=nProton;j++)
k=int(Re(po(i))); l=int(Re(po(j)));
    dHH += h_dHH(sys,a,b,g,k,l,i,j);
   // for
  return dHH;

//
//-------------------------------------------------
//
spin_op h_Z(spin_sys &sys, double b0, int k_spin)
   return  protonOmega(b0) * Iz(sys,k_spin);

//
//-------------------------------------------------
//
spin_op zeemanHamiltonian(spin_sys &sys, double b0)
  int nProton=sys.spins()-1;  // uncount the 0th (electron) spin
  spin_op hZ;
  for(int k_spin=1; k_spin <= nProton; k_spin++)  hZ += h_Z(sys,b0,k_spin);
  return hZ;

//
//-------------------------------------------------
//
spin_op h_HF_zOffset(spin_sys &sys, double a, double b, double g, int k_space, int k_spin)
  return 0.5*hyperfineGz(a,b,g,k_space)*Fz(sys,k_spin);

//
//-------------------------------------------------
//
spin_op hfHamiltonian_zOffset(spin_sys &sys, double a, double b, double g, col_vector &po)
  int nProton=sys.spins()-1;  // uncount the 0th (electron) spin
  spin_op hZ;
  for(int k=1; k<=nProton; k++)  hZ += h_HF_zOffset(sys,a,b,g,int(Re(po(k))),k);
  return hZ;

//
//-------------------------------------------------
//
double icpSweepOffset_inGauss(double width_inGauss, double tau, double time)
           // symmetric sweep
   return width_inGauss*(time-0.5*tau)/tau;

//
//-------------------------------------------------
//
double icpSweepOffset_inGauss(double bi_inGauss, double bf_inGauss, double tau, double time)
   return bi_inGauss + time*(bf_inGauss - bi_inGauss)/tau;

//
//-------------------------------------------------
```

```
//
double omegaZFS(double d, double e, double alpha, double beta)
   double cb=cos(beta*PI/180.0);
   double sb=sin(beta*PI/180.0);
   double c2a=cos(2*alpha*PI/180.0);
   return 2*PI*((0.5*d*(1-(3.0*cb*cb))) + (1.5*e*sb*sb*c2a));

//
//-----------------------------------------------
//
spin_op zfsHamiltonian(spin_sys &sys, double alpha, double beta, double d, double e)
  spin_op hzfs=(Iz(sys,0)*Iz(sys,0))-((2/3)*Ie(sys,0));
  return omegaZFS(d,e,alpha,beta)*hzfs;

//
//-----------------------------------------------
//
spin_op hfcH(spin_sys &sys, double a, double b, double g, int k_space, int k_spin)
  return hyperfineGz(a,b,g,k_space)*Iz(sys,k_spin)
        + hyperfineGPlus(a,b,g,k_space)*Ip(sys,k_spin)
        + hyperfineGMinus(a,b,g,k_space)*Im(sys,k_spin);

//
//-----------------------------------------------
//
spin_op hfcHamiltonian(spin_sys &sys, double a, double b, double g, col_vector &po)
  spin_op h_total;
  int nProton=sys.spins()-1;
  for (int j=1; j<=nProton; j++)
    h_total += hfcH(sys,a,b,g, int(Re(po(j))),  // index for the spatial part
                               j);              // index for the spin part

  h_total=h_total*Iz(sys,0);
  return h_total;

//
//-----------------------------------------------
//
spin_op nuclearZeemanHamiltonian_aux(spin_sys &sys)
  spin_op h_z;
  int nProton=sys.spins()-1;
  for (int j=1; j<=nProton; j++)
    h_z += Iz(sys,j);

  return h_z;

//
//-----------------------------------------------
//
//
//***********************************************
//
//
//-----------------------------------------------
//
int main(int argc, char *argv[])


//*************** init. setup 1 ***************
col_vector po( PENTACENE_NH + 1 );
setDefaultPosition(po);
     //
     // This function MUST BE implemented
     //        before reading a parameter file.
     //
//***********************************************

switch(argc)
      case 2: break;
      default:
        cout << "Usage: icp <par file>" << endl;
        exit(1);
 //switch
```

```
ifstream fin;
ofstream fout,fout2;
char finName[100];
  strcpy(finName, argv[1]);
  strcat(finName, ".par");

//+++++ Open parameter file +++++
  fin.open(finName);
  if(!fin)
     cout << finName << ": Cannot open file."
          << endl;
     exit(1);


//++++++ declaration of parameters to be read from the file ++++++
double ZFS_D=0; // zero-field splitting D parameter
double ZFS_E=0; // zero-field splitting E parameter
double population1,population2,population3;
int nProton=1;
double dt=1e-9; // default: 1 ns;
double sweepTime=15e-6;  // 15 us
double db0_ini_inGauss, db0_fin_inGauss, signedSweepWidth_inGauss;
double b1_frequency_Hz=9.0e9; // microwave freq. (in Hz)
double omega=2*3.141592*b1_frequency_Hz; // microwave freq. (in rad s^-1)
double b1_inGauss=1000;   // in Gauss
double b0=0.3187;  // B0 in Tesla
double iniTemp=300; // ini. spin temp (proton)
double a=0,b=90,g=0; // Euler angles
int obs_step=10;
char outputFileName[100]; // output filename

double protonBroadening_inGauss=0.0;
     // proton resonance broadening (due to the unconsidered protons)
int n_protonBroadening=1;

//+++++ Read parameters ++++++
char ach[100];
while(!fin.eof())
fin >> ach;
    if(!strcmp(ach,"ZFS_D"))
      fin >> ZFS_D;
      cout << "ZFS D parameter: " << ZFS_D << " Hz" << endl;

    else if(!strcmp(ach,"ZFS_E"))
      fin >> ZFS_E;
      cout << "ZFS E parameter: " << ZFS_E << " Hz" << endl;

    else if(!strcmp(ach,"population1"))
      fin >> population1;
      cout << "population1: " << population1 << " (no dimension)" << endl;

    else if(!strcmp(ach,"population2"))
      fin >> population2;
      cout << "population2: " << population2 << " (no dimension)" << endl;

    else if(!strcmp(ach,"population3"))
      fin >> population3;
      cout << "population3: " << population3 << " (no dimension)" << endl;

    else if(!strcmp(ach,"nProton"))
      fin >> nProton;
      cout << "nProton: " << nProton << " (no dimension)" << endl;

    else if(!strcmp(ach,"dt"))
      fin >> dt;
      cout << "dt: " << dt << " s." << endl;

    else if(!strcmp(ach,"sweepTime"))
      fin >> sweepTime;
      cout << "sweepTime: " << sweepTime << " s." << endl;

    else if(!strcmp(ach,"b1_frequency_Hz"))
      fin >> b1_frequency_Hz;
      cout << "b1_frequency_Hz: " << b1_frequency_Hz << " Hz." << endl;
```

```
      omega=2*3.141592*b1_frequency_Hz;

    else if(!strcmp(ach,"b1_inGauss"))
      fin >> b1_inGauss;
      cout << "b1_inGauss: " << b1_inGauss << " Gauss." << endl;

    else if(!strcmp(ach,"b0"))
      fin >> b0;
      cout << "b0: " << b0 << " Tesla." << endl;

    else if(!strcmp(ach,"iniTemp"))
      fin >> iniTemp;
      cout << "iniTemp: " << iniTemp << " K." << endl;

    else if(!strcmp(ach,"a"))
      fin >> a;
      cout << "a: " << a << " degree." << endl;

    else if(!strcmp(ach,"b"))
      fin >> b;
      cout << "b: " << b << " degree." << endl;

    else if(!strcmp(ach,"g"))
      fin >> g;
      cout << "g: " << g << " degree." << endl;

    else if(!strcmp(ach,"obs_step"))
      fin >> obs_step;
      cout << "obs_step: " << obs_step << " (no dimension)" << endl;

    else if(!strcmp(ach,"db0_ini_inGauss"))
     fin >> db0_ini_inGauss;
      cout << "db0_ini_inGauss: " << db0_ini_inGauss << " Gauss." << endl;

    else if(!strcmp(ach,"signedSweepWidth_inGauss"))
     fin >> signedSweepWidth_inGauss;
      cout << "signedSweepWidth_inGauss: " << signedSweepWidth_inGauss
           << " Gauss." << endl;

    else if(!strcmp(ach,"outputFileName"))
      fin >> outputFileName;
      cout << "outputFileName: " << outputFileName << "." << endl;

    else if(!strcmp(ach,"hydrogenSites"))
      cout << "hydrogen sites to be taken into account: ";
      for(int q=1; q<=nProton; q++)
int qq;
        fin >> qq; po(q)=qq;
        cout << qq << "  ";

      cout << endl;

    else if(!strcmp(ach,"protonBroadening_inGauss"))
     fin >> protonBroadening_inGauss;
      cout << "protonBroadening_inGauss: " << protonBroadening_inGauss
           << " Gauss." << endl;

    else if(!strcmp(ach,"n_protonBroadening"))
     fin >> n_protonBroadening;
      cout << "n_protonBroadening: " << n_protonBroadening
           << " (no dimension)." << endl;

    else if(!strcmp(ach,"#")) break;
    else ;
  // while
fin.close();  // file close

//+++++++++++++++++++++++++++++++++++++++++++++++++++++++++++++
int obs_count=0;
int q; // counter variable
int br_count=0;
int nobs=(int)(sweepTime/dt/obs_step);
spin_sys pen(nProton+1);
  pen.isotope(0,"2H"); // 0th spin: triplet state (S=1)
```

```
                      // imitated by deuterium (spin 1)
spin_op rho0; gen_op rho;
spin_op H, H_t; // time-indep. and time-dep. Hamiltonians;
spin_op H_aux, H_aux2;
double t; // time
double *pp,*tp1,*tp2,*tp3;

pp = new double[nobs];
tp1 = new double[nobs];
tp2 = new double[nobs];
tp3 = new double[nobs];

db0_fin_inGauss = db0_ini_inGauss + signedSweepWidth_inGauss;

double protonOmega_Lab;
double protonOmega_Lab_increment;
double electronOmega_Rot;
double electronOmega_Rot_increment;
double ddt;
//+++++++++++++++++++++++++++++++++++++++++++++++++++++++++++++
char buf[10];
char fn[100];
fout2.open(outputFileName);
  if(!fout2)
     cout << outputFileName << ": Cannot open file."
          << endl;
     exit(1);

for (int simCount=1; simCount<=1000; simCount++)
  strcpy(fn, outputFileName);
  sprintf(buf, "%d", simCount);
  strcat(fn, "_"); strcat(fn, buf);strcat(fn, ".dat");

//*****************  Time independent terms ******************

H = dipolarHamiltonian_HH(pen, a, b, g, po)  // H-H dipolar int.
    + zfsHamiltonian(pen,a,b,ZFS_D,ZFS_E)     // ZFS
   + 1e-4*b1_inGauss*ELECTRONGAMMA*Ix(pen,0) // microwave
   + hfcHamiltonian(pen, a, b, g, po);   // HFC

H_aux = nuclearZeemanHamiltonian_aux(pen);
H_aux2 = Fz(pen,0);
//*****************  initial (t=0) setup 2 ******************

for(q=0; q<nobs; q++)
  pp[q]=0; tp1[q]=0; tp2[q]=0; tp3[q]=0;
  // initialization
//*************************************************************
for(br_count=0; br_count<n_protonBroadening; br_count++)
//
  cout << simCount << " :  " << br_count+1 << endl;
//
rho0=initialDensityOperator(pen,b0,iniTemp,
               population1,population2,population3);
rho=rho0;
t=0.0; q=0;

//
protonOmega_Lab = protonOmega(b0 + (db0_ini_inGauss*1.0e-4));
protonOmega_Lab +=
    protonOmega(protonBroadening_inGauss*1.0e-4*(1-n_protonBroadening)/(2*n_protonBroadening));
protonOmega_Lab +=
    protonOmega(protonBroadening_inGauss*1.0e-4*br_count/n_protonBroadening);

protonOmega_Lab_increment =
             protonOmega(1.0e-4*dt*signedSweepWidth_inGauss/sweepTime);
electronOmega_Rot = electronOmega(b0 + (db0_ini_inGauss*1.0e-4)) - omega;
electronOmega_Rot_increment =
             electronOmega(1.0e-4*dt*signedSweepWidth_inGauss/sweepTime);
ddt=obs_step*dt;
//
//*****************  TIME EVOLUTION LOOP *********************
//
while(t<=sweepTime)
```

```
         pp[q] += protonPolarization(pen,rho);
         tp1[q] += tripletPopulation1(pen,rho);
         tp2[q] += tripletPopulation2(pen,rho);
         tp3[q] += tripletPopulation3(pen,rho);

for(obs_count=0; obs_count<obs_step; obs_count++)
   H_t = H + (electronOmega_Rot * H_aux2) + (protonOmega_Lab * H_aux);
   rho = evolve(rho, H_t, dt);
   protonOmega_Lab += protonOmega_Lab_increment;
   electronOmega_Rot += electronOmega_Rot_increment;
 // for
   t += ddt;   // time increment
   q++;       // counter increment
 // while
//
 // br_count
//
//**************  END OF TIME EVOLUTION LOOP *****************
//
for(q=0; q<nobs; q++)
  pp[q] = pp[q]/n_protonBroadening;
  tp1[q] = tp1[q]/n_protonBroadening;
  tp2[q] = tp2[q]/n_protonBroadening;
  tp3[q] = tp3[q]/n_protonBroadening;

//
fout.open(fn);
  if(!fout)
     cout << fn << ": Cannot open file." << endl;
     exit(1);

//
for(q=0; q<nobs; q++)
   fout << q*dt
        << "  " << pp[q]
        << "  " << tp1[q]
        << "  " << tp2[q]
        << "  " << tp3[q] << endl;

  fout.close();
//
//
  fout2 << b1_inGauss
        << "  " << pp[nobs-1]
        << "  " << tp1[nobs-1]
        << "  " << tp2[nobs-1]
        << "  " << (tp1[nobs-1]-tp2[nobs-1])/(tp1[nobs-1]+tp2[nobs-1])
        << "  " << tp3[nobs-1] << endl;

  b1_inGauss += 0.005;

 // simCount
  fout2.close();
  delete[] pp;
  delete[] tp1; delete[] tp2; delete[] tp3;
```

■□■ An example of the input parameter file ■□■

```
ZFS_D  1381.5e6
```

```
ZFS_E   42.5e6
population1 0.12
population2 0.76
population3 0.12
nProton 4
hydrogenSites 3 4 5 6
dt 1e-8
sweepTime 15e-6
db0_ini_inGauss -36.0
signedSweepWidth_inGauss 72.0
b1_frequency_Hz 9.7e9
b1_inGauss 0
b0 0.3187
iniTemp 3000000
a 0
b 90
g 0
obs_step 10
outputFileName r
#
------ comments ------
ZFS_D  1381.5e6    ZFS D parameter (1/s)
ZFS_E   42.5e6     ZFS E parameter (1/s)
population1 0.12   population on the triplet substate |1> (no dimension)
population2 0.76   population on the triplet substate |2> (no dimension)
population3 0.12   population on the triplet substate |3> (no dimension)
nProton 4          number of proton to be considered (no dimension)
hydrogenSites 3 4 5 6  proton positions j
dt 1e-8
sweepTime 15e-6    ICP sweep time
db0_ini_inGauss -36.0   initial field offset (Gauss)
signedSweepWidth_inGauss 72.0  sweep width (Gauss);
                               positive (negative) for up(down)field sweep
b1_frequency_Hz 9.7e9  microwave frequency (1/s)
b1_inGauss 0
b0 0.3187         field strength (Tesla)
iniTemp 3000000   initial proton spin temperature (Kelvin)
a 0
b 90      Euler angles specifying the orientation
g 0       of a pentacene molecule (degree)
obs_step 10        data sampling interval (no dimension)
outputFileName  r  output filename (the extension ".dat" will be appended automatically)
```

9.2 Program list for the simulation of the ^{1}H polarization buildup

```
 #include <stdlib.h>
#include <time.h>
#include <iostream.h>
#include <fstream.h>
#include <string.h>
#include <math.h>

#define RANDOM_0_1 rand()/(1.0+RAND_MAX)


int n, nSquare, nCube; // n: boxels per side
                       // nSquare: n^2
                       // nCube: n^3 = total number of boxels
```

```
double rDelayICP; // ICP recycle delay

int nt;      // number of time steps during rDelayICP
int nt_half; // nt/2
             // NOTE: nt must be set to an
             //       even number in a parameter file.

int nICP;    // total repetition of ICP sequences

int nGuest;  // number of guest molecules
int nObs;    // number of the ICP operations during which
             //     the nuclear polarization is recorded

double thermalPolarization=0;
double electronPolarization=0;
double averagePolarization=0;

double dConst_xx, dConst_yy, dConst_zz; // (anisotropic) spin diffusion constant
double molecularWeight;  // molecular weight of the host molecule
                         // e.g.: naphthalene --> 128 g/mol
double density; // density of the host
                // e.g.: naphthalene --> 1.16E6 g/m^3
double nSpinsPerMolecule;
                // number of (proton) spins in a host molecule
                // e.g.: naphthalene --> 8
double guestConcentration;
             // concentration of the guest (in mol/mol)
const double avogadroNumber=6.0221367E23;

double exchangeProb; // Probability of spin exchange
double fictitiousSpinFraction; //
char fileName[100]; // output filename

int i,j,k,m,u,c; // counter variables
int aInt, ax, ay, az;     // aux. integers
double aReal;             // aux. real numbers

int randomInt(int min, int max);

void main(int argc, char **argv)

//
//################################
//####   Initialization (1)  ####
//################################
 cout << "---------------------------------" << endl
      << "---------------------------------" << endl
      << "    bup version 6.0    "           << endl
      << "      2003/1/14  by K. Takeda"      << endl
      << "---------------------------------" << endl
      << "---------------------------------" << endl;
switch(argc)
      case 2: break;
      default:
        cout << "Usage: bup5 <par file>" << endl;
        exit(1);
 // end of switch
//
//*****  read parameter file  *****
//
ifstream fin;
ofstream fout,fout1,fout_bup;
char fName[100], finName[100];
  strcpy(fName, argv[1]);
  strcpy(finName, fName);
  strcat(finName, ".par");
  fin.open(finName);
  if(!fin)
     cout << finName << ": Cannot open file."
          << endl;
     exit(1);


  char ach[100];
```

```
while(!fin.eof())
fin >> ach;
  if(!strcmp(ach,"dConst_xx"))
    fin >> dConst_xx;
    cout << "dConst_xx: " << dConst_xx << " m^2/s." << endl;

  else if(!strcmp(ach,"dConst_yy"))
    fin >> dConst_yy;
    cout << "dConst_yy: " << dConst_yy << " m^2/s." << endl;

  else if(!strcmp(ach,"dConst_zz"))
    fin >> dConst_zz;
    cout << "dConst_zz: " << dConst_zz << " m^2/s." << endl;

  else if(!strcmp(ach,"molecularWeight"))
    fin >> molecularWeight;
    cout << "molecularWeight: " << molecularWeight
         << " g/mol." << endl;

  else if(!strcmp(ach,"density"))
    fin >> density;
    cout << "density: " << density << " g/m^3." << endl;

  else if(!strcmp(ach,"nSpinsPerMolecule"))
    fin >> nSpinsPerMolecule;
    cout << "nSpinsPerMolecule: " << nSpinsPerMolecule
         << " (no dimension)." << endl;

  else if(!strcmp(ach,"guestConcentration"))
    fin >> guestConcentration;
    cout << "guestConcentration: " << guestConcentration
         << " mol/mol." << endl;

  else if(!strcmp(ach,"electronPolarization"))
    fin >> electronPolarization;
    cout << "electronPolarization: " << electronPolarization
         << " (no dimension)." << endl;

  else if(!strcmp(ach,"rDelayICP"))
    fin >> rDelayICP;
    cout << "rDelayICP: " << rDelayICP << " s." << endl;

  else if(!strcmp(ach,"n"))
    fin >> n;
    cout << "n: " << n << " (no dimension)." << endl;

  else if(!strcmp(ach,"nt"))
    fin >> nt;
    cout << "nt: " << nt << " (no dimension)." << endl;

  else if(!strcmp(ach,"nICP"))
    fin >> nICP;
    cout << "nICP: " << nICP << " (no dimension)." << endl;

  else if(!strcmp(ach,"nGuest"))
    fin >> nGuest;
    cout << "nGuest: " << nGuest << " (no dimension)." << endl;

  else if(!strcmp(ach,"fileName"))
    fin >> fileName;
    cout << "fileName: " << fileName << "." << endl;

  else if(!strcmp(ach,"nObs"))
    fin >> nObs;
    cout << "nObs: " << nObs << " (no dimension)" << endl;

  else if(!strcmp(ach,"exchangeProb"))
    fin >> exchangeProb;
    cout << "exchangeProb: " << exchangeProb
         << " (no dimension)" << endl;

  else if(!strcmp(ach,"fictitiousSpinFraction"))
    fin >> fictitiousSpinFraction;
    cout << "fictitiousSpinFraction: " << fictitiousSpinFraction
```

```
          << " (no dimension)" << endl;

    else if(strcmp(ach,"#")) break;
   // while
  fin.close();
//
//*****  Reset random number  *****
//
  srand((unsigned int) time(0));
//
//
//################################################
//####                                        ####
//####  Initialization (2)                    ####
//####                                        ####
//####   variables that need to be declared   ####
//####   (or to be assigned)                  ####
//####   AFTER reading a parameter file       ####
//################################################
//
if(div(nt,2).rem==1) // Is nt odd integer?
  cout << "Warning! nt must be an even integer." << endl;
  exit(1);

nt_half = div(nt,2).quot;

nSquare = n*n;
nCube = n*n*n;  cout << "nCube: " << nCube << endl;

double volume = nGuest*molecularWeight
               /(guestConcentration*avogadroNumber*density);
              //  total volume under consideration (in m^3)

cout << "volume: " << volume << endl;
double L = pow(volume, (1.0/3.0));

cout << "Length: " << L << endl;
              //  Length;
double dx = L/n; // boxel size
cout << "dx: " << dx << endl;

double dGuest = (double)nGuest/nCube;
               // average number of guest molecules
               //     per unit boxel
               //  NOTE: (dGuest << 1) is necessary.
cout << "dGuest: " << dGuest << endl;
if(dGuest>0.1)
  cout << "Warning! dGuest (" << dGuest << ") is too large!"
       << endl << "larger n than " << n
       << " or smaller nGuest than "<< nGuest
       << " is necessary." << endl;
  exit(1);


double nSpinsPerBoxel;
nSpinsPerBoxel = dGuest*nSpinsPerMolecule/guestConcentration;
cout << "Spins per boxel: " << nSpinsPerBoxel << endl;

double dP;

double dt = rDelayICP/nt;
cout << "dt: " << dt << " s" << endl;

double lambda_xx = dConst_xx*dt/(dx*dx);
double lambda_yy = dConst_yy*dt/(dx*dx);
double lambda_zz = dConst_zz*dt/(dx*dx);

cout << "lambda_xx: " << lambda_xx << endl;
cout << "lambda_yy: " << lambda_yy << endl;
cout << "lambda_zz: " << lambda_zz << endl;

if((lambda_xx>=0.15) || (lambda_yy>=0.15) || (lambda_zz>=0.15))
   cout << "Warning: lambda_?? = dConst_??*dt/(dx*dx) must be
       smaller than 0.15 (stability condition)." << endl;
```

```
   exit(1);


double eta = 1.0 - (2.0*lambda_xx) - (2.0*lambda_yy) - (2.0*lambda_zz);

cout << "eta: " << eta << endl;

//
//***** positions of polarization sources *****
//
  bool occupied[nCube];
  int gpx[nGuest], gpy[nGuest], gpz[nGuest];

  for(c=0; c<nCube; c++) occupied[c]=false;
  c=0;
  while(c<nGuest)
    aInt = randomInt(0,nCube);  //cout << aInt << "   ";
    if(occupied[aInt]==false)  // unoccupied yet?
      occupied[aInt]=true;

      gpz[c]=div(aInt, nSquare).quot;
      aInt = div(aInt, nSquare).rem;
      gpy[c]=div(aInt,n).quot;
      gpx[c]=(int)div(aInt,n).rem;

      //cout << gpx[c] << " " << gpy[c] << " " << gpz[c] << endl;
      c++;
       // if
   // while
//***** output guest positions *****
  char distFileName[100];
  strcpy(distFileName, fileName);
  strcat(distFileName, ".dist");
  fout.open(distFileName);
  if(!fout)
     cout << distFileName << ": Cannot open file."
          << endl;
     exit(1);

  for(c=0; c<nGuest; c++)
     fout << gpx[c] << "  " << gpy[c] << "  " << gpz[c] << endl;

  fout.close();
//
//***** initialization of boxels P & Q *****
//
double P[n][n][n],
       Q[n][n][n]; // nuclear polarization
for(i=0;i<n;i++)for(j=0;j<n;j++)for(k=0;k<n;k++)
  P[i][j][k] = 0.0; Q[i][j][k] = 0.0;
 // k,j,i

//
//############################
//####   Calc. start   #####
//############################
//
//***** data file *****
//
  char datFileName[100];
  char bupFileName[100];
  strcpy(datFileName, fileName); strcat(datFileName, ".dat");
  strcpy(bupFileName, fileName); strcat(bupFileName, ".bup");

  fout1.open(datFileName);
  if(!fout)
     cout << datFileName << ": Cannot open file." << endl; exit(1);


  fout_bup.open(bupFileName);
  if(!fout_bup)
     cout << bupFileName << ": Cannot open file."
          << endl;
     exit(1);
```

```
//
//*****  repetition of ICP *****
//
for(u=0; u<nICP; u++)

//
// ***********************************************
//
 if(!div(u,nObs).rem)   // time to observe?

   // --- output to a dat file ---
   for(j=0;j<n;j++)  for(i=0;i<n;i++)
     fout1 << P[n-1][i][j] << " ";

   fout1 << endl;

   // --- output to a bup file ---
   aReal=0;
   for(i=0; i<n; i++)  for(j=0; j<n; j++)  for(k=0; k<n; k++)
      aReal += P[i][j][k];

   averagePolarization = aReal/nCube;
   fout_bup << u*rDelayICP << "  " << averagePolarization << endl;

   // --- display the status of a calculation ---
   cout << u*rDelayICP << " s: " << averagePolarization << endl;
  // if
//
// ***********************************************
//

//***** Polarization transfer by ICP *****
  srand((unsigned int) time(0));
  for(c=0; c<nGuest; c++)
    ax = gpx[c]; ay = gpy[c]; az = gpz[c];
    aReal = RANDOM_0_1;
    if(aReal<fictitiousSpinFraction)
      aReal = RANDOM_0_1;
      if(aReal<exchangeProb)
       dP = (electronPolarization-P[ax][ay][az])/nSpinsPerBoxel;
       P[ax][ay][az] += dP;


   // c
//
//*****  time evolution during rDelayICP  *****
//
for(m=0; m<nt_half; m++)

//
//
//==== 3-D Diffusion with periodic boundary cond. ===
//
//++++++ 1st stage: P ---> Q  ++++++
//
//+=+=+=+ CASE A: (k=0) +=+=+=+
// CASE A1: (i=0, j=0, k=0)
  Q[0][0][0] = eta*P[0][0][0]
             + lambda_xx * ( P[n-1][0][0] + P[1][0][0] )
             + lambda_yy * ( P[0][n-1][0] + P[0][1][0] )
             + lambda_zz * ( P[0][0][n-1] + P[0][0][1] );
// CASE A2: (i=n-1, j=0, k=0)
  Q[n-1][0][0] = eta*P[n-1][0][0]
               + lambda_xx * ( P[n-2][0][0]   + P[0][0][0] )
               + lambda_yy * ( P[n-1][n-1][0] + P[n-1][1][0] )
               + lambda_zz * ( P[n-1][0][n-1] + P[n-1][0][1] );
// CASE A3: (i=n-1, j=n-1, k=0)
  Q[n-1][n-1][0] = eta*P[n-1][n-1][0]
                 + lambda_xx * ( P[n-2][n-1][0]   + P[0][n-1][0] )
                 + lambda_yy * ( P[n-1][n-2][0]   + P[n-1][0][0] )
                 + lambda_zz * ( P[n-1][n-1][n-1] + P[n-1][n-1][1] );
// CASE A4: (i=0, j=n-1, k=0)
  Q[0][n-1][0] = eta*P[0][n-1][0]
```

```
               + lambda_xx * ( P[n-1][n-1][0] + P[1][n-1][0] )
               + lambda_yy * ( P[0][n-2][0]   + P[0][0][0] )
               + lambda_zz * ( P[0][n-1][n-1] + P[0][n-1][1] );
// CASE A5: (0<i<n-1, j=0, k=0)
for(i=1; i<n-1; i++)
  Q[i][0][0] = eta*P[i][0][0]
             + lambda_xx * ( P[i-1][0][0] + P[i+1][0][0] )
             + lambda_yy * ( P[i][n-1][0] + P[i][1][0] )
             + lambda_zz * ( P[i][0][n-1] + P[i][0][1] );
// i
// CASE A6: (i=n-1, 0<j<n-1, k=0)
for(j=1; j<n-1; j++)
  Q[n-1][j][0] = eta*P[n-1][j][0]
               + lambda_xx * ( P[n-2][j][0]   + P[0][j][0] )
               + lambda_yy * ( P[n-1][j-1][0] + P[n-1][j+1][0] )
               + lambda_zz * ( P[n-1][j][n-1] + P[n-1][j][1] );
 // j
// CASE A7: (0<i<n-1, j=n-1, k=0)
for(i=1; i<n-1; i++)
  Q[i][n-1][0] = eta*P[i][n-1][0]
               + lambda_xx * ( P[i-1][n-1][0] + P[i+1][n-1][0] )
               + lambda_yy * ( P[i][n-2][0]   + P[i][0][0] )
               + lambda_zz * ( P[i][n-1][n-1] + P[i][n-1][1] );
 // i
// CASE A8: (i=0, 0<j<n-1, k=0)
for(j=1; j<n-1; j++)
  Q[0][j][0] = eta*P[0][j][0]
             + lambda_xx * ( P[n-1][j][0] + P[1][j][0] )
             + lambda_yy * ( P[0][j-1][0] + P[0][j+1][0] )
             + lambda_zz * ( P[0][j][n-1] + P[0][j][1] );
 // j
// CASE A9: (0<i<n-1, 0<j<n-1, k=0)
for(i=1; i<n-1; i++)
for(j=1; j<n-1; j++)
  Q[i][j][0] = eta*P[i][j][0]
             + lambda_xx * ( P[i-1][j][0] + P[i+1][j][0] )
             + lambda_yy * ( P[i][j-1][0] + P[i][j+1][0] )
             + lambda_zz * ( P[i][j][n-1] + P[i][j][1] );
// j
// i

//
//+=+=+=+ CASE B: (0<k<n-1) +=+=+=+
// CASE B1: (i=0, j=0, 0<k<n-1)
for(k=1; k<n-1; k++)
  Q[0][0][k] = eta*P[0][0][k]
             + lambda_xx * ( P[n-1][0][k] + P[1][0][k] )
             + lambda_yy * ( P[0][n-1][k] + P[0][1][k] )
             + lambda_zz * ( P[0][0][k-1] + P[0][0][k+1] );
 // k
// CASE B2: (i=n-1, j=0, 0<k<n-1)
for(k=1; k<n-1; k++)
  Q[n-1][0][k] = eta*P[n-1][0][k]
               + lambda_xx * ( P[n-2][0][k]   + P[0][0][k] )
               + lambda_yy * ( P[n-1][n-1][k] + P[n-1][1][k] )
               + lambda_zz * ( P[n-1][0][k-1] + P[n-1][0][k+1] );
 // k
// CASE B3: (i=n-1, j=n-1, 0<k<n-1)
for(k=1; k<n-1; k++)
  Q[n-1][n-1][k] = eta*P[n-1][n-1][k]
                 + lambda_xx * ( P[n-2][n-1][k]   + P[0][n-1][k] )
                 + lambda_yy * ( P[n-1][n-2][k]   + P[n-1][0][k] )
                 + lambda_zz * ( P[n-1][n-1][k-1] + P[n-1][n-1][k+1] );
 // k
// CASE B4: (i=0, j=n-1, 0<k<n-1)
for(k=1; k<n-1; k++)
  Q[0][n-1][k] = eta*P[0][n-1][k]
               + lambda_xx * ( P[n-1][n-1][k] + P[1][n-1][k] )
               + lambda_yy * ( P[0][n-2][k]   + P[0][0][k] )
               + lambda_zz * ( P[0][n-1][k-1] + P[0][n-1][k+1] );
 // k
// CASE B5: (0<i<n-1, j=0, 0<k<n-1)
for(k=1; k<n-1; k++)
for(i=1; i<n-1; i++)
```

```
  Q[i][0][k] = eta*P[i][0][k]
             + lambda_xx * ( P[i-1][0][k] + P[i+1][0][k] )
             + lambda_yy * ( P[i][n-1][k] + P[i][1][k] )
             + lambda_zz * ( P[i][0][k-1] + P[i][0][k+1] );
 // i
 // k
// CASE B6: (i=n-1, 0<j<n-1, 0<k<n-1)
for(k=1; k<n-1; k++)
for(j=1; j<n-1; j++)
  Q[n-1][j][k] = eta*P[n-1][j][k]
               + lambda_xx * ( P[n-2][j][k]   + P[0][j][k] )
               + lambda_yy * ( P[n-1][j-1][k] + P[n-1][j+1][k] )
               + lambda_zz * ( P[n-1][j][k-1] + P[n-1][j][k+1] );
 // j
 // k
// CASE B7: (0<i<n-1, j=n-1, 0<k<n-1)
for(k=1; k<n-1; k++)
for(i=1; i<n-1; i++)
  Q[i][n-1][k] = eta*P[i][n-1][k]
               + lambda_xx * ( P[i-1][n-1][k] + P[i+1][n-1][k] )
               + lambda_yy * ( P[i][n-2][k]   + P[i][0][k] )
               + lambda_zz * ( P[i][n-1][k-1] + P[i][n-1][k+1] );
 // i
 // k
// CASE B8: (i=0, 0<j<n-1, 0<k<n-1)
for(k=1; k<n-1; k++)
for(j=1; j<n-1; j++)
  Q[0][j][k] = eta*P[0][j][k]
             + lambda_xx * ( P[n-1][j][k] + P[1][j][k] )
             + lambda_yy * ( P[0][j-1][k] + P[0][j+1][k] )
             + lambda_zz * ( P[0][j][k-1] + P[0][j][k+1] );
 // j
 // k
// CASE B9: (0<i<n-1, 0<j<n-1, 0<k<n-1)
for(k=1; k<n-1; k++)
for(i=1; i<n-1; i++)
for(j=1; j<n-1; j++)
  Q[i][j][k] = eta*P[i][j][k]
             + lambda_xx * ( P[i-1][j][k] + P[i+1][j][k] )
             + lambda_yy * ( P[i][j-1][k] + P[i][j+1][k] )
             + lambda_zz * ( P[i][j][k-1] + P[i][j][k+1] );
 // j
 // i
 // k

//+=+=+=+ CASE C: (k=n-1) +=+=+=+
// CASE C1: (i=0, j=0, k=n-1)
  Q[0][0][n-1] = eta*P[0][0][n-1]
               + lambda_xx * ( P[n-1][0][n-1] + P[1][0][n-1] )
               + lambda_yy * ( P[0][n-1][n-1] + P[0][1][n-1] )
               + lambda_zz * ( P[0][0][n-2]   + P[0][0][0] );
// CASE C2: (i=n-1, j=0, k=n-1)
  Q[n-1][0][n-1] = eta*P[n-1][0][n-1]
                 + lambda_xx * ( P[n-2][0][n-1]   + P[0][0][n-1] )
                 + lambda_yy * ( P[n-1][n-1][n-1] + P[n-1][1][n-1] )
                 + lambda_zz * ( P[n-1][0][n-2]   + P[n-1][0][0] );
// CASE C3: (i=n-1, j=n-1, k=n-1)
  Q[n-1][n-1][n-1] = eta*P[n-1][n-1][n-1]
                   + lambda_xx * ( P[n-2][n-1][n-1] + P[0][n-1][n-1] )
                   + lambda_yy * ( P[n-1][n-2][n-1] + P[n-1][0][n-1] )
                   + lambda_zz * ( P[n-1][n-1][n-2] + P[n-1][n-1][0] );
// CASE C4: (i=0, j=n-1, k=n-1)
  Q[0][n-1][n-1] = eta*P[0][n-1][n-1]
                 + lambda_xx * ( P[n-1][n-1][n-1] + P[1][n-1][n-1] )
                 + lambda_yy * ( P[0][n-2][n-1]   + P[0][0][n-1] )
                 + lambda_zz * ( P[0][n-1][n-2]   + P[0][n-1][0] );
// CASE C5: (0<i<n-1, j=0, k=n-1)
for(i=1; i<n-1; i++)
  Q[i][0][n-1] = eta*P[i][0][n-1]
               + lambda_xx * ( P[i-1][0][n-1] + P[i+1][0][n-1] )
               + lambda_yy * ( P[i][n-1][n-1] + P[i][1][n-1] )
               + lambda_zz * ( P[i][0][n-2]   + P[i][0][0] );
 // i
// CASE C6: (i=n-1, 0<j<n-1, k=n-1)
```

```
for(j=1; j<n-1; j++)
  Q[n-1][j][n-1] = eta*P[n-1][j][n-1]
                 + lambda_xx * ( P[n-2][j][n-1]   + P[0][j][n-1] )
                 + lambda_yy * ( P[n-1][j-1][n-1] + P[n-1][j+1][n-1] )
                 + lambda_zz * ( P[n-1][j][n-2]   + P[n-1][j][0] );
 // j
// CASE C7: (0<i<n-1, j=n-1, k=n-1)
for(i=1; i<n-1; i++)
  Q[i][n-1][n-1] = eta*P[i][n-1][n-1]
                 + lambda_xx * ( P[i-1][n-1][n-1] + P[i+1][n-1][n-1] )
                 + lambda_yy * ( P[i][n-2][n-1]   + P[i][0][n-1] )
                 + lambda_zz * ( P[i][n-1][n-2]   + P[i][n-1][0] );
 // i
// CASE C8: (i=0, 0<j<n-1, k=n-1)
for(j=1; j<n-1; j++)
  Q[0][j][n-1] = eta*P[0][j][n-1]
               + lambda_xx * ( P[n-1][j][n-1] + P[1][j][n-1] )
               + lambda_yy * ( P[0][j-1][n-1] + P[0][j+1][n-1] )
               + lambda_zz * ( P[0][j][n-2]   + P[0][j][0] );
 // j
// CASE C9: (0<i<n-1, 0<j<n-1, k=n-1)
for(i=1; i<n-1; i++)
for(j=1; j<n-1; j++)
  Q[i][j][n-1] = eta*P[i][j][n-1]
               + lambda_xx * ( P[i-1][j][n-1] + P[i+1][j][n-1] )
               + lambda_yy * ( P[i][j-1][n-1] + P[i][j+1][n-1] )
               + lambda_zz * ( P[i][j][n-2]   + P[i][j][0] );
 // j
 // i

//++++++ 2nd stage: Q ---> P  ++++++
//
//+=+=+=+ CASE A: (k=0) +=+=+=+
// CASE A1: (i=0, j=0, k=0)
  P[0][0][0] = eta*Q[0][0][0]
             + lambda_xx * ( Q[n-1][0][0] + Q[1][0][0] )
             + lambda_yy * ( Q[0][n-1][0] + Q[0][1][0] )
             + lambda_zz * ( Q[0][0][n-1] + Q[0][0][1] );
// CASE A2: (i=n-1, j=0, k=0)
  P[n-1][0][0] = eta*Q[n-1][0][0]
               + lambda_xx * ( Q[n-2][0][0]   + Q[0][0][0] )
               + lambda_yy * ( Q[n-1][n-1][0] + Q[n-1][1][0] )
               + lambda_zz * ( Q[n-1][0][n-1] + Q[n-1][0][1] );
// CASE A3: (i=n-1, j=n-1, k=0)
  P[n-1][n-1][0] = eta*Q[n-1][n-1][0]
                 + lambda_xx * ( Q[n-2][n-1][0]   + Q[0][n-1][0] )
                 + lambda_yy * ( Q[n-1][n-2][0]   + Q[n-1][0][0] )
                 + lambda_zz * ( Q[n-1][n-1][n-1] + Q[n-1][n-1][1] );
// CASE A4: (i=0, j=n-1, k=0)
  P[0][n-1][0] = eta*Q[0][n-1][0]
               + lambda_xx * ( Q[n-1][n-1][0] + Q[1][n-1][0] )
               + lambda_yy * ( Q[0][n-2][0]   + Q[0][0][0] )
               + lambda_zz * ( Q[0][n-1][n-1] + Q[0][n-1][1] );
// CASE A5: (0<i<n-1, j=0, k=0)
for(i=1; i<n-1; i++)
  P[i][0][0] = eta*Q[i][0][0]
             + lambda_xx * ( Q[i-1][0][0] + Q[i+1][0][0] )
             + lambda_yy * ( Q[i][n-1][0] + Q[i][1][0] )
             + lambda_zz * ( Q[i][0][n-1] + Q[i][0][1] );
// i
// CASE A6: (i=n-1, 0<j<n-1, k=0)
for(j=1; j<n-1; j++)
  P[n-1][j][0] = eta*Q[n-1][j][0]
               + lambda_xx * ( Q[n-2][j][0]   + Q[0][j][0] )
               + lambda_yy * ( Q[n-1][j-1][0] + Q[n-1][j+1][0] )
               + lambda_zz * ( Q[n-1][j][n-1] + Q[n-1][j][1] );
 // j
// CASE A7: (0<i<n-1, j=n-1, k=0)
for(i=1; i<n-1; i++)
  P[i][n-1][0] = eta*Q[i][n-1][0]
               + lambda_xx * ( Q[i-1][n-1][0] + Q[i+1][n-1][0] )
               + lambda_yy * ( Q[i][n-2][0]   + Q[i][0][0] )
               + lambda_zz * ( Q[i][n-1][n-1] + Q[i][n-1][1] );
 // i
```

```
// CASE A8: (i=0, 0<j<n-1, k=0)
for(j=1; j<n-1; j++)
  P[0][j][0] = eta*Q[0][j][0]
             + lambda_xx * ( Q[n-1][j][0] + Q[1][j][0] )
             + lambda_yy * ( Q[0][j-1][0] + Q[0][j+1][0] )
             + lambda_zz * ( Q[0][j][n-1] + Q[0][j][1] );
 // j
// CASE A9: (0<i<n-1, 0<j<n-1, k=0)
for(i=1; i<n-1; i++)
for(j=1; j<n-1; j++)
  P[i][j][0] = eta*Q[i][j][0]
             + lambda_xx * ( Q[i-1][j][0] + Q[i+1][j][0] )
             + lambda_yy * ( Q[i][j-1][0] + Q[i][j+1][0] )
             + lambda_zz * ( Q[i][j][n-1] + Q[i][j][1] );
// j
// i

//
//+=+=+=+ CASE B: (0<k<n-1) +=+=+=+
// CASE B1: (i=0, j=0, 0<k<n-1)
for(k=1; k<n-1; k++)
  P[0][0][k] = eta*Q[0][0][k]
             + lambda_xx * ( Q[n-1][0][k] + Q[1][0][k] )
             + lambda_yy * ( Q[0][n-1][k] + Q[0][1][k] )
             + lambda_zz * ( Q[0][0][k-1] + Q[0][0][k+1] );
 // k
// CASE B2: (i=n-1, j=0, 0<k<n-1)
for(k=1; k<n-1; k++)
  P[n-1][0][k] = eta*Q[n-1][0][k]
               + lambda_xx * ( Q[n-2][0][k]   + Q[0][0][k] )
               + lambda_yy * ( Q[n-1][n-1][k] + Q[n-1][1][k] )
               + lambda_zz * ( Q[n-1][0][k-1] + Q[n-1][0][k+1] );
 // k
// CASE B3: (i=n-1, j=n-1, 0<k<n-1)
for(k=1; k<n-1; k++)
  P[n-1][n-1][k] = eta*Q[n-1][n-1][k]
                 + lambda_xx * ( Q[n-2][n-1][k]   + Q[0][n-1][k] )
                 + lambda_yy * ( Q[n-1][n-2][k]   + Q[n-1][0][k] )
                 + lambda_zz * ( Q[n-1][n-1][k-1] + Q[n-1][n-1][k+1] );
 // k
// CASE B4: (i=0, j=n-1, 0<k<n-1)
for(k=1; k<n-1; k++)
  P[0][n-1][k] = eta*Q[0][n-1][k]
               + lambda_xx * ( Q[n-1][n-1][k] + Q[1][n-1][k] )
               + lambda_yy * ( Q[0][n-2][k]   + Q[0][0][k] )
               + lambda_zz * ( Q[0][n-1][k-1] + Q[0][n-1][k+1] );
 // k
// CASE B5: (0<i<n-1, j=0, 0<k<n-1)
for(k=1; k<n-1; k++)
for(i=1; i<n-1; i++)
  P[i][0][k] = eta*Q[i][0][k]
             + lambda_xx * ( Q[i-1][0][k] + Q[i+1][0][k] )
             + lambda_yy * ( Q[i][n-1][k] + Q[i][1][k] )
             + lambda_zz * ( Q[i][0][k-1] + Q[i][0][k+1] );
 // i
 // k
// CASE B6: (i=n-1, 0<j<n-1, 0<k<n-1)
for(k=1; k<n-1; k++)
for(j=1; j<n-1; j++)
  P[n-1][j][k] = eta*Q[n-1][j][k]
               + lambda_xx * ( Q[n-2][j][k]   + Q[0][j][k] )
               + lambda_yy * ( Q[n-1][j-1][k] + Q[n-1][j+1][k] )
               + lambda_zz * ( Q[n-1][j][k-1] + Q[n-1][j][k+1] );
 // j
 // k
// CASE B7: (0<i<n-1, j=n-1, 0<k<n-1)
for(k=1; k<n-1; k++)
for(i=1; i<n-1; i++)
  P[i][n-1][k] = eta*Q[i][n-1][k]
               + lambda_xx * ( Q[i-1][n-1][k] + Q[i+1][n-1][k] )
               + lambda_yy * ( Q[i][n-2][k]   + Q[i][0][k] )
               + lambda_zz * ( Q[i][n-1][k-1] + Q[i][n-1][k+1] );
 // i
 // k
```

```
// CASE B8: (i=0, 0<j<n-1, 0<k<n-1)
for(k=1; k<n-1; k++)
for(j=1; j<n-1; j++)
  P[0][j][k] = eta*Q[0][j][k]
             + lambda_xx * ( Q[n-1][j][k] + Q[1][j][k] )
             + lambda_yy * ( Q[0][j-1][k] + Q[0][j+1][k] )
             + lambda_zz * ( Q[0][j][k-1] + Q[0][j][k+1] );
 // j
 // k
// CASE B9: (0<i<n-1, 0<j<n-1, 0<k<n-1)
for(k=1; k<n-1; k++)
for(i=1; i<n-1; i++)
for(j=1; j<n-1; j++)
  P[i][j][k] = eta*Q[i][j][k]
             + lambda_xx * ( Q[i-1][j][k] + Q[i+1][j][k] )
             + lambda_yy * ( Q[i][j-1][k] + Q[i][j+1][k] )
             + lambda_zz * ( Q[i][j][k-1] + Q[i][j][k+1] );
 // j
 // i
 // k

//+=+=+=+ CASE C: (k=n-1) +=+=+=+
// CASE C1: (i=0, j=0, k=n-1)
  P[0][0][n-1] = eta*Q[0][0][n-1]
               + lambda_xx * ( Q[n-1][0][n-1] + Q[1][0][n-1] )
               + lambda_yy * ( Q[0][n-1][n-1] + Q[0][1][n-1] )
               + lambda_zz * ( Q[0][0][n-2]   + Q[0][0][0] );
// CASE C2: (i=n-1, j=0, k=n-1)
  P[n-1][0][n-1] = eta*Q[n-1][0][n-1]
                 + lambda_xx * ( Q[n-2][0][n-1]   + Q[0][0][n-1] )
                 + lambda_yy * ( Q[n-1][n-1][n-1] + Q[n-1][1][n-1] )
                 + lambda_zz * ( Q[n-1][0][n-2]   + Q[n-1][0][0] );
// CASE C3: (i=n-1, j=n-1, k=n-1)
  P[n-1][n-1][n-1] = eta*Q[n-1][n-1][n-1]
                   + lambda_xx * ( Q[n-2][n-1][n-1] + Q[0][n-1][n-1] )
                   + lambda_yy * ( Q[n-1][n-2][n-1] + Q[n-1][0][n-1] )
                   + lambda_zz * ( Q[n-1][n-1][n-2] + Q[n-1][n-1][0] );
// CASE C4: (i=0, j=n-1, k=n-1)
  P[0][n-1][n-1] = eta*Q[0][n-1][n-1]
                 + lambda_xx * ( Q[n-1][n-1][n-1] + Q[1][n-1][n-1] )
                 + lambda_yy * ( Q[0][n-2][n-1]   + Q[0][0][n-1] )
                 + lambda_zz * ( Q[0][n-1][n-2]   + Q[0][n-1][0] );
// CASE C5: (0<i<n-1, j=0, k=n-1)
for(i=1; i<n-1; i++)
  P[i][0][n-1] = eta*Q[i][0][n-1]
               + lambda_xx * ( Q[i-1][0][n-1] + Q[i+1][0][n-1] )
               + lambda_yy * ( Q[i][n-1][n-1] + Q[i][1][n-1] )
               + lambda_zz * ( Q[i][0][n-2]   + Q[i][0][0] );
 // i
// CASE C6: (i=n-1, 0<j<n-1, k=n-1)
for(j=1; j<n-1; j++)
  P[n-1][j][n-1] = eta*Q[n-1][j][n-1]
                 + lambda_xx * ( Q[n-2][j][n-1]   + Q[0][j][n-1] )
                 + lambda_yy * ( Q[n-1][j-1][n-1] + Q[n-1][j+1][n-1] )
                 + lambda_zz * ( Q[n-1][j][n-2]   + Q[n-1][j][0] );
 // j
// CASE C7: (0<i<n-1, j=n-1, k=n-1)
for(i=1; i<n-1; i++)
  P[i][n-1][n-1] = eta*Q[i][n-1][n-1]
                 + lambda_xx * ( Q[i-1][n-1][n-1] + Q[i+1][n-1][n-1] )
                 + lambda_yy * ( Q[i][n-2][n-1]   + Q[i][0][n-1] )
                 + lambda_zz * ( Q[i][n-1][n-2]   + Q[i][n-1][0] );
 // i
// CASE C8: (i=0, 0<j<n-1, k=n-1)
for(j=1; j<n-1; j++)
  P[0][j][n-1] = eta*Q[0][j][n-1]
               + lambda_xx * ( Q[n-1][j][n-1] + Q[1][j][n-1] )
               + lambda_yy * ( Q[0][j-1][n-1] + Q[0][j+1][n-1] )
               + lambda_zz * ( Q[0][j][n-2]   + Q[0][j][0] );
 // j
// CASE C9: (0<i<n-1, 0<j<n-1, k=n-1)
for(i=1; i<n-1; i++)
for(j=1; j<n-1; j++)
  P[i][j][n-1] = eta*Q[i][j][n-1]
```

```
              + lambda_xx * ( Q[i-1][j][n-1] + Q[i+1][j][n-1] )
              + lambda_yy * ( Q[i][j-1][n-1] + Q[i][j+1][n-1] )
              + lambda_zz * ( Q[i][j][n-2]   + Q[i][j][0] );
 // j
 // i
//
//================================
//
 // m
 // u
//
//*****  End of calc.  *****
//
 fout1.close();     // close data dile
 fout_bup.close(); // close bup file

//
// End of main
//


//
//--------------------------------
//
int randomInt(int min, int max)
        // returns a random integer between min and max
 return min + (int)(rand()*(max-min+1.0)/(1.0+RAND_MAX));
 // randomInt
//
//--------------------------------
//
```

■□■ An example of the input parameter file ■□■

```
molecularWeight 128.0
density 1.16E6
nSpinsPerMolecule 8
dConst_xx 2.18E-16
dConst_yy 2.17E-16
dConst_zz 12.4E-16
guestConcentration 1.83E-4
electronPolarization 0.68
rDelayICP 2E-2
nt 24
nICP 5000
nObs 50
nGuest 540
n 30
fictitiousSpinFraction 0.7
exchangeProb 0.158
fileName a
#
------ comments ------
dConst_xx, dConst_yy, dConst_zz:
    anisotropic spin diffusion const. (m^2/s)
molecularWeight: (g/mol)
density: (g/m^3)
nSpinsPerMolecule: (no dimension)
guestConcentration: (mol/mol -> no dimension)
```

```
electronPolarization: (no dimension)
rDelayICP: ICP repetition delay (s)
nt: number of time steps during rDelayICP (no dimension)
nICP: total number of the ICP operations (no dimension)
nObs: number of the ICP operations during which
      the nuclear polarization is recorded.
nGuest: number of guest molecules in a
        volume under consideration (no dimension)
n: number of grids (no dimension)
fictitiousSpinFraction:
exchangeProb: probability for exchange (no dimension)
fileName: Output filename
```

Bibliography

[1] F. Bloch, W.W. Hansen, and M. Packard. Nuclear induction. *Phys. Rev.*, 69:127, 1946.

[2] F. Bloch, W.W. Hansen, and M. Packard. The nuclear induction experiment. *Phys. Rev.*, 70:474, 1946.

[3] F. Bloch. Nuclear induction. *Phys. Rev.*, 70:460, 1946.

[4] E.M. Purcell, H.C. Torrey, and R.V. Pound. Resonance absorption by nuclear magnetic moment in a solid. *Phys. Rev.*, 69:37, 1946.

[5] A. Abragam. *Principles of Nuclear Magnetism*. Clarendon, Oxford, 1961.

[6] A.W. Overhauser. Polarization of nuclei in metals. *Phys. Rev.*, 92:411, 1953.

[7] T.R. Carver and C.P. Slichter. Polarization of nuclear spins in metals. *Phys. Rev.*, 92:212, 1953.

[8] T.R. Carver and C.P. Slichter. Experimental verification of the overhauser nuclear polarization effect. *Phys. Rev.*, 102:975, 1956.

[9] A. Abragam. Overhauser effect in nonmetals. *Phys. Rev.*, 98:1729, 1955.

[10] I. Solomon. Relaxation process in a system of two spins. *Phys. Rev.*, 99:559, 1955.

[11] S. Un, T. Prisner, R.T. Weber, M.J. Seaman, K.W. Fishbein, A.E. McDermott, D.J. Singel, and R.G. Griffin. Pulsed dynamic nuclear polarization at 5t. *Chem. Phys. Lett.*, 189:54, 1992.

[12] C.D. Jeffries. Dynamic orientation of nuclei by forbidden transitions in paramagnetic resonance. *Phys. Rev.*, 117:1056, 1960.

[13] A. Abragam and M. Goldman. *Nuclear magnetism: order and disorder*. Clarendon, Oxford, 1982.

[14] R.A. Wind and H. Lock. Electron-nuclear polarization transfer in the nuclear rotating frame. *Adv. Magn. Opt. Reson.*, 15:51, 1990.

[15] G.J. Gerfen, L.R. Becerra, D.A. Hall, R.G. Griffin, R.J. Temkin, and D.J. Singel. High frequency (140 ghz) dynamic nuclear polarization: Polarization transfer to a solute in frozen aqueous solution. *J. Chem. Phys.*, 102:9494, 1995.

[16] A. Henstra, P. Dirksen, J. Schmidt, and W.Th. Wenckebach. Nuclear spin orientation via electron spin locking (novel). *J. Magn. Reson.*, 77:389–393, 1988.

[17] A. Henstra, P. Dirksen, and W.Th. Wenckebach. Enhanced dynamic nuclear polarization by the integrated solid effect. *Phys. Lett. A*, 134:134, 1988.

[18] G. Maier, U. Haeberlen, H.C. Wolf, and K.H. Hausser. Optische kernspin-polarisation in anthracen-kristallen. *Phys. Lett.*, 25A:384, 1967.

[19] H. Schuch, D. Stehlik, and K.H. Hausser. Optische kern-spin polarisation in moleckül-kristallen. *Z. Naturforsch*, 26a:1944, 1971.

[20] J.P. Colpa, K.H. Hausser, and D. Stehlik. Optical nuclear polarization by selective population of nuclear substates. *Z. Naturforsch*, 26a:1792–1799, 1971.

[21] J.P. Colpa and D. Stehlik. A mechanism for the optical nuclear spin alignment in zero magnetic field. *Z. Naturforsch*, 27a:1695–1704, 1972.

[22] P. Lau, D. Stehlik, and K.H. Hausser. Optical nuclear polarization of protons in fluorene-d8,h2 single crystals. *J. Magn. Reson.*, 15:270–282, 1974.

[23] D. Stehlik, A. Doehring, J.P. Colpa, E. Callaghan, and S. Kesmarky. Optical nuclear polarization in molecular crystals through an optical excitation cycle. *Chem. Phys.*, 7:165–186, 1975.

[24] G. Dittrich, D. Stehlik, and K.H. Hausser. Optische kernspin polarisation (onp) in anthracen dotiert mit phenazin im temperaturbereich 1,4...300k. *Z. Naturforsch*, 32a:652–658, 1977.

[25] J.P. Colpa and D. Stehlik. Optical nuclear polarization as a consequence of the non-crossing rule (level-anticrossing) i. analytical treatment of onp in the level-crossing region. *Chem. Phys.*, 21:273–288, 1977.

[26] D. Stehlik and J.P. Colpa. Optical nuclear polarization as a consequence of the non-crossing rule (level-anticrossing) ii. the influence of electronic relaxation. *Chem. Phys.*, 21:289–299, 1977.

[27] D. Stehlik, P. Rösch, P. Lau, H. Zimmermann, and K.H. Hausser. Optical nuclear polarization as a consequence of the non-crossing rule (level-anticrossing) iii. experimental results and evidence for guest-host complexes in doped fluorene crystals. *Chem. Phys.*, 21:301–309, 1977.

[28] J. Allgeier, V. Macho, D. Stehlik, H.M. Vieth, W. Auch, and J.U. von Schütz. Optical nuclear polarization via hyperfine relaxation. polarization mechanism in anthracene/tetracyanobenzene charge-transfer crystals. *Chem. Phys. Lett.*, 86:522, 1982.

[29] J. Allgeier, G. Buntkowsky, S. Hentrich, M. Nack, and H.-M. Vieth. Mobility in single crystals studied by optical nuclear polarization. *Ber. Bunsenges. Phys. Chem.*, 93:1281–1285, 1989.

[30] M. Deimling, H. Brunner, K.P. Dinse, K.H. Hausser, and J.P. Colpa. Microwave-induced optical nuclear polarization (mionp). *J. Magn. Reson.*, 39:185–202, 1980.

[31] A. Henstra, T.-S. Lin, J. Schmidt, and W.Th. Wenckebach. High dynamic nuclear polarization at room temperature. *Chem. Phys. Lett.*, 165:6, 1990.

[32] K. Takeda, K. Takegoshi, and T. Terao. Dynamic nuclear polarization by photoexcited-triplet electron spins in polycrystalline samples. *Chem. Phys. Lett.*, 345:166–170, 2001.

[33] M. Iinuma, Y. Takahashi, I. Shaké, M. Oda, A. Masaike, T. Yabuzaki, and H.M. Shimizu. High proton polarization by microwave-induced optical nuclear polarization at 77k. *Phys. Rev. Lett*, 84:171, 2000.

[34] H.W. van Kesteren, W.Th. Wenckebach, J. Schmidt, and N.J. Poulis. Dynamic nuclear polarization of proton spins via photoexcited triplet states: The system phenanthrene in fluorene. *Chem. Phys. Lett.*, 89:67, 1982.

[35] H.W. van Kesteren, W.Th. Wenckebach, and J. Schmidt. Production of high long-lasting, dynamic proton polarization by way of photoexcited triplet states. *Phys. Rev. Lett.*, 55:1642, 1985.

[36] M. Iinuma, I. Shake, R. Takizawa, M. Daigo, H.M. Shimizu, Y. Takahashi, A. Masaike, and T. Yabuzaki. High proton polarization in crystalline naphthalene by dynamic nuclear polarization with laser excitation at room temperature and liquid nitrogen temperature. *Phys. Lett. A*, 208:251–256, 1995.

[37] K. Takeda, K. Takegoshi, and T. Terao. Dynamic nuclear polarization by electron spins in the photoexcited triplet state: I. attainment of proton polarization of 0.7 at 105 k in naphthalene. *Phys. Rev.*, submitted, 2003.

[38] K. Takeda, K. Takegoshi, and T. Terao. Dynamic nuclear polarization by electron spins in the photoexcited triplet state: Ii. high polarization of dilute protons in deuterated naphthalene. *Phys. Rev.*, submitted, 2003.

[39] K. Takeda, K. Takegoshi, and T. Terao. Zero-field electron spin resonance and theoretical studies of light penetration into single crystal and polycrystalline material doped with molecules photoexcitable to the triplet state via intersystem crossing. *J. Chem. Phys.*, 117:4940, 2002.

[40] D.J. Sloop, H.-L. Yu, T.-S. Lin, and S.I. Weissman. Electron spin echoes of a photoexcited triplet: pentacene in *p*-terphenyl crystals. *J. Chem. Phys.*, 75:3746, 1981.

[41] C. Hellner, L. Lindqvist, and P.C. Roberge. Absorption spectrum decay kinetics of triplet pentacene in solution, studied by flash photolysis. *J. Chem. Soc. Faraday Trans. II*, 68:1928, 1972.

[42] S. Astilean, V. Chitta, A. Corval, R.J.D. Miller, and H.P. Trommsdorff. Singlet-triplet level crossing in matrix-isolated pentacene. *Chem. Phys. Lett.*, 219:95–100, 1994.

[43] A. Corval, C. Kryschi, S. Astilean, and H.P. Trommsdorff. Resonant intersystem crossing in pentacene. *J. Phys. Chem.*, 98:7376–7381, 1994.

[44] H. de Vries and D.A. Wiersma. Fluorescence transient and optical free induction decay spectroscopy of pentacene in mixed crystals at 2K. determination of intersystem crossing and internal conversion rates. *J. Chem. Phys.*, 70:5807, 1979.

[45] W.R. Lambert and A.H. Zewail. Intersystem crossing rates of pentacene in naphthalene at 1.9k following single-mode laser excitation. *Chem. Phys. Lett.*, 69:270, 1980.

[46] R.W. Olson and M.D. Fayer. Site-dependent vibronic line widths and relaxation in the mixed molecular crystal pentacene in *p*-terphenyl. *J. Phys. Chem.*, 84:2001–2004, 1980.

[47] F.G. Patterson, H.W.H. Lee, W.L. Wilson, and M.D. Fayer. Intersystem crossing from singlet states of molecular dimers and monomers in mixed molecular crystals: Picosecond stimulated photon echo experiments. *Chem. Phys.*, 84:51–60, 1984.

[48] J. Köhler, A.C.J. Brouwer, E.J.J. Groenen, and J. Schmidt. On the intersystem crossing of pentacene in *p*-terphenyl. *Chem. Phys. Lett.*, 250:137–144, 1996.

[49] J.O. Williams, A.C. Jones, and M.J. Davies. Radiationless transitions in *p*-terphenyl crystals doped with anthrecene, tetracene, and pentacene. *J. Chem. Soc. Faraday Trans. 2*, 79:263–269, 1983.

[50] C. Kryschi, H.-C. Fleischhauser, and B. Wagner. The mechanism of singlet to triplet transitions of pentacene guests in p-terphenyl and benzoic acid crystals. *Chem. Phys.*, 161:485–491, 1992.

[51] M. Gouterman and W. Moffitt. Origin of zero-field splittings in triplet states of aromatic hydrocarbons. *J. Chem. Phys.*, 30:1107, 1959.

[52] M. Gouterman. Calculation on the zero-field splitting in triplet states of various aromatic hydrocarbons. ii. *J. Chem. Phys.*, 30:1369, 1959.

[53] A.J. van Strien and J. Schmidt. An EPR study of the triplet state of pentacene by electron spin-echo techniques and laser flash excitation. *Chem. Phys. Lett.*, 70:513, 1980.

[54] J.-L. Ong, D.J. Sloop, and T.-S. Lin. Deuteration effect on the spin dynamics of the photo-excited triplet state of pentacene in *p*-terphenyl crystals. *Chem. Phys. Lett.*, 241:540–546, 1995.

[55] A. McLachlan and A.D. Carrington. *Introduction to Magnetic Resonance With Applications to Chemistry and Chemical Physics*. Thomson Learning, 1999.

[56] H.M. McConnell and R.E. Robertson. Comments on "Theory of Isotropic hyperfine interactions in π-electron radicals". *J. Chem. Phys.*, 28:991, 1958.

[57] H.M. McConnell. Spin density matrices for paramagnetic molecules. *J. Chem. Phys.*, 28:1188, 1958.

[58] H.M. McConnell and D.B. Chesnut. Theory of isotropic hyperfine interactions in π-electron radicals. *J. Chem. Phys.*, 28:107, 1958.

[59] A.D. McLachlan. Self-consistent field theory of the electron spin distribution in π-electron radicals. *Mol. Phys.*, 3:233, 1960.

[60] A.D. McLachlan. Spin density and spin correlation in triplet states. *Mol. Phys.*, 5:51, 1962.

[61] C.P. Keijzers, E.J. Reijerse, and J. Schmidt. *Pulsed EPR: a new field of applications*. North Holland, Amsterdam/Oxford/Tokyo, 1989.

[62] S.R. Hartmann and E.L. Hahn. Nuclear double resonance in the rotating frame. *Phys. Rev.*, 128:2042, 1962.

[63] C.P. Slichter. *Principles of Magnetic Resonance, Third Enlarged and Updated Edition*. Springer-Verlag, 1990.

[64] M. Mehring. *Principles of high resolution NMR in solids*. Springer-Verlag, Berlin, Heidelberg, New York, 1983.

[65] A. Pines, M.G. Gibby, and J.S. Waugh. Proton-enhanced nmr of dilute spins in solids. *J. Chem. Phys.*, 59:569, 1973.

[66] M. Iinuma. Dynamic nuclear polarization at high temperature for polarized proton target. *phD thesis*, 1997.

[67] J.U. von Schütz and H.C. Wolf. Bewegungen der CH_3-gruppen in methyl-naphthalin-kristallen. *Z. Naturforsch*, 27a:42–50, 1972.

[68] S.C. Abrahams, J.M. Robertson, and J.G. White. The crystal and molecular structure of naphthalene. i. x-ray measurements. *Acta Cryst.*, 2:233, 1949.

[69] D.W. Cruickshank. A detailed refinement of the crystal and molecular structure of naphthalene. *Acta Cryst.*, 10:504, 1957.

[70] M. Iinuma. *private communication*.

[71] B. Ghim, G.A. Rinard, R.W. Quine, S.S. Eaton, and G.R. Eaton. Design and fabrication of copper-film loop-gap resonators. *J. Magn. Reson.*, A120:72–76, 1996.

[72] A.E. McDermott, F.J. Creuzet, A.C. Kolbert, and R.G. Griffin. High-resolution magic-angle-spinning NMR spectra of protons in deuterated solids. *J. Magn. Reson.*, 98:408, 1992.

[73] B. Reif, C.P. Jaroniec, C.M. Rienstra, M. Hohwy, and R.G. Griffin. ^{1}H-^{1}H MAS correlation spectroscopy and distance measurements in a deuterated peptide. *J. Magn. Reson.*, 151:320, 2001.

[74] A. Pines, D.J. Ruben, S. Vega, and M. Mehring. New approach to high-resolution proton NMR in solids: Deuterium spin decoupling by multiple-quantum transitions. *Rhys. Rev. Lett.*, 36:110, 1976.

[75] C. Kittel and E. Abrahams. Dipolar broadening of magnetic resonance lines in magnetically diluted crystals. *Phys. Rev.*, 90:238, 1953.

[76] J.S. Waugh, O. Gonen, and P. Kuhns. Fourier transform nmr at low temperatures. *J. Chem. Phys.*, 86:3816, 1987.

[77] S. Vega. Fictitious spin 1/2 operator formalism for multiple quantum nmr. *J. Chem. Phys.*, 68:5518, 1978.

[78] N. Bloembergen. On the interaction of nuclear spins in a crystalline lattice. *Physica*, 15:386, 1949.

[79] I.J. Lowe and S. Gade. Density-matrix derivation of the spin-diffusion equation. *Phys. Rev.*, 156:817, 1967.

[80] A.G. Redfield and W.N. Yu. Moment-method calculation of magnetization and interspin-energy diffusion. *Phys. Rev.*, 169:443, 1968.

[81] A.G. Redfield and W.N. Yu. Erratum: Moment-method calculation of magnetization and interspin-energy diffusion. *Phys. Rev.*, 177:177, 1969.

[82] T.T.P. Cheung. Spin diffusion in nmr in solids. *Phys. Rev.*, B23:1404, 1981.

[83] C. Tang and J.S. Waugh. Dynamics of classical spins on a lattice: Spin diffusion. *Phys. Rev.*, B45:748, 1992.

[84] J. Clauss, K. Schmidt-Rohr, and H.W. Spiess. Determination of domain sizes in heterogeneous polymers by solid-state nmr. *Acta Polymer*, 44:1–17, 1993.

[85] W. Zhang and D.G. Cory. Pulsed gradient NMR probes for solid state studies. *J. Magn. Reson.*, 132:144, 1998.

[86] R. Loudon. *The quantum theory of light, 2nd edition,*. Clarendon Press, Oxford, 1983.

[87] R.S. Becker. *Theory and interpretation of fluorescence and phosphorescence*. Wiley Interscience, 1969.

[88] C.W. Ashpole and S.J. Formosinho. Triplet-triplet absorption spectra of aromatic vapors. *J. Mol. Spec.*, 53:489–492, 1974.

[89] M.B. van der Mark, M.P. van der Albada, and A. Lagendijk. Light scattering in strongly scattering media: Multiple scattering and weak localization. *Phys. Rev.*, B37:3575, 1988.

[90] J.H. Meyling and D.A. Wiersma. The second-order stark effect on the $^1B_{2u}$ electronic origin of tetracene and pentacene in *p*-terphenyl. *Chem. Phys. Lett.*, 20:383, 1973.

[91] B. Soep, A. Kellmann, M. Martin, and L. Lindqvist. Study of triplet quantum yields using a tunable dye laser. *Chem. Phys. Lett.*, 13:241, 1972.

[92] I.Y. Chan, W.G. van Dorp, T.J. Schaafsma, and J.H. van der Waals. The lowest triplet state of zn porphin i. modulation of its phosphorescence by microwaves. *Mol. Phys.*, 22:741–751, 1971.

[93] I.Y. Chan, W.G. van Dorp, T.J. Schaafsma, and J.H. van der Waals. The lowest triplet state of zn porphin ii. investigation of its dynamics by microwave induced delayed phosphorescence. *Mol. Phys.*, 22:753–760, 1971.

[94] D.G. Crabb, C.B. Higley, A.D. Krisch, R.S. Raymond, J.A. Stewart, and G.R. Court. Observation on a 96% proton polarization in irradiated ammonia. *Phys. Rev. Lett.*, 64:2627, 1990.

[95] A. Ozarowski, A. Misra, S. Ghosh, and A.H. Maki. Spin-lattice relaxation of the tryptophan triplet state varies with its protein environment. *J. Phys. Chem.*, B106:5099, 2002.

[96] A. Ozarowski, J.Q. Wu, and A.H. Maki. Electron spin-lattice relaxation of the triplet state in disordered solids exhibits dispersion. *Chem. Phys. Lett.*, 286:433–438, 1998.

[97] J. Zuclich. Triplet-state electron spin resonance of aromatic amino acid and proteins. *J. Chem. Phys.*, 52:3586, 1970.

[98] H.W. Long, H.C. Gaede, J. Shore, L. Reven, C.R. Bowers, J. Kritzenberger, T. Pietrass, A. Pines, P. Tang, and J.A. Reimer. High-field cross-polarization NMR from laser-polarized xenon to a polymer surface. *J. Am. Chem. Soc.*, 115:8491, 1993.

[99] J. Smith, K. Knagge, L.J. Smith, E. MacNamara, and D. Raftery. Investigating hyperpolarized ^{129}Xe and CPMAS for spin polarization transfer to surface nuclei: a model study. *J. Magn. Reson.*, 159:111, 2002.

[100] S.A. Smith, T.O. Levante, B.H. Meier, and R.R. Ernst. Computer simulations in magnetic resonance. An object-oriented programming approach. *J. Magn. Reson.*, 106a:75–104, 1994.

Index

adiabatic condition, 29, 77

Bloch, F., 1
Bloembergen, N, 87

Carver, T.R., 5
Cory, D.G., 87
CREST, iii
cross polarization, 21, 23, 25, 29, 30, 59, 60, 62, 78

Deimling, M., 7
DNP (dynamic nuclear polarization), i, iii, 1, 5–9, 11, 13, 31, 32, 40, 45, 50, 53, 55, 65, 97, 102, 109–111, 129, 133, 134

effective field, 22, 77

Fictitious spin $\frac{1}{2}$, 73

Gade, S, 87

Hahn, E.L., 24
Hartmann, S.R., 24
Hartmann-Hahn
  condition, 24–26, 28, 29, 61, 79, 83
  matching, 25, 27, 83
Henstra, A., 7, 25, 30

IC (internal conversion), 11
ICP (Integrated Cross Polarization), 21, 25, 29
  sequence, 37
inhomogeneous broadening, 20
ISC (intersystem crossing), 11, 107, 121, 126, 128
  quantum yield, 11, 13, 33, 126
    of pentacene, 13, 33
  rate, 32, 33, 121, 128

Lambert-Beer law, 107
Larmor frequency, 21, 22
Lowe, I,J, 87

Overhauser effect, 5
Overhauser, A.H., 5

penetration depth, 32, 108, 109, 120, 121, 126, 128
pentacene, 11, 98, 100
  -doped naphthalene, 97
photo-bleaching, 108
polarization, 3

Purcell, E.M., 1

sample shuttle system, 61
Slichter, C.P., 5, 24
Sloop, D.J., 11
Solomon, I., 5
spin diffusion, 53, 68–70, 87, 88, 93
    constant, 68, 87–89, 93
spin packet, 7, 20, 21, 25–30, 34, 88, 104

triplet excitation depth, 32, 33, 119, 121, 124, 128
triplet-triplet absorption, 108

zero-field splitting, 14, 109
ZFS (zero-field splitting), 13, 14, 109
    tensor, 16
Zhang, W, 87